



**Politecnico
di Torino**

Politecnico di Torino

Corso di Laurea

A.a. 2024/2025

Sessione di Laurea Marzo 2025

Fragility functions of unreinforced masonry aggregate buildings under varying unit-interconnectivity conditions

Supervisor:

Prof. Paolo Castaldo

External supervisor:

Prof. Fabio di Trapani

Co-supervisor:

Ing. Sofia Villar

Dr. Antonio Sberna

Candidate:

Luca Biancotto

Sommario

Nella regione mediterranea, in particolare in Italia, gli edifici in muratura in configurazione aggregata costituiscono una parte significativa del patrimonio architettonico. Queste strutture sono il risultato della graduale trasformazione di singole unità strutturali che, nel corso del tempo, vengono unite e fuse in un unico organismo edilizio. La valutazione delle prestazioni sismiche degli aggregati murari è un argomento complesso principalmente a causa delle incertezze derivanti dalle interazioni tra le singole unità e anche a causa del fatto che le attuali normative non trattano tale materia in modo esaustivo. Di conseguenza, lo studio di configurazioni elementari di aggregati edilizi, costituiti da unità regolari e simili tra loro, ha recentemente acquisito importanza in quanto, in questo modo, è possibile porre in evidenza l'impatto che le connessioni fra le diverse unità hanno nelle prestazioni finali dell'intero aggregato edilizio. Questa tesi è strutturata in due parti. La prima presenta un'analisi di fragilità di un aggregato edilizio di riferimento composto da tre unità strutturali simili, valutato in tre diverse condizioni al contorno: (i) configurazione in aggregato con connessione rigida tra le unità, (ii) configurazione in aggregato con una connessione che si degrada e (iii) come edifici isolati. La probabilità di superare lo stato limite di collasso è stimata utilizzando come parametro lo spostamento in piano dei pannelli in muratura (EDP), misurato nel contesto di un'analisi dinamica incrementale (IDA) costituita da una serie di trenta terremoti. La seconda parte applica quanto sviluppato nella prima ad un caso studio reale - il Palazzo Ducale di Popoli (Pescara) - per il quale è stato creato un modello numerico al fine di studiarne il comportamento dinamico, considerando l'edificio come parte di un complesso architettonico più esteso. La presenza di strutture adiacenti è stata simulata introducendo dei vincoli. L'edificio è stato valutato utilizzando il framework precedente con un numero ridotto di moti al suolo a causa della maggiore scala della struttura. Tutti i modelli numerici sono stati sviluppati utilizzando la piattaforma software STKO per OpenSees, che consente il calcolo parallelo per analisi su larga scala. Per la modellazione è stata adottata una tecnica di omogeneizzazione della muratura, utilizzando elementi di tipo “layered shell” inelastici 2D. I risultati mostrano l'impatto del cosiddetto “effetto aggregato” e i suoi potenziali benefici nel contesto delle prestazioni sismiche delle singole unità strutturali, sottolineando inoltre l'influenza che le scelte di modellazione delle condizioni al contorno hanno in termini dell'evoluzione dei meccanismi di rottura globali e locali.

Abstract

Within the Mediterranean region, particularly in Italy, masonry aggregate buildings constitute a significant portion of the architectural heritage. These structures result from the gradual transformation and interconnection of originally isolated structural units over time, shaping the evolution of urban areas. Assessing the seismic performance of masonry aggregates is challenging due to the significant uncertainties arising from interactions between individual units. Moreover, existing building codes and standards lack comprehensive guidance on this topic, impacting the reliability of modeling assumptions and the accuracy of analytical outcomes. Consequently, studying masonry aggregates at an elementary level, with similar regular units, to isolate the effects of unit interconnectivity has recently gained interest. This thesis is structured into two parts. The first part presents a fragility analysis of a reference building aggregate composed of three similar structural units, evaluated under three different boundary conditions: (i) in-aggregate configuration with a rigid connection between units, (ii) in-aggregate configuration with a degrading connection, and (iii) as isolated buildings. The probability of exceeding the collapse limit state is estimated using the in-plane drift on masonry panels as the engineering demand parameter (EDP), measured during an Incremental Dynamic Analysis (IDA) with a set of thirty ground motions. The second part applies the lessons learned to a real case study—the Palazzo Ducale of Popoli (Pescara)—for which a detailed numerical model was created to study its dynamic behaviour, considering the building as part of a more complex architectural arrangement. The presence of adjacent structures was simulated by introducing constraints. The building was assessed using the previous framework with a reduced number of ground motions due to the large scale of the structure. All numerical models are developed using the STKO software platform for OpenSees, enabling parallel computing for large-scale analyses. A homogenized masonry approach is adopted, employing 2D layered inelastic shell elements. The results showcase the impact of the so-called “aggregate effect” and its potential benefits for the seismic performance of individual structural units. They also emphasize the critical influence of boundary condition modelling choices on the evolution of global and local failure mechanisms.

Content

1. Introduction	1
2. Seismic behaviour of unreinforced masonry aggregate buildings	3
2.1 The current state of the art of unreinforced masonry aggregates	4
2.1.1 NTC2018	4
2.1.2 Definition of the Limit States	5
2.1.3 Inter-story drift ratio	6
2.2 Behaviour of masonry	8
2.2.1 Mortar.....	9
2.2.2 Units	9
2.3 Global failure mechanisms of masonry	10
2.4 Local collapse mechanisms	11
2.5 The “aggregate effect”	13
2.5.1 Impact of different floor typologies	14
2.5.2 Impact of degrees of interconnection between units	17
2.6 Modelling approaches.....	18
3. Numerical modelling of aggregate buildings in Opensees using STKO	19
3.1 Introduction to OpenSees	19
3.1.1 OpenSees Objects	20
3.1.2 ModelBuilder.....	20
3.1.3 Domain	21
3.1.4 Analysis	21
3.1.5 Recorder.....	22
3.2 STKO.....	23
3.2.1 Definition of the geometry.....	23
3.2.2 Physical and element properties	24
3.2.3 Conditions	24

3.2.4	Analysis Steps.....	25
3.3	Python as a tool to automate OpenSees.....	25
3.4	Numerical modelling approach.....	27
3.4.1	Masonry structure modelling approach.....	27
3.4.2	Modelling of the slab and of floor beams.....	33
3.4.3	Modelling of openings in masonry walls.....	35
3.4.4	Modelling of connection between units of the URM aggregate.....	36
4.	Fragility curves of a masonry aggregate building.....	38
4.1	Introduction to fragility analyses.....	38
4.2	Incremental Dynamic Analysis.....	39
4.2.1	General properties of IDA curves	40
4.2.2	Multi-record IDAs.....	41
4.2.3	Spline interpolation of IDA curves: Centripetal method	42
4.3	Multi-stripe analysis	43
4.4	Performance-based earthquake engineering assessment framework.....	44
4.4.1	Engineering characterization of ground motions: Arias intensity, energetic criteria for ground motion truncation.....	46
4.4.2	Selection of the DM and post-processing of the results.....	48
4.5	Probability	49
4.5.1	Conditional probability	49
4.5.2	Definition of the fragility function.....	49
5.	Description of the elementary aggregate case study.....	53
5.1	Numerical modelling	53
5.1.1	Geometry	53
5.1.2	Material properties.....	55
5.1.3	Loads, masses and conditions.....	57
5.1.4	Mesh architecture	58
5.2	Dynamic properties of the elementary aggregate	60

5.2.1	Vertical analysis.....	60
5.2.2	Modal analysis	60
5.2.3	Non-linear dynamic analysis	61
5.3	Dynamic characteristics of the models	62
5.4	Non-linear dynamic analysis results – derivation of fragility curves	65
5.4.1	Ground motion selection	65
5.4.2	Intensity measure.....	65
5.4.3	Engineering demand parameter (EDP).....	65
5.4.4	IDA curves	68
5.4.5	Multi Stripe Analysis (MSA).....	73
5.4.6	Damage Analysis.....	77
5.4.7	Proposed fragility curves	79
6.	Description of a real example of aggregate: Palazzo Ducale in Popoli, Abruzzo	81
6.1	Evolution of the aggregate.....	82
6.2	Numerical modelling	83
6.2.1	Geometry and simplification hypothesis.....	83
6.2.2	Material properties.....	86
6.2.3	Loads, masses and conditions.....	87
6.2.4	Mesh architecture	87
6.3	Dynamic properties of Palazzo Ducale	88
6.4	Non-linear dynamic analysis results	90
6.4.1	Damage Analysis.....	91
7.	Conclusions.....	95
7.1.1	Future developments	97
8.	Appendix.....	98
9.	References.....	100

List of figures

Figure 1: Building Aggregate, Popoli, Italy.....	3
Figure 2: Schematic configuration of the arrangement of a masonry aggregate.....	4
Figure 3: Minimum reliability requirements depending on the class of the building. Tab2.1 CNR [3]	6
Figure 4: Schematization of the element for the computation of the inter-story drift ratio [3].	6
Figure 5: Regular and irregular masonry.....	8
Figure 6: Typical in-plane failure modes of masonry walls: (a) sliding shear failure; (b) rocking; and (c) diagonal cracking (Cakir et al. 2015).....	11
Figure 7: Overturning mechanisms	11
Figure 8: Vertical flexural mechanisms	12
Figure 9: Horizontal flexural mechanisms	12
Figure 10: Composed overturning mechanisms	13
Figure 11: Examples of planimetric and altimetric positions that SUs can occupy within the aggregate [4].....	14
Figure 12: schematizations of: (a) rigid floor (b) flexible floor	15
Figure 13: Scheme, rigid diaphragm	15
Figure 14: Scheme, flexible diaphragm.....	16
Figure 15: Examples of damage mechanisms observed after the Central Italy, pounding mechanism [4].....	17
Figure 16: Comparison between the structure behind a traditional code and the one of the OpenSees framework	19
Figure 17: OpenSees objects	20
Figure 18: OpenSees model.....	21
Figure 19: Opensees Analysis object [7]	22
Figure 20: STKO work tree	23
Figure 21: Example of the articulation of folders for the creation of a set of models.....	26
Figure 22: Layered Shell section [29]	27
Figure 23: Nodes, Gauss points, local coordinate system, warped and flat geometry [10].....	28
Figure 24: Nodes, Gauss points and local coordinate system for ASDShellT3 [10].....	28
Figure 25: A schematic representation of the elastic predictor followed by the plastic and damage correctors in a representative uniaxial case. [10].....	31
Figure 26: Energy dissipated by $e1$ and $e2$	33

Figure 27: Rigid diaphragms of the three cases considered: a) fully connected, b) semi-connected, c) isolated model.	34
Figure 28: Example of fibre discretization of a beam-column element for a reinforced concrete cross-section	35
Figure 29: Lintel geometry [26]	36
Figure 30: Details of the mesh refinement and of the EqualDOF connection between masonry and mortar.	37
Figure 31: IDA curves of a $T_1 = 18$ sec, 5-storey steel braced frame subjected to 4 different records. [17]	41
Figure 32: Structural resurrection on the IDA curve of a $T_1 = 13$ sec, 3-storey steel moment-resisting frame with fracturing connections [17]	41
Figure 33: Non-fitted IDA curve vs fitted IDA curve using the centripetal model	43
Figure 34: Example of IDA curves and MSA data [15]	44
Figure 35: Performance-based earthquake engineering framework (Yang et al. 2009) [19]... ..	44
Figure 36: Illustration of significant duration for the Treasure Island ground motion during the 1989, based on 5% and 95% thresholds [20]	47
Figure 37: Capacity curves of the same accelerogram scaled for different factors: Figure a) smooth capacity curve, Figure b) discontinuities given by the non-convergence of the analysis.	48
Figure 38: Cumulative density functions for different IMs and the related probability of exceedance of the imposed threshold.	51
Figure 39: Probability Density Function for the collapsing events and the relative Cumulative Density Function.	52
Figure 40: Fragility curve as the sum of the 2 terms.	52
Figure 41: Reference aggregate's geometry: (a) Front wall; (b) Back wall [24].....	53
Figure 42: STKO 3D model of the aggregate building	54
Figure 43: Front wall, mid wall and back wall.....	54
Figure 44: From left to right: example of external wall, internal wall and partitioning wall between the units	54
Figure 45: Model geometry for the three cases considered, emphasizing the rigid diaphragm.	58
Figure 46: Visual representation of the model partition	59
Figure 47: Example of Rayleigh damping introduced for the Semi-connected model	61

Figure 48: Example of monitor placement and naming for the front wall of the semi-connected model.....	66
Figure 49: IDA curves obtained for a set of 30 ground motions. a) Fully-connected case, b.1) Semi-connected case, m1 b.2) semi-connected case, m3	68
Figure 50: IDA curves obtained for a set of 30 ground motions. c) Isolated cases	69
Figure 51: Interpolated IDA curves obtained for a set of 30 ground motions. a) Fully-connected case, b.1) Semi-connected case, m1	69
Figure 52: Interpolated IDA curves obtained for a set of 30 ground motions. b.2) semi-connected case, m3 c) Isolated cases	70
Figure 53: Capacity curves for the fully-connected model.	71
Figure 54: Capacity curves for the semi-connected model	72
Figure 55: MSA analysis for the Fully Connected case (a) and Semi Connected case (b)	73
Figure 56: Figure 50: MSA analysis for the isolated cases (c)	74
Figure 57: Cumulative Density Function for the a) fully-connected case b) semi-connected case c) isolated models.....	75
Figure 58: MSA for converging analyses and PDF of the intensity measures obtained for the fully-connected and semi-connected cases	75
Figure 59: MSA for converging analyses and PDF of the intensity measures obtained for the semi-connected and isolated cases.	76
Figure 60: IDA curves for the fully connected and semi connected m1 cases (accelerograms 9 and 15 are highlighted in red and in blue respectively).	77
Figure 61: Initial damage for the fully-connected and the semi-connected model.	78
Figure 62: Crushing of the back wall of the external units for the fully-connected case.....	78
Figure 63: Final damage for the fully-connected and the semi-connected model, for the accelerogram 9 and 15.....	79
Figure 64: Comparison of the fragility curves for different degrees of interconnection between units.	79
Figure 65: The case study aggregate in the historical centre of Popoli (Italy). The façades facing the square, reported with the ten units (from U1 to U10 from left to right)	81
Figure 66: Hypothesis about the evolution of the aggregate over time	82
Figure 67: Proposed schematization and simplification of the structural layout for the four levels of the structure.	83
Figure 68: Front and back wall (model from Revit).....	84
Figure 69: 3D STKO model for front, back and lateral walls.	84

Figure 70: Modelling hypothesis regarding the placement and the typologies of constraint to simulate the interaction between the aggregate and the other buildings.....	85
Figure 71: 3D STKO model, vaults and rigid diaphragms.....	85
Figure 72: Fix condition to emulate the interaction between the aggregate and the rest of the structure	86
Figure 73: Shell thicknesses and the related number of elements	87
Figure 74: Partitioning of the Palazzo Ducale model.....	88
Figure 75: Acceleration time-history for the two components of the Norcia ground motion.	90
Figure 76: Comparison between the inter-story drift and the accelerations time-histories	91
Figure 77: Initial damage for the two cases considered. a) constrained model, b) isolated model.	92
Figure 78: Damage for the back wall. a) constrained model, b) isolated model.	92
Figure 79: Damage for the back wall, detail of the large displacements attained for the towering units. a) constrained model, b) isolated model.	93
Figure 80: Damage of the aggregate front wall. a) constrained model, b) isolated model.....	93

List of tables

Table 1: Indicative ranges of drift and residual strength values for different damage states [3].	7
Table 2: Table C8.5II from NTC18, masonry characteristics and classifications.	8
Table 3: Tab. 4.5.Ia from NTC18 classification of the masonry units.	10
Table 4: Wood physical properties and embedded settings	55
Table 5: Masonry physical properties calibration from study	55
Table 6: Tab C8.5.1, NTC2018 - Masonry categories	56
Table 7: Properties used in the model for the different typologies of mortar considered.....	56
Table 8: Lintel physical properties.....	56
Table 9: User-defined mortar parameters.....	57
Table 10: Eigenvalues analysis results for the fully-connected and the semi-connected cases.	62
Table 11: Eigenvalues analysis results for the isolated model.....	62
Table 12: First 3 modal shapes of the Fully-Connected aggregate [24]	63
Table 13: First 3 modal shapes of the isolated units [24].	63
Table 14: First 3 modal shapes of the Semi-Connected aggregate [24].	64
Table 15: Ground motion selection.....	67
Table 16: Masonry physical properties.....	87
Table 17: Eigenvalues analysis results for the constrained and the isolated model.....	88
Table 18: Five modal shapes for the constrained and the isolated model.....	89
Table 19: Parameters for the ground motion selection.	90

1. Introduction

The upcoming chapters address the topic of masonry buildings in aggregate configuration. This structural typology is widely spread across Europe as the result of urban development in cities and, in particular, of small historic towns, which now face issues related to the maintenance and the preservation of the cultural heritage.

The analysis of this structural typology is affected mainly by three factors:

- The lack of adequate coverage in the regulations: Current building codes and standards do not comprehensively address the structural behaviour of masonry aggregates.
- The lack of understanding of the interaction between different units: the influence that one unit has on the others is affected by lots of uncertainties, so it is difficult to predict a priori the final distribution of forces and stresses within the aggregate.
- The simplifications that are conventionally performed with masonry structures, can now lead to the rise of major uncertainties that can mislead the final result of the analysis.

The present work is structured in two parts:

1. **Fragility Analysis of an elementary case study:** The first part is about a fragility analysis conducted on a selected three-story case study; the building in the aggregate configuration is subjected to a set of thirty earthquakes to perform an Incremental Dynamic Analysis (IDA) and to explore the impact of different levels of interconnection between the units.
2. **Application to a real historical aggregate:** The second part focuses on a real historical masonry aggregate, the Palazzo Ducale located in Popoli (Pescara), so it has been conducted an in-depth analysis of the geometry of the building, its construction details and the modifications that have occurred during its existence, followed then by a numerical simulation of the structural behaviour using OpenSees and STKO (Scientific Tool Kit for OpenSees).

This study aims to enhance the understanding of the aggregate effect and the interaction between different units performing a fragility analysis on a simplified theoretical case study and, once the methodological framework is set, the same approach is applied to a real case study. The first case study examines a simplified and regular elementary aggregate with rigid diaphragms, while the second case study focuses on a real structure that is irregular in elevation

and features flexible diaphragms. The decision of modelling a real case study is based on the need to complement the initial analysis conducted on a simplified, regular model. While the simplified model is useful for exploring how different levels of interconnection between units influence the overall building behaviour, it does not accurately represent the structural configurations commonly found in the Mediterranean region. Analyzing the historical aggregate of Palazzo Ducale di Popoli, the second part of this study evaluates the impact of key factors such as height irregularities, the presence of flexible floors, and the effects of connections between structural elements.

2. Seismic behaviour of unreinforced masonry aggregate buildings

The constructions that compose the majority of the city centres in Europe are the result of a centuries-lasting process of evolution: often the operations of demolition or addition of new floors, features or even entire new buildings were done without following any rules except satisfying the needs of that very moment. This can be demonstrated by the fact that in Italy one of the first anti-seismic codes containing basic recommendations such as provisions about the materials, the minimum width of some structural elements, etc., was developed after the earthquake occurred in Norcia in 1859 and up to this moment the urban expansion of the city centres led to the diffusion of this particular structural typology of the “building aggregate”.

To further explain, these aggregates comprise multiple “open” units that share one or more walls with adjacent structures and, as a consequence of this non-planned and non-homogeneous construction process, it is not easy to correctly interpret their structural behaviour.



Figure 1: Building Aggregate, Popoli, Italy.

Vulnerability studies have shown that one important parameter to enhance the performance of a building under an earthquake is the number of stories [1]. This issue is a relevant one, especially in the Italian context noted the large diffusion of URM buildings in aggregate in Italy, this fact is demonstrated from the data available in the Da.Do. platform (Database of Observed Damage, Dolce et al. 2019) referring only to residential URM buildings; the number

of buildings in aggregate is about 3 times (i.e. 35,261/12,624) higher than the individual buildings by considering all municipalities and even higher, namely 4 (i.e. 26,205/7045) focusing only on small municipalities (< 2000 residents). The ratio is even larger only focusing on historical centres [2]

Lastly, one other aspect that should be mentioned is the state of maintenance of the building itself, which, in the following decades, is destined to become a crucial factor because it will be a direct consequence of gentrification and the negative demographic trends that can be seen almost everywhere in Europe and in particular in Italy.

2.1 The current state of the art of unreinforced masonry aggregates

2.1.1 NTC2018

Even in the NTC2018, all the limitations that are linked with this particular structural typology are underlined, in particular, chapter 8 reports the following: *“In the presence of buildings in aggregate, contiguous, in contact with or interconnected with adjacent buildings, general verification methods for new buildings may be inadequate”*, so the rule itself admits the lack of an adequate standardized approach for dealing with buildings in aggregate.

Nevertheless, NTC18 contains some general provisions and definitions, the regulation defines as “structural unit” a unit that “must have continuity from top to ground” and that can be delimited “either by open spaces, or by structural joints, or by buildings that are structurally contiguous but, at least typologically, different”. It is also necessary to “take into account the possible interactions deriving from structural contiguity with adjacent buildings” and, lastly, differently from what can happen with isolated masonry buildings, particular attention should be put in identifying the local effects that may arise due to “the unbalanced thrusts on walls in common with adjacent US”, caused by height offset between different floors.



Figure 2: Schematic configuration of the arrangement of a masonry aggregate

So, to sum up, the first step is to identify the structural unit (US), highlighting the actions that may derive from contiguous structural units, and understanding the evolution of the building.

The absence of specific regulations regarding the seismic assessment of unreinforced masonry aggregates resulted in multiple study typologies among which it is possible to distinguish:

Empirical methods: consist in a large-scale approach that defines vulnerability classes based on post-earthquake data. This enables the calibration of a vulnerability model for each recognized class through statistical analyses, which can be performed quickly with minimal data, making it suitable for analysing numerous structures or an entire large city.

Holistic methods: usually based on assessing the expected damage considering components such as vulnerability, hazard, and exposure. Useful for a multi-scale analysis that also consider the interconnection between these factors to have an integrated understanding of the situation.

Analytical/mechanical methods: use numerical models and building simulations to determine the structural capacity of buildings. A complete comprehension of the building's characteristics and extensive structural calculations are required, but this is unsuitable for large-scale analysis.

2.1.2 Definition of the Limit States

In the CNR-DT 212/2013 a precise definition of the limit states is provided; they are identified with reference to the performance of the construction as a whole, including structural elements, non-structural elements and supply systems.

There are three limit states considered by the regulation:

- **Damage Limit State (SLD):** the construction maintains the integrity of the structural elements (negligible structural damage that does not require repair) and remains serviceable despite light damage to non-structural elements.
- **Severe Damage Limit State (SLS):** the building undergoes breakage and collapse of the non-structural and plant components and damage to the structural components which is associated with a significant loss of stiffness in relation to horizontal actions; the building instead retains a part of the resistance and stiffness for vertical actions and a margin of safety against collapse for horizontal seismic actions; this state defines the limit beyond which the damage is such as to make repair economically uneconomic.
- **Collapse Prevention Limit State (SLC):** the building suffers very serious damage to structural components while still maintaining a residual capacity to withstand vertical loads. The residual safety against horizontal actions is negligible [3].

Stato limite	Classe I	Classe II	Classe III	Classe IV
SLD	64.0	45.0	30.0	22.0
SLS	6.8	4.7	3.2	2.4
SLC	3.3	2.3	1.5	1.2

Figure 3: Minimum reliability requirements depending on the class of the building. Tab2.1 CNR [3]

2.1.3 Inter-story drift ratio

For the current thesis, the first term of the formula is neglected since the numerical modelling of the walls has been conducted using shell elements that are not able to catch the rotations

The element drift is defined as the sum of flexural and shear deformation. It can be evaluated at both ends of the panel, referring to the flexural point, or, alternatively, formulations can be adopted that consider an average drift of the panel, e.g. provided by the expression [3]:

$$\theta = \frac{\varphi_i + \varphi_j}{2} + \frac{u_j - u_i}{h}$$

With:

- $\varphi_{i,j}$ are the nodal rotations
- $u_{i,j}$ are the transverse displacements of the two nodes
- h is the interstory height of the element
- h' shear span

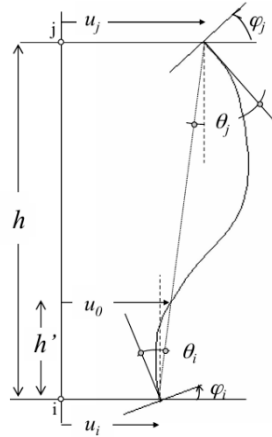


Figure 4: Schematization of the element for the computation of the inter-story drift ratio [3]

In the following pages, the inter-story drift is limited to 0,5%, this condition is obtained from the Table 3.2 of the CNR-DT 212/2013, which suggests the adoption of limit values for the

drifts. These thresholds are functions of the predominant collapse mechanism and of three damage levels (3-severe, 4-very severe, 5-collapse).

The limit value considered in the following analyses is obtained considering that the main collapse mechanism observed is due to shear and taking into account the range suggested by the regulations (that is between 0.25% - 0.6%, corresponding to the first two damage levels).

Table 1: Indicative ranges of drift and residual strength values for different damage states [3].

Tabella 3.2. Intervalli indicativi dei valori del *drift* e della resistenza residua per i diversi stati di danno.

danno	Drift (%)			Resistenza residua	
	3	4	5	3→4	4→5
pressoflessione	0.4 ÷ 0.8	0.8 ÷ 1.2	1.2 ÷ 1.8	1.0	0.8 ÷ 0.9
taglio	0.25 ÷ 0.4	0.4 ÷ 0.6	0.6 ÷ 0.9	0.6 ÷ 0.8	0.25 ÷ 0.6

2.2 Behaviour of masonry

By the term masonry, we mean an assembly of natural or artificial elements called units (or even bricks or blocks, depending on their size) that are arranged with regularity and are kept together with mortar; the final result is an element that has both a structural/resisting function and also a load distribution function. According to the size and the regularity of the elements we can distinguish two categories:

- a) Regular masonry
- b) Irregular masonry

Irregular masonry



Disorderly stone



Hewed blocks



Split stones with good texture

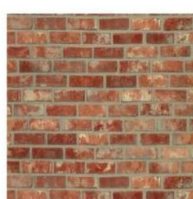


Soft stone (tuff / calcarenite)

Regular masonry



Squared stone blocks



Solid brick



Semi-filled bricks

Figure 5: Regular and irregular masonry

Table 2: Table C8.5II from NTC18, masonry characteristics and classifications.

Tipologia di muratura	f (N/mm ²)	τ_0 (N/mm ²)	f_{v0} (N/mm ²)	E (N/mm ²)	G (N/mm ²)	w (kN/m ³)
	min-max	min-max		min-max	min-max	
Muratura in pietrame disordinata (ciottoli, pietre erratiche e irregolari)	1,0-2,0	0,018-0,032	- -	690-1050	230-350	19
Muratura a conci sbozzati, con paramenti di spessore disomogeneo (*)	2,0	0,035-0,051	- -	1020-1440	340-480	20
Muratura in pietre a spacco con buona tessitura	2,6-3,8	0,056-0,074	- -	1500-1980	500-660	21
Muratura irregolare di pietra tenera (tufo, calcarenite, ecc.)	1,4-2,2	0,028-0,042	- -	900-1260	300-420	13 ÷ 16(**)
Muratura a conci regolari di pietra tenera (tufo, calcarenite, ecc.) (**)	2,0-3,2	0,04-0,08	0,10-0,19	1200-1620	400-500	
Muratura a blocchi lapidei squadriati	5,8-8,2	0,09-0,12	0,18-0,28	2400-3300	800-1100	22
Muratura in mattoni pieni e malta di calce (***)	2,6-4,3	0,05-0,13	0,13-0,27	1200-1800	400-600	18
Muratura in mattoni semipieni con malta cementizia (es.: doppio UNI foratura ≤40%)	5,0-8,0	0,08-0,17	0,20-0,36	3500-5600	875-1400	15

The correct assessment of the category of masonry is a crucial phase because the way in which the masonry is composed has a great influence in the way the cracks will form and propagate through the elements it-self because in the case of irregular masonry, there will be mainly diagonal cracks, while in the other case, due to the regularity of the assembly it mainly experiences sliding failure of mortar joints.

This phase begins with a visual inspection of the elements and then can be further detailed by performing in-depth analysis like the use of infrared thermography, radar investigations, flat jack tests, or even destructive tests such as compression tests and shear tests.

Once the category of masonry is determined, the regulations allow the designers to use in the structural analyses a range of values that is given in the table C8.5.II of NTC18, limiting the need to perform the amount of tests that would be necessary to completely characterize the masonry elements, that, in the end, will be characterized by its compressive strength and by its shear resistance.

2.2.1 Mortar

The mortar has both the function of unifying and distributing the loads.

The technical code classifies mortar in 2 classes:

- **Performance-guaranteed mortar** (this type of mortar is being produced in specialized factories).
- **Prescribed composition mortar** (this type of mortar is being produced directly on-site).

Since the behaviour of mortar is brittle, the typical tests that are performed on mortar specimens are a 3-point bending test and then the 2 halves are tested in compression to characterize the material by its mean compressive strength.

2.2.2 Units

One of the fundamental components of a masonry panel is the units, that can be classified according to their origin into:

- Natural blocks (stone)
- Artificial bricks - Regular or lightened brick elements in paste form, with improved thermal insulation properties.
- Artificial concrete elements

Units can also be classified according to the percentage of the hole area and by their characteristic compressive strength in the 2 orthogonal directions (since the material has an anisotropic behaviour it is important to characterize both the directions).

Table 3: Tab. 4.5.1a from NTC18 classification of the masonry units.

Elementi	Percentuale di foratura φ	Area f della sezione normale del foro
Pieni	$\varphi \leq 15\%$	$f \leq 9 \text{ cm}^2$
Semipieni	$15\% < \varphi \leq 45\%$	$f \leq 12 \text{ cm}^2$
Forati	$45\% < \varphi \leq 55\%$	$f \leq 15 \text{ cm}^2$

Due to their anisotropic behaviour, the elements are characterized by their characteristic compressive strength in 2 directions (the direction in which the load is applied and in the direction orthogonal to this one).

2.3 Global failure mechanisms of masonry

Unreinforced masonry buildings undergoing seismic actions often exhibit local failure mechanisms which represent a serious life-safety hazard, as recent strong earthquakes have shown. Compared to new buildings, older unreinforced masonry buildings are more vulnerable, not only because they have been designed without or with limited seismic loading requirements, but also because horizontal structures and connections amid the walls are not always effective.

Secondary (or global) mechanisms are named after the fact that they are activated only when local mechanisms do not occur, so even if the degree of connection may vary within a range, the main assumption is that the connection between orthogonal walls is rigid and it is assumed that all structural elements contribute to the overall resistance of the building.

According to the crack patterns, the in-plane failure mechanism can be classified into three categories: shear cracking, sliding, and rocking failure (Figure 6).

- **Shear sliding:** This collapse mechanism forms when there are low vertical loads and/or in the case of insufficient mortar cohesion and friction; it can be seen in the development of horizontal tensile cracks along horizontal mortar joints, forming sliding planes.
- **Rocking:** In the presence of vertical eccentric loads, as the horizontal loads or displacements increase, tension cracks form in the bed joints, shifting the load to the compressed masonry, and the failure is due to crushing at one corner and the overturning of the pier, while tensile cracks may appear at the opposite corner.

- **Shear cracking:** This typology of cracks (also called “stepped” cracking) occurs when the cracks propagate along mortar joints or even through bricks (in the case of weak masonry).

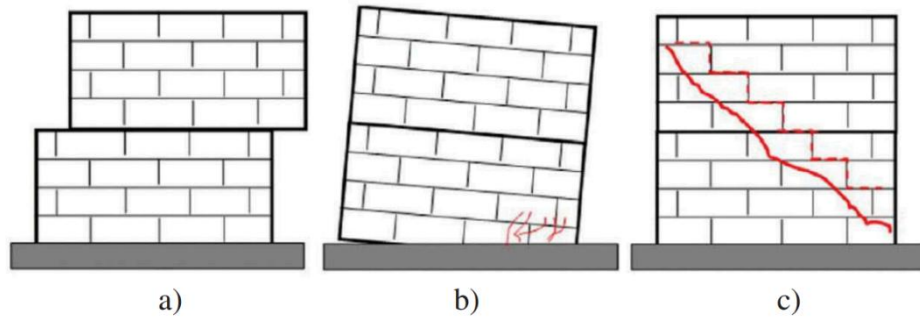


Figure 6: Typical in-plane failure modes of masonry walls: (a) sliding shear failure; (b) rocking; and (c) diagonal cracking (Cakir et al. 2015)

2.4 Local collapse mechanisms

Overturning mechanism of the facades

The overturning mechanism of facades involves the rotation of an entire wall perpendicular to the earthquake direction around a hinge, usually located at its base. This mechanism is enhanced by the lack of a proper connection at the top of masonry panels (such as low degree of connection between the floor slab and the walls or the absence of floor curbs or chains). It can develop at different levels of the structure and may affect one or multiple walls depending on several factors like the presence of openings or the already mentioned lack of good connections.

The presence of this type of collapse can be seen if there are cracks in the correspondence of the wall-to-wall connections near the corners, so one way of mitigating the problem is the introduction of metal ties that can improve the wall connectivity and structural integrity.

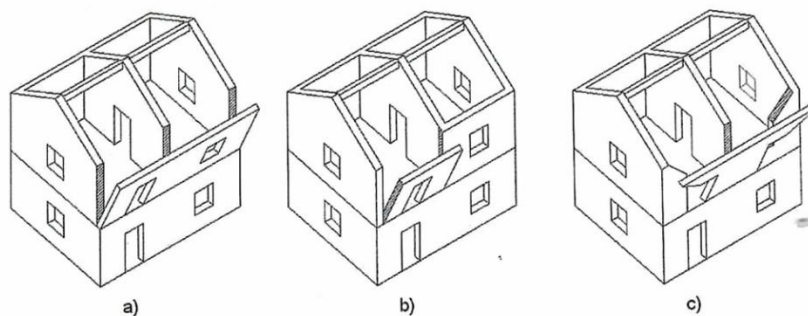


Figure 7: Overturning mechanisms

Vertical flexural mechanism

The vertical-flexural mechanism occurs when a cylindrical hinge develops into the wall dividing it into two rotating segments with hinges at their extremities; as a result, the central portion of the wall perpendicular to the earthquake may bulge outward due to hinge formation at its upper and lower borders. This mechanism typically arises due to poor connections at the floor level, allowing the thrust from intermediate floors to push against the wall (Figure 8). The presence of a concrete curb at the base and roof level or a rigid connection of a wall between two floor slabs (especially in the case of slender walls) can enhance the development of this kinematic mechanism.

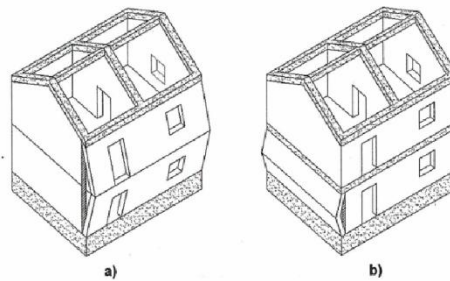


Figure 8: Vertical flexural mechanisms

Horizontal flexural mechanism

The horizontal flexural mechanism occurs when orthogonal walls are well connected, while the connection between the facade and the roof is weak (Figure 9). Consequently, the roof system exerts thrust on the wall, leading to the formation of oblique plastic hinges and causing the subsequent out-of-plane rotation of the upper section of the wall.

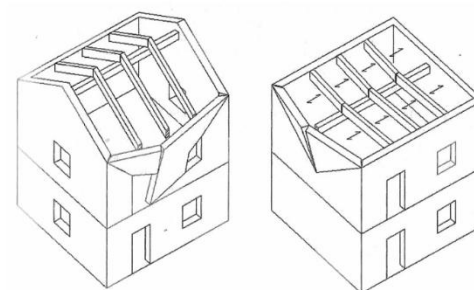


Figure 9: Horizontal flexural mechanisms

Composed overturning mechanism

The composed overturning mechanism takes place when multiple local failure mechanisms occur at the same time. This is common in cases where there is a good connection between walls, but the orthogonal walls are weak and so they are more susceptible to cracking. Openings in transverse walls often serve as critical points where detachment is more likely to initiate.

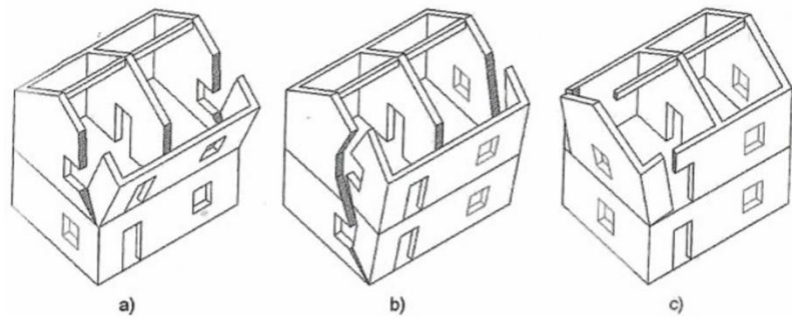


Figure 10: Composed overturning mechanisms

2.5 The “aggregate effect”

As previously stated in the introduction, the category of “buildings in aggregate configuration” comprises a wide range of structures that are interconnected with a certain degree of effectiveness and are distinguished by a predominant direction, defined by the walls of the multiple adjacent units, resulting in distinct behaviours along the longitudinal and transverse directions; on the contrary, isolated buildings, if their plan is relatively regular, there are typically no significant variations in behaviour between the two main directions.

During earthquakes, it is believed that the presence of other adjacent units can have a beneficial effect since it can provide mutual support for the others, stabilizing and redistributing the stresses among the whole ensemble; each unit can have both a function of transmitting the forces to the next structure and a sort of “buttress effect” supporting the previous unit. Given the great variability of the factors involved and the possibility of their mutual interaction, the beneficial effect related to the aggregate configuration is currently being debated.

Vulnerability factors of URM buildings in aggregate certainly include those common to isolated buildings such as the quality of materials and of the execution, the state of maintenance, the in-plane and in elevation regularity, the quality of connections among walls that identify the SU, the opening's misalignments and the foundations' condition [4] but, additionally, factors like the in-plan position of the structural unit, the presence of staggered floors, the quality of interconnections and also the presence of towering units can have an impact in the final behaviour of the structural aggregate.

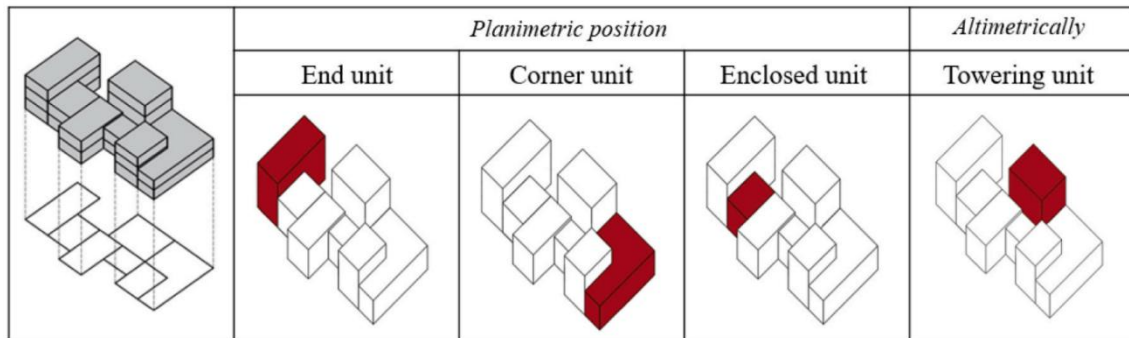


Figure 11: Examples of planimetric and altimetric positions that SUs can occupy within the aggregate [4]

As a matter of fact, from empirical studies, it is possible to assert that units located at the periphery of the aggregates tend to demonstrate higher vulnerability due to a greater torsional effect induced by the absence of constraints imposed by adjacent units [5] and when one unit is located in between shorter buildings, the creation of soft story mechanism in the upper levels is enhanced.

The following paragraphs will elaborate on two additional factors, namely the stiffness at the floor level and the unit-to-unit connection.

2.5.1 Impact of different floor typologies

In addition to the risk factors previously mentioned, like the presence of inadequate wall-to-wall connection, the presence of openings or the unbalanced trust coming from staggered floor slabs belonging to different units; another aspect that can impact the response of a masonry ensemble is the floor-to-wall connection and rigidity of said floor. The possibility of the existence of a range in the rigidity of the floor slab represents an issue that should be correctly addressed since it affects the distribution of forces and stresses among the masonry elements.

In general, two extreme cases can be considered: a rigid floor and a flexible floor.

The concrete slab is the typical example of a rigid floor. Its deformability is very low, therefore, the in-plane infinite stiffness hypothesis can be assumed. This means that the slab is assumed

to have only 3 degrees of freedom: two perpendicular in-plane displacements and in-plane rotation; the more rigid, the higher the capacity of absorbing forces, and the seismic response improves. However, this assumption often cannot be verified, for instance if the slab is made of wood or due to poor slab-to wall connection or to damages, the slab exhibits a finite stiffness and can deform even out of its plane.



Figure 12: schematizations of: (a) rigid floor (b) flexible floor

In the case of an infinitely rigid diaphragm, inertial forces on walls will be distributed proportionally to their relative stiffness. The following scheme (Figure 13) can be adopted to estimate the forces.

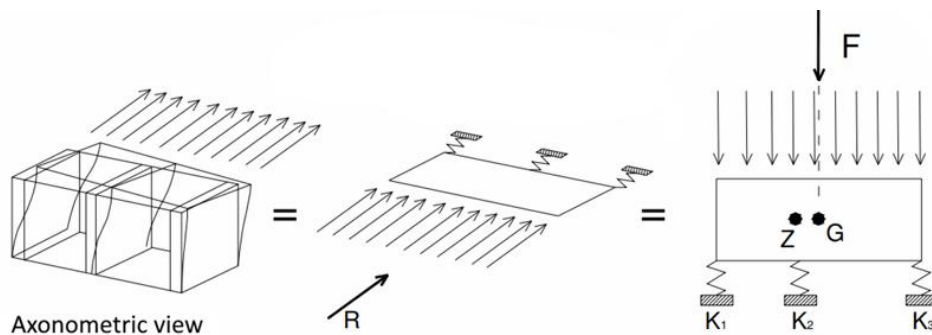


Figure 13: Scheme, rigid diaphragm

In the picture (Figure 13):

- Z: barycentre of stiffness
- G: barycentre of masses
- F: resultant of the seismic force developed

The walls are modelled as springs and the slab as an infinitely rigid beam supported by them. The beam behaves as a rigid body, rotating and translating without experiencing deformation.

The position of the floor barycentre is:

$$x_z = \frac{\sum_{j=1}^n k_j x_j}{\sum_{j=1}^n k_j}$$

Then, the reaction of each spring is:

$$R_i = F \frac{k_i}{\sum_{j=1}^n k_j} + F K_i \frac{(x_i - x_z)(x_G - x_z)}{\sum k_i (x_i - x_z)^2}$$

Where the first term stands for the translation effect, while the second one is related to rotation. It should be noticed that in cases where the mass and the stiffness centroids coincide, the second term of equation is null.

The flexible floor is characterized by a flexible slab or a series of flexural beams. They provide finite to almost null stiffness. As we can see below, the lack of rigidity causes the walls that are perpendicular to the direction of the force to go out of plane. The following scheme is used instead:

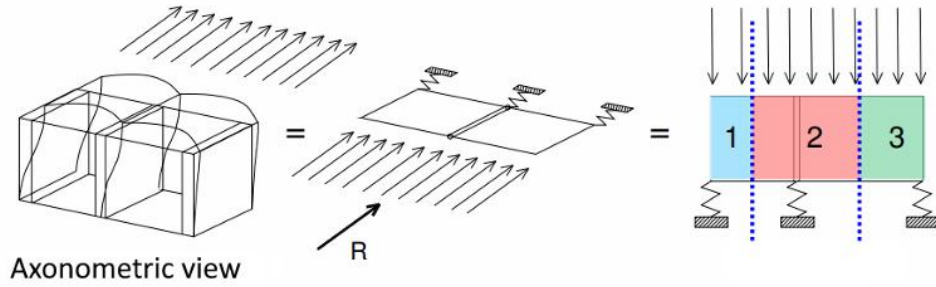


Figure 14: Scheme, flexible diaphragm

In this case, the inertial forces are distributed among transverse walls according to the masses applied on each floor. The mass corresponding to each wall can be evaluated using the tributary area method. The reaction force of each wall is:

$$R_1 = \frac{R}{L_1 + L_2} \frac{L_1}{2}$$

$$R_2 = \frac{R}{L_1 + L_2} \frac{L_1 + L_2}{2}$$

$$R_3 = \frac{R}{L_1 + L_2} \frac{L_2}{2}$$

2.5.2 Impact of degrees of interconnection between units

In the context of buildings in aggregate configuration, newly constructed units in proximity to existing ones are often connected by interlocking joints or mortar. These interfaces are more susceptible to failure during seismic events since there is a concentration of high stress and damage and the initiation of failure mechanisms. Previous studies have highlighted the critical role these interfaces play in the development of horizontal cracks in correspondence with adjacent discontinuities or of vertical cracks at the contact of adjacent units or cracks induced by differential motion of adjacent structures. Figure 15 provides an illustrative example of the formation of cracks at the interface between units due to pounding between two separate units after seismic activity.

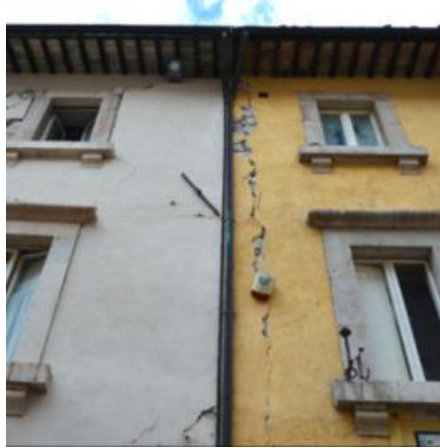


Figure 15: Examples of damage mechanisms observed after the Central Italy, pounding mechanism [4].

The modelling of unreinforced masonry aggregates is commonly simplified using 3D elements or 2D shell elements, but the aggregate units are often considered as either perfectly connected or isolated. However, even if a simplified approach results in a satisfying or conservative value, there is a risk of overlooking possible damage and collapse mechanisms [6]. Additionally, considering the units completely independent from each other leads to the impossibility of properly capturing the "aggregate effect."

In optimal circumstances, aggregates are modelled in three dimensions (3D) using either 3D elements or 2D shell elements. However, the perfectly rigid connection frequently assumed during the modelling stage can be a simplification that significantly alters the response during analysis. Consequently, various studies reported to use interface elements with materials based on Coulomb friction theory and Herz impact theory to reproduce friction and pounding effects between units.

2.6 Modelling approaches

Several approaches for assessing seismic vulnerability have been developed in recent decades, such as:

- a) **Finite Element Models (FEM) – Brick 3D elements**: the structure is schematized in a set of nodes and elements, it is possible to assign material properties and define the boundary conditions of the model it is possible to obtain the unknowns that are the nodal displacements. This specific type of model with 3D elements is mostly used for historic and monumental buildings where modelling simplifications are not possible.
- b) **FE models – 2D Shell Elements**: used for medium-complex buildings.
- c) **Micro-modelling with discrete element method (DEM)**: used for research topics, since masonry elements are constituted by solid blocks joined together with mortar, their behaviour can be captured using discrete element methods (DEM); the solid blocks and their mortar interface can be individually modelled and, consequently it is possible to catch the behaviour of the structure in the non-linear field.
- d) **Micro-modelling (FEM - DEM)**: hybrid techniques have been developed over time, trying to overcome the limitations linked both to FEM and DEM.
- e) **Macro-elements models**: This technique is used for regular buildings; masonry panels are not explicitly modelled in their components but they are considered as an homogeneous material. This can be useful to be employed in large models in order to decrease the computational time without a loss in terms of accuracy.
- f) **Equivalent frame modelling**: This method was first proposed by prof. Dolce and it is based on the assumption that it is possible to conceptually schematize a masonry panel using a frame structure composed of piers, spandrels, and the rigid nodes; the columns are not uniformly rigid, but a section called “effective length” (which depends on the inter-story height) is assumed to be flexible, while near the nodes a rigid zone is assumed. Evidently, the employment of this methodology has become increasingly significant in the past due to the savings in terms of computational time, however, this is often accompanied by a compromise in accuracy.

3. Numerical modelling of aggregate buildings in Opensees using STKO

3.1 Introduction to OpenSees

OpenSees is an open-source object-oriented software framework, developed under the sponsor of the *Pacific Earthquake Engineering Research Center*, and used to create finite element applications for earthquake engineering simulations, covering both structural and geotechnical engineering.

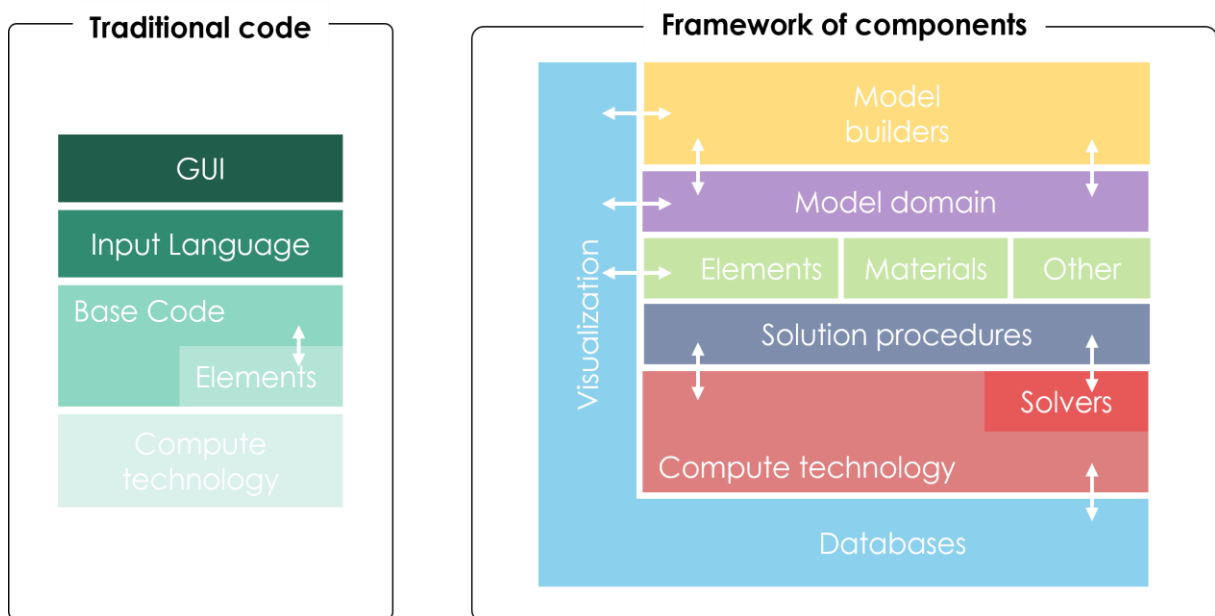


Figure 16: Comparison between the structure behind a traditional code and the one of the OpenSees framework

The software is predominantly written in C++ and Fortran, but to use its features, the user must also write some files in the Tcl (Tool Command Language) programming language. Through this process, the user can create geometry and sections, assign loads, and define the type of analysis. These components are then integrated into the "main" file, thereby generating the complete model.

The complete list of Tcl files that are required to create a model in OpenSEES is:

- a) analysis_steps
- b) definitions
- c) elements

- d) materials
- e) nodes
- f) sections
- g) main

3.1.1 OpenSees Objects

The OpenSees framework (object-oriented) is comprised of a set of modules to perform the creation of the finite element model (Figure 17), each of them associated with a C++ procedure linked to FORTRAN libraries for solving linear systems of equations [7].

An OpenSees' finite element model is composed of 4 main objects:

- **ModelBuilder**: Constructs the objects in the model and adds them to the domain.
- **Analysis**: Moves the model from state at time t_i to state at time and $(t_i + dt)$.
- **Recorder**: Monitors user-defined parameters in the model during the analysis.
- **Domain**: Holds the state of the model at each time and stores the objects created by the ModelBuilder, the Analysis and the Recorder.

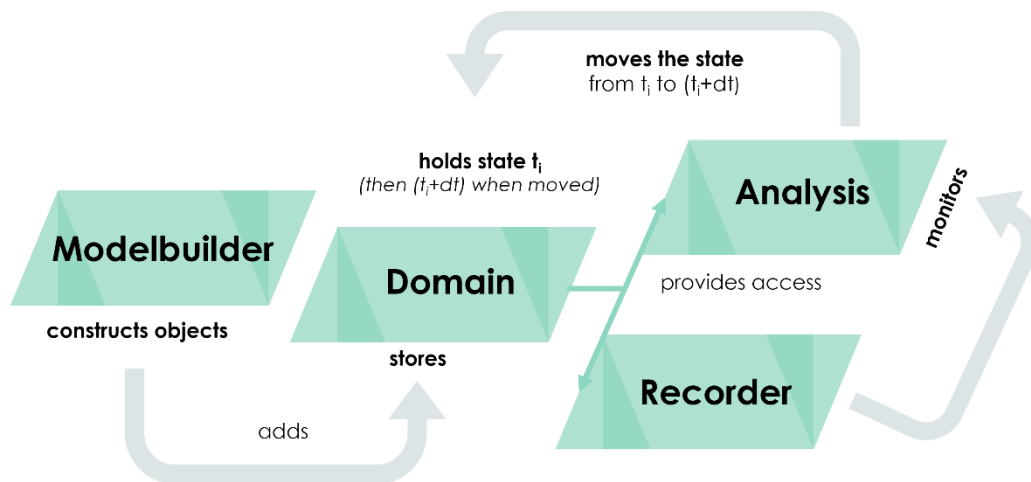


Figure 17: OpenSees objects

3.1.2 ModelBuilder

A finite element model (FEM) consists of Nodes, Elements, Constraints and Loads (McKenna, 1997). The ModelBuilder allows to build these objects and add them to the domain (Figure 16) and define the spatial dimension of the subsequent nodes to be added on the number of degrees-of-freedom (DOFs) at each node [7]. In total there are 5 classes (type of commands) to define the model (Figure 17).

3.1.3 Domain

The Domain object is responsible for storing the objects created by the ModelBuilder object and for providing the Analysis and Recorder objects access to these objects [7]

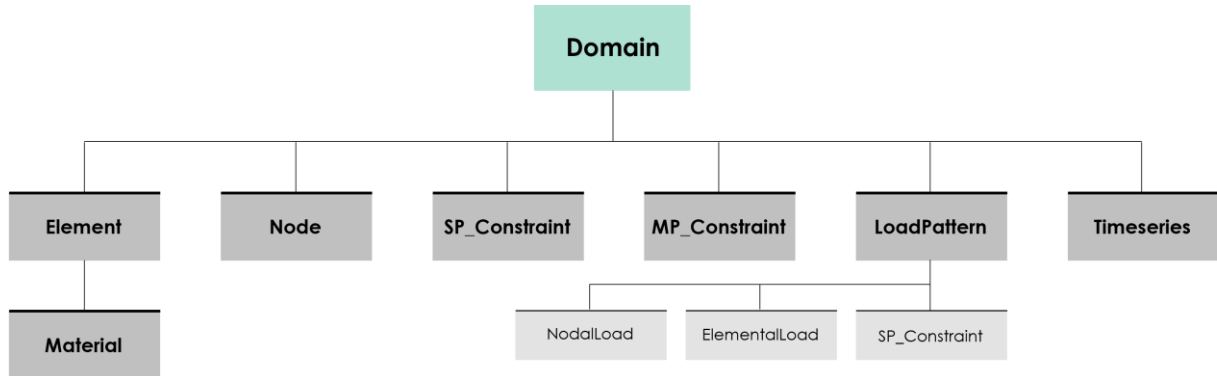


Figure 18: OpenSees model

3.1.4 Analysis

The Analysis objects are responsible for performing the analysis; this object moves the model along from state at time t to state at time $t + dt$. This may vary from a simple static linear analysis, an eigenvalue analysis or a transient non-linear analysis. In OpenSees, each analysis object is comprised of multiple objects which delineate the nature of the analysis and the manner in which it is to be executed.

The finite-element method discretizes the governing partial differential equations of equilibrium, kinematics, and constitution for a structural problem into a system of nonlinear ordinary differential equations (ODEs) [8].

The typical approach that has been taken to the Analysis class is the black box approach of traditional finite element programming [9], so a number of subclasses of Analysis are provided but the analyst has no control over the classes used to create these objects [9].

There are six different classes required to define an analysis object (Figure 19) [7]:

- **Constrain Handler:** The ConstraintHandler object determines how the constraint equations are enforced in the analysis. Constraint equations enforce a specified value for a DOF, or a relationship between DOFs.
- **DOF Numberer:** The DOF_Numberer object determines the mapping between equation numbers and degrees-of-freedom, so it conveys the way in which the degrees of freedom are numbered.

- **SystemOfEqn & Solver:** it specifies how to store and solve the system of equations in the analysis.
- **Convergence Test:** detects when convergence has been achieved on the system of equations at each time step.
- **Solution Algorithm:** determines the sequence of steps taken to solve the nonlinear equation at the current time step.
- **Integrator:** The Integrator object is used to determine the predictive step for time $t + dt$, to specify the tangent matrix and residual vector at any iteration and to determine the corrective step based on the displacement increment dU .

As summarised in Figure 19, all these objects can then be defined using different algorithms, accordingly to the dimension and the typology of the model and analysis to be performed.

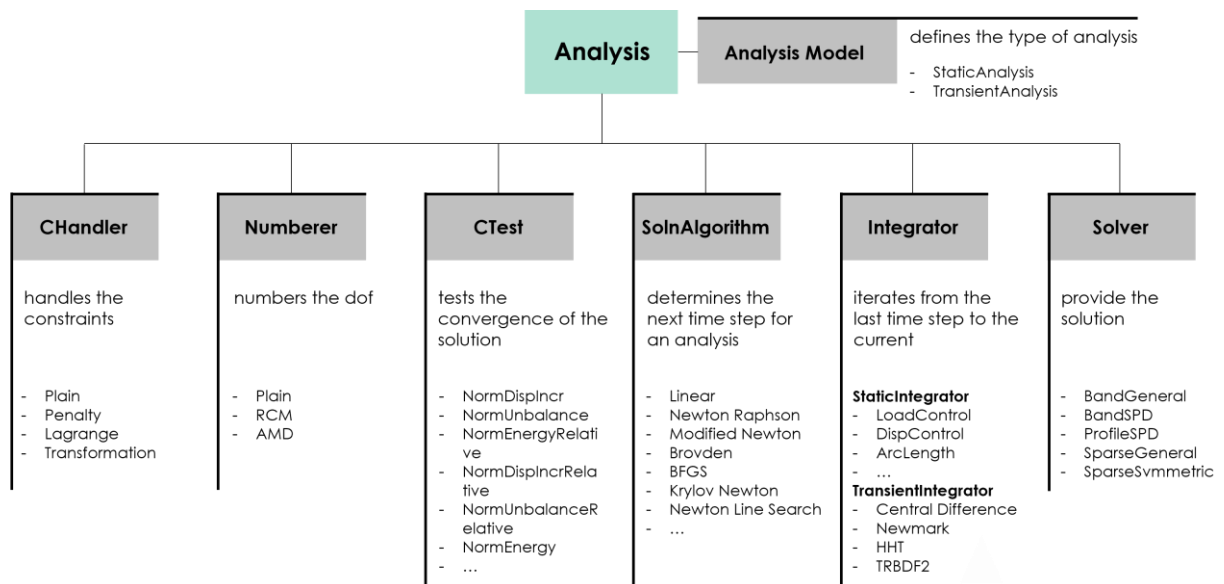


Figure 19: OpenSees Analysis object [7]

3.1.5 Recorder

The recorder object monitors user-defined parameters in the model during the analysis; this, for example, could be the displacement history at a node in a transient analysis, or the entire state of the model at each step of the solution procedure [7]. The pieces of information are then stored in a file (.plt file) for being plotted or manipulated in the post-processing phase.

3.2 STKO

OpenSees provides a robust framework, however, modelling complex structures using the Tcl programming language is a non-trivial process, since each node has to be manually defined. ASDEA software (an Italian software development company) has developed a software called STKO (Scientific Tool Kit for OpenSees), which simplifies the modelling stage and the analysis phase.

STKO is an advanced graphic user interface that integrates a CAD modeler and some graphic tools in the OpenSees framework; additionally, STKO provides new materials and elements, improving the computation capabilities of OpenSees and it also integrates the only pre and post-processor for OpenSees, offering the flexibility of working with Python instead of Tcl.

The modelling workflow of STKO is structured following the same order as the .tcl files that are needed to create the final model (Figure 20)

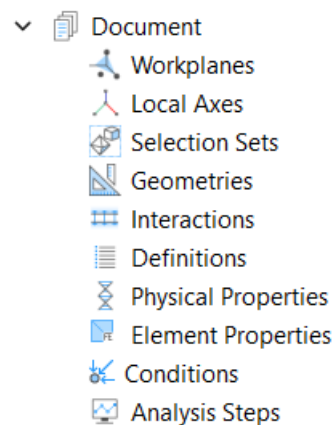


Figure 20: STKO work tree

3.2.1 Definition of the geometry

In STKO, nodes, faces, and volumes can be intuitively generated in a CAD environment, recalling the same commands used in any CAD software, using a global reference system; each category has a precise meaning: nodes represent discrete points in space, while faces define two-dimensional surfaces and volumes model three-dimensional regions.

Each geometry category is considered on its own as a distinct entity, but it is possible to connect different geometries through merging or interactions:

- The **"merge" command** allows the user to combine multiple structural entities into a unified one.

- **Interactions** are tools used to connect nodes of different geometrical entities, specifying the type and degree of connection, associating specific conditions. When creating an interaction, it is necessary to define master and slave nodes, this implies that the behaviour of the slave nodes directly depends on that of the master nodes and on the nature of the connection between them.

Furthermore, it is possible to divide the model into different selection sets, selecting groups of components and assigning them a name; this subdivision is merely used for the purpose of better user management of different entities, without interfering with how the elements are analysed by OpenSees (but this is particularly useful for the phase of creation of the monitors for the post-processing analysis of the results and when there are some issues related to the creation of the model itself).

3.2.2 Physical and element properties

Once the geometry of the model has been defined, it is necessary to associate the geometry with its element and physical properties.

The element property defines the computational behaviour of the component (for instance, in this phase, the software states that a particular element should be interpreted as a shell or as a *ForceBeamColumn* element or a truss element).

On the other hand, physical properties govern the constitutive behaviour of the material assigned to each structural element, describing how it responds to the applied stress (in this phase both the material and the section of the elements are assigned). It is possible to use both a library of sets of pre-inserted properties and materials and also to customize them directly in the software.

A common error is to directly assign a material to elements (on the contrary, it is necessary to first define the section and then assign the material). Another typical mistake is to not respect the coherence between the material used and the type of element.

3.2.3 Conditions

In this step, the association between boundary constraints, loads, masses and the entities previously defined is established.

To further explain the meaning of each condition: “Boundary conditions” define how the structure is constrained, so the type of constraint and the nodal degrees of freedom (DOFs) that are limited in the analysis are defined. “Loading conditions” contains the definition of all the

external forces, displacements, or other effects (like prestressing or temperature variations) that act on the structure; since OpenSees makes a distinction between masses and self-weight of elements, it is necessary to compute both of them and to ensure their correct assignment. In OpenSees, loads and masses are directly applied to nodes, but one of the useful features introduced by STKO is the straightforward application of forces or masses on edges or faces, which are then automatically lumped among nodes by the software.

3.2.4 Analysis Steps

In the "analysis steps" section, the software is guided on how to set up the entire analysis process. The user is required to respect a sequence of inputs:

- **Recorder:** the parameters and the frequency with which the software will store them during the analysis are specified.
- **constraintPattern:** the list of constraints that should be included into the model is introduced here.
- **loadPattern:** the set of loads and masses that should be taken into account by the model is introduced here.
- **Monitors:** through this command it is possible to evaluate the evolution of specific parameters (such as time, nodal displacements, reaction forces, ...) during the progression of the numerical simulation and to save them in a specific .plt output file.
- **AnalysesCommand:** The type of analysis (static or transient), the DOF numberer, the system solver and the solution algorithm are chosen in this stage.

3.3 Python as a tool to automate OpenSees

Since the final aim of this thesis is to perform some incremental dynamic analyses of different masonry structures, the same model is processed by applying different accelerograms every time scaled by a different intensity measure; Python can be integrated into the workflow to optimize the time needed for creating and running the models.

Once the model is built using the CAD modeller in STKO and after having inserted the conditions, the physical and element properties, it is possible to write the .tcl files that stand behind the model directly using STKO (in this way a model called “original model” is created in its folder -). After that, Python scripts were used to modify the Tcl files named definitions.tcl and analysis_steps.tcl.

The full structure of Python scripts that are required to create the model is the following:

1. **cut_records(file_txt).py**: this script takes as input a file .txt which contains all the data concerning an accelerogram related to a particular ground motion and, after having applied an energetic equivalence through the Arias Intensity, the script cuts the data to the right length, reducing the computational time required to perform the analyses.
2. **update_definitions_tcl.py**: this script takes as input the definitions.tcl file and updates the list of values named “timeSeries_list_of_values_3” with the data taken from the accelerogram:

```
set timeSeries_list_of_values_3 {11.36808 6.0314 0.0929 -2.18678 -0.64389 0.62252}
```

and then to correctly scale the accelerogram, the script also modifies the scaling factor updating the value `-factor 0.6` in the following line:

```
timeSeries Path 3 -dt 0.005 -values $timeSeries_list_of_values_3 -factor 0.6
```

3. **update_analysis_steps_tcl**: this script takes as input the analysis_steps.tcl file and updates the total duration of the dynamic analysis and the number of increments:

```
# duration and initial time step
set total_duration 1.0
set initial_num_incr 10
```

4. **create_directories_events.py**: this script takes as input the names of all the earthquakes and all the intensity measures that are going to be considered in the project and creates the directories (one for each event and inside this main folder one directory for each intensity measure) in a main folder called “Set_aggregato_output”.
5. **script_launch_seq_write_status.py**: this script runs all the directories of the same project scaled for the different intensity measure’s values.

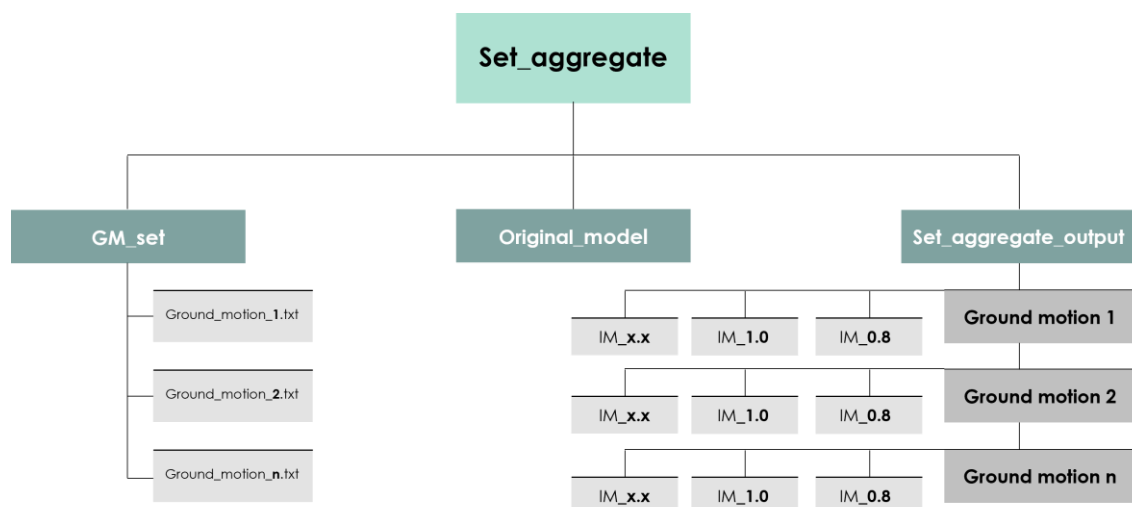


Figure 21: Example of the articulation of folders for the creation of a set of models.

3.4 Numerical modelling approach

In the paragraph that follows, details about the modelling choices behind the creation of the models of the two case studies are going to be enucleated, particularly focusing on the modelling of the masonry, of the slab and of the connection between the units (used for the modelling of the elementary aggregate building).

3.4.1 Masonry structure modelling approach

Layered shell

The layered shell command in STKO is used for the purpose of creating the section of a multilayer shell element; this specific section has been developed to emulate the behaviour of composite structures, consequently, the user can define the total number of the separated layers, their thicknesses, and the types of materials associated with each layer.

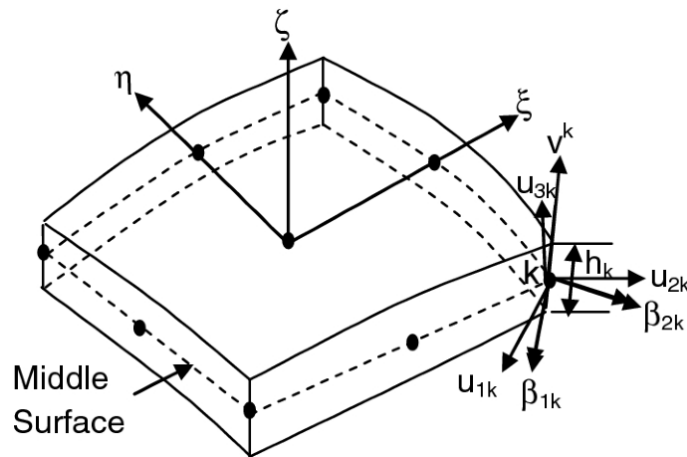


Figure 22: Layered Shell section [29]

From a numerical point of view, the axial deformation and curvature of the intermediate layer of the shell are primarily evaluated and, subsequently, the deformation of the other layers is computed considering the hypothesis of section planarity. The stresses are evaluated at each integration point using the constitutive law (specific for each layer) and the internal actions are derived using numerical integration.

ASDShellQ4

ASDShellQ4 element is a 4-node general-purpose thick shell element designed to integrate membrane behaviour, bending behaviour, and out-of-plane shear behaviour [10]. The macro-element's capability to support three-dimensional constitutive models enables it to capture both

in-plane and out-of-plane failure modes. Additionally, its advanced numerical membrane behaviour ensures insensitivity to geometric distortions, so it can be used to model both flat and warped geometries; it uses a full 2x2 Gauss quadrature, so it has a total of 4 integration points [10].

This element was selected to model both masonry walls and mortar interfaces of the first case study, offering an accurate description of complex behaviours like non-linear stress-strain relationships, cracking, and collapse mechanisms.

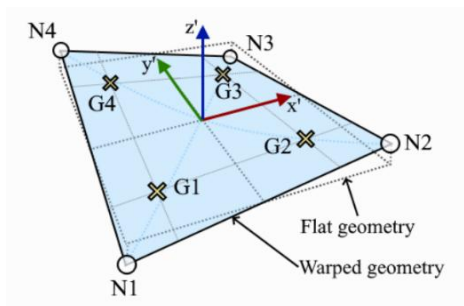


Figure 23: Nodes, Gauss points, local coordinate system, warped and flat geometry [10]

ASDShellT3

The ASDShellT3 element is a 3-node general-purpose thick shell element in which the membrane behaviour is based on the corner rotational DOFs (using the ANDeS formulation), and the plate bending is treated using the MITC3 formulation for thick plate elements;

ASDShellT3 uses 3 integration points to have a full rank for the ANDeS formulation and the MITC3 formulation. However, for computational efficiency, the user can optionally choose a single-point integration scheme. [10]

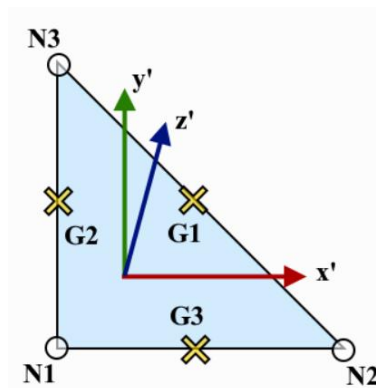


Figure 24: Nodes, Gauss points and local coordinate system for ASDShellT3 [10]

The advantage of using this three-node element stands in the fact that the mesh can better adapt to irregular and more complicated geometries such as the ones of the second case study, without the need for subdividing the geometry into regular parts using additional lines that would make the model more complex to be managed.

ASDConcrete3D

The ASDConcrete3D constitutive model was employed for the physical property of the homogenized masonry walls. This material object is a plastic-damage model for concrete materials and it is based on continuum-damage theory (the stress tensor can be obtained from the total strain tensor, without internal iterations at the constitutive level) making it fast and robust, suitable for the simulation of large-scale structures. Plasticity is added in a simplified way, in order to have the overall effect of inelastic deformation, but keeping the simplicity of continuum-damage models.

To improve the robustness and convergence of the simulation in case of strain-softening, this model optionally allows to use the IMPL-EX integration scheme (a mixed IMPLicit EXplicit integration scheme) [10] and autoregularization algorithms.

The constitutive model uses two damages indexes d^+ and d^- , tensile and compressive damage indexes, respectively, affecting the positive σ^+ and negative σ^- components of the effective stress σ . These damage indexes are scalar variables ranging from 0 (intact material) to 1 (completely damaged material). [11]

The aim is to update the stress tensor $\tilde{\sigma}$ for the step n when a new deformation is added, assuming to know the stress and the deformation at the step $n - 1$.

At the beginning a trial stress tensor is defined, assuming the material is working in the elastic regime:

$$\tilde{\sigma} = \bar{\sigma}_n + C_0 : (\varepsilon - \varepsilon_n)$$

With:

- $\bar{\sigma}_n$ previous effective stress
- $C_0 : (\varepsilon - \varepsilon_n)$ trial elastic stress increment

Then the stress tensor is split into its positive and negative components $\tilde{\sigma}^+, \tilde{\sigma}^-$.

From the trial effective stress tensor two equivalent scalar stress values are defined using the damage surfaces: $\tau^+ \tau^-$ related to tensile and to compressive behaviour respectively.

$$\tilde{\tau}^+ = f(\tilde{\sigma}) = H(\tilde{\sigma}_{max}) \left[\frac{1}{1-\alpha} \left(\alpha \tilde{I}_1 + \sqrt{3\tilde{J}_2} + \beta \langle \tilde{\sigma}_{max} \rangle \right) \frac{1}{\Phi} \right]$$

$$\tilde{\tau}^- = f(\tilde{\sigma}^-) = \left[\frac{1}{1-\alpha} \left(\alpha \tilde{I}_1 + \sqrt{3\tilde{J}_2} + \gamma \langle -\tilde{\sigma}_{max} \rangle \right) \right]$$

With:

- \tilde{I}_1 is the first invariant of $\tilde{\sigma}$
- \tilde{J}_2 is the second invariant of the deviator of $\tilde{\sigma}$
- $\tilde{\sigma}_{max}$ is the maximum principal stress
- $\alpha = \frac{4}{33}, \beta = \frac{23}{3}, \gamma = 3 \frac{(1-K_c)}{(2K_c-1)}, \Phi = 10$

By considering the equivalent plastic strain from the previous step ($x_{pl,n}$), the equivalent stress measures τ^+ and τ^- can be converted into their trial total-strain counterparts:

$$\tilde{x}^\pm = \frac{\tilde{\tau}^\pm}{E} + x_{pl,n}$$

The strain so obtained should be updated to impose the damage irreversibility and to account for rate-dependency:

$$\tilde{x}^\pm = \begin{cases} \frac{\eta}{\eta + \Delta t} x_n^\pm + \frac{\Delta t}{(\eta + \Delta t)} \tilde{x}^\pm, & \text{if } \tilde{x}^\pm \geq x_n^\pm \\ x_n^\pm, & \text{otherwise} \end{cases}$$

The plastic damage and cracking variables (d_{pl} and d_{cr}) are derived from the hardening softening law and the effective stress tensors are obtained as:

$$\bar{\sigma}^+ = (1 - d_{pl}^+) \tilde{\sigma}^+$$

$$\bar{\sigma}^- = (1 - d_{pl}^-) \tilde{\sigma}^-$$

$$\bar{\sigma} = \bar{\sigma}^+ + \bar{\sigma}^-$$

Hence, the nominal stress tensors are:

$$\sigma = (1 - d_{cr}^+) \bar{\sigma}^+ + (1 - d_{cr}^-) \bar{\sigma}^-$$

This procedure is schematized in Figure 25 where, at first, the elastic predictor is evaluated and then it is corrected to consider plasticity and damage in the uniaxial scenario.

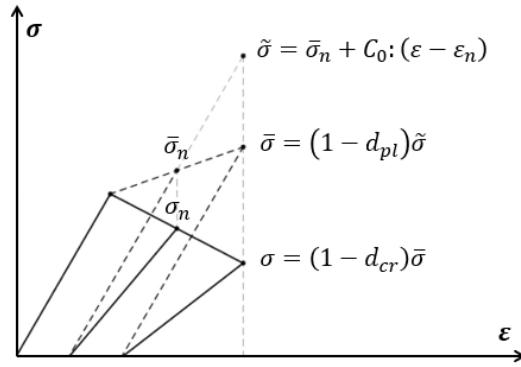


Figure 25: A schematic representation of the elastic predictor followed by the plastic and damage correctors in a representative uniaxial case. [10]

It is possible to directly customize the material parameters using STKO, choosing to control between 1 and 9 parameters. Additionally, the user can further define the stress-strain relationship by placing custom vectors.

For both the case studies, the 6 parameters (6P) version was used.

DamageTC3D

DamageTC3D was used for mortar layer interfaces between units of the first case study and is the predecessor of the ASDConcrete3D. As ASDConcrete3D it enables autoregularization features, but on the contrary it is not capable to withstand multiple failure mechanism; this implies that when a component fails in tension, the resistance is then reduced in all directions, resulting in null compression resistance as well. This mechanism emulates what happens in reality when mortar reaches its failure point and the material exhibits a complete or a partial disintegration, consequently its resistance is drastically reduced for all the directions.

IMPL-EX algorithm

Explicit integration schemes are in many cases conditionally stable (so they often have a limitation of the time step length) but the problem results to be linear or quasi-linear; on the other hand, implicit integration schemes are generally unconditionally stable, but they are highly non-linear. Consequently, explicit integration schemes are robust but expensive solving algorithms, whereas implicit integration schemes are accurate but less robust [12].

The IMPL-EX algorithm can overcome the drawbacks of both integration schemes. As its name would suggest, it is a combination of the standard implicit integration scheme of the stresses and explicit extrapolation of the involved internal variables.

In a first stage the explicit evaluation of the stresses, $\tilde{\sigma}_{n+1}$, and the stress-like variable \tilde{q}_{n+1} is done; in a second stage the standard implicit integration of the constitutive model is performed and the implicitly integrated stresses, σ_{n+1} , are obtained.

One key aspect of this algorithm is the dependence of the extrapolation error to the length of the time step, Δt . Therefore, to limit the error it is the necessity to control this length.

Autoregularization tool

In discrete problems, to achieve invariance of the response with respect to the discretization size, the softening law must be modified according to the size of the damaging zone (l_{dis}) [11]; so what the autoregularization tool does is to facilitate a mesh-size independent response.

This tool is important because real structures have imperfections (due to material heterogeneity) which can be conceptualized as points in which stress accumulates, and damage starts to propagate. For instance, considering two elements e_1 , e_2 , which both have the same geometries and materials and in which the stress is equally increased, due to the presence of larger imperfections in one of them, one element should show damages before than the other; But, since the imperfections are not considered, the numerical model cannot determine which element will fail and stress localization never occurs. Additionally, as it is displayed in Figure 26, if element e_1 enters in the softening field, element e_2 will unload to maintain equilibrium, reaching the same stress value as e_1 . As a consequence, the fracture energy related to e_2 (orange area) will be much lower than the one related to e_1 (brown area).

To further explain this topic, for brittle materials (which have a low tensile resistance), the tensile fracture energy is one of the most important parameters because it is able to characterize their behaviour in the cracked stage, considering the energy required to propagate a crack in a material due to tension (visually it is represented by the area under the softening curve).

The value of fracture energy depends on various factors such as the type and characteristics of the material, as well as the dimensions and geometry of the element.

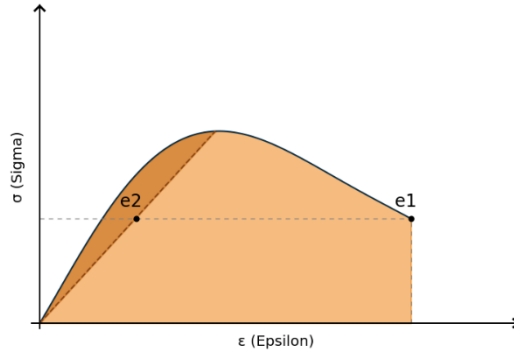


Figure 26: Energy dissipated by *e1* and *e2*.

In absence of experimental data, both fracture energies can be calculated using the following formulation as a function of the compressive strength.

According to the Model Code [13] the tensile fracture energy can be calculated as:

$$G_t = 0.073 f_{cm}^{0.18} \quad [N/mm]$$

Where f_{cm} is the compressive tensile strength of the masonry in MPa.

The calculation of the compressive fracture energy is instead carried out following the formulation of "Guidelines for Nonlinear Finite Element Analysis of concrete structures", which can be also used for masonry [14].

$$G_c = 250 G_t \quad [N/mm]$$

These formulas provide values that are useful to be used as a starting point to later define the constitutive model for the material, but it is important to remark the relevance of the calibration process in order to establish a connection between the experimental data and the model.

3.4.2 Modelling of the slab and of floor beams

Rigid diaphragm

The rigid diaphragm condition is modelled using a node-to-node or a node-to-element interaction which establish a relative relationship between DOFs of different nodes and applying to this interaction a *rigidDiaphragm* condition that ensures the nodes to move as if they were on a rigid plane with the constrained node, which is typically located at the floor's centre of gravity. This constraint imposes a zero axial strain condition on the connecting elements and allows the nodes to translate only along the x and y axes while rotating about the z axis.

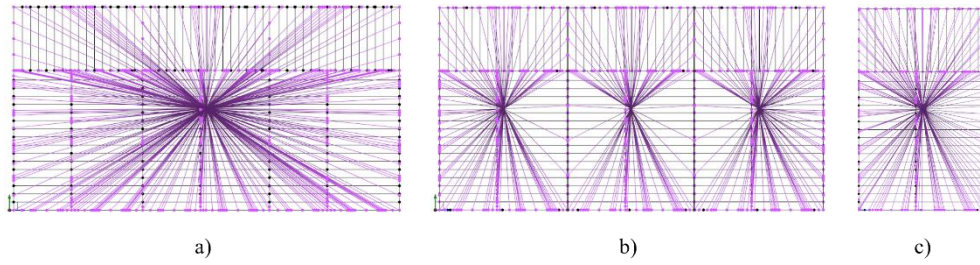


Figure 27: Rigid diaphragms of the three cases considered: a) fully connected, b) semi-connected, c) isolated model.

Fiber section

There are several methods that can be used to take into account for the plasticity in the model and that can be gathered into two main categories: lumped and distributed plasticity.

The concentrated plasticity approach assumes that the entire element is elastic, and the plastic deformation is localized only at specific points, achieved either considering plastic hinges or by incorporating nonlinear springs; the inelastic behaviour is defined assigning a specific Moment-Rotation relationship to these points. This is a simplified way of taking into account the non-linearities but it requires the predefinition of the position of the plastic hinges within the element. Conversely, the distributed plasticity approach facilitates the automatic identification of plastic deformation points; this is done decomposing the element's cross-section into fibres and assigning to each fibre a peculiar constitutive law that helps determine when sections reach their plastic limit (this is particularly useful to model sections that are not regular in geometry and/or in their composition, such as reinforced concrete sections - Figure 28).

Two primary types of fibre elements are used in modelling: displacement-based (DB) and force-based (FB) elements. DB elements are exclusively used for distributed plasticity analysis and are formulated based on displacement fields. Meanwhile, FB elements use force and moment fields, ensuring equilibrium through stiffness-based governing equations. For the model of the beams in OpenSees in both the case studies, a force-based approach was used by the means of the *ForceBeamColumn* property.

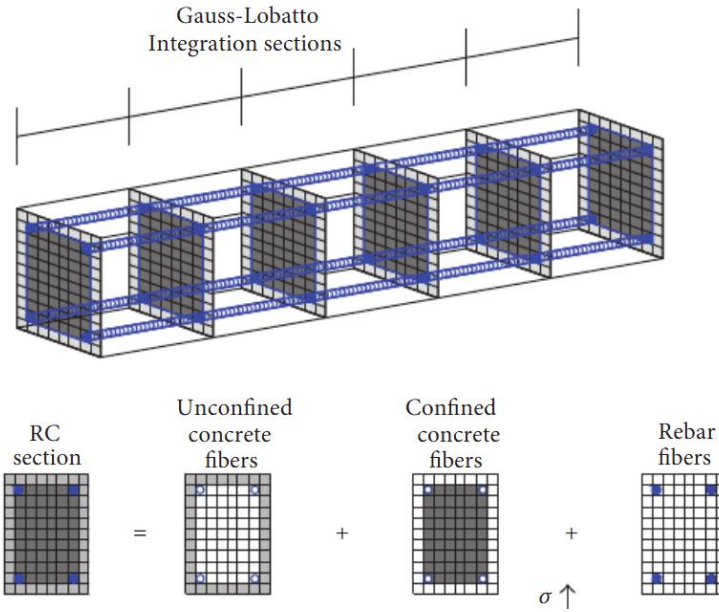


Figure 28: Example of fibre discretization of a beam-column element for a reinforced concrete cross-section

Connection beams-vertical walls

The connection between beam floors and vertical walls was modelled using two approaches: in the case of the elementary aggregate building, a node-to-element interaction was modelled, where the masonry faces act as master elements and the beam ends as slave nodes. This interaction is assigned the *ASDEmbeddedNodeElement* condition, which directly defines the degree of connection between the two components. The key aspect is that with the embedded condition, the penalty approach is used to enforce constraints without altering the system size; this is done adding large penalty parameters to the stiffness matrix.

While, in the Palazzo Ducale case the connection was modelled using node-to-node interactions and then assigning an *equalDOF* condition. By its means it is possible to associate the behaviour in terms of DOFs of the slave nodes with the ones of the master node.

3.4.3 Modelling of openings in masonry walls

In the early developments of the model of the first case study, it became clear that it was necessary to include lintels to accurately model the building. As a demonstration of that, in real masonry structures, it is common to find lintels as horizontal elements over the openings, having the structural role of resisting both to tension and bending forces caused by the weight of the bricks above. Lintels also facilitate the distribution of load from the wall above to the sides of

the opening, thereby contributing to the support of the structure and enhancing the strength of the spandrels.



Figure 29: Lintel geometry [26]

ASDConcrete3D was used even in this case to model the material properties of the lintel. A thin layer of mortar was introduced between the lintel and the wall, instead of merging the two elements together; this choice was done to prevent overestimating the resistance of the spandrel.

3.4.4 Modelling of connection between units of the URM aggregate

The first case study analysed comprises three cases: Fully-connected, Semi-connected and isolated model, exploring 3 different degrees of constraint between the units; in the semi-connected case, the junction between the units has been modelled by the introduction of a mortar layer between units, which emulates the connection through a cohesion-friction law. This law accounts for variations between compression and tensile actions while considering material degradation.

The mortar layer is modelled using shell elements, having the same thickness as the masonry walls it connects and using the *DamageTC3D* material model. As it will be explained in chapter 5, to optimize the computation time needed to perform the analysis, a global coarse mesh was used for the entire building, while for these interface layers a finer mesh was preferred in order to increase the accuracy (Figure 30).

The connection between the mortar layer and the masonry wall is implemented using an *EqualDOF* interaction, which constrains all internal degrees of freedom except for rotation around the axis perpendicular to the wall. In this setup, master nodes are assigned to edges with the larger mesh size, while slave nodes correspond to edges with the finer mesh.

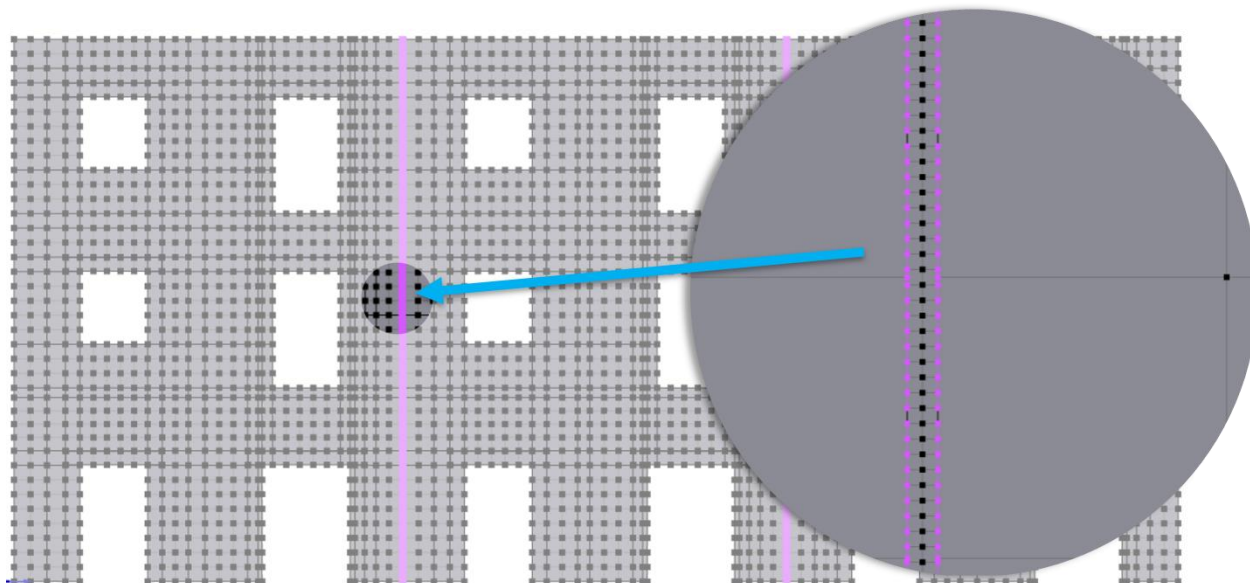


Figure 30: Details of the mesh refinement and of the EqualDOF connection between masonry and mortar.

4. Fragility curves of a masonry aggregate building

4.1 Introduction to fragility analyses

Fragility curves are a crucial tool for assessing seismic risk, as each building or structure can be characterized by its own fragility curve.

Fragility analysis aims to describe the conditional probability that the seismic demand of a structure exceeds its capacity at a given level of intensity measure (IM) for a given damage state [15].

According to [16], there are four primary methods for developing fragility curves: (1) Expert-based methods, (2) Empirical methods, (3) Analytical methods, and (4) Hybrid methods.

1. **Expert-based Method:** The expert-based method is the oldest and simplest of the four approaches. It relies on expert judgment, typically gathered through questionnaires and consultations with multiple specialists. However, the reliability of the results is heavily affected by the subjectivity of the method itself.
2. **Empirical Method:** This approach derives fragility curves from observed data from past earthquake events. Its primary advantage is that it reflects actual structural performance, providing a realistic representation of seismic fragility, but it requires a great knowledge of the behaviour of the structure during the previous decades, which often is not available.
3. **Analytical Method:** The analytical method is the most commonly used one, it is based on deriving the fragility curves on simulated data obtained from time-history analyses of structural models. This approach is favoured due to its reduced bias in comparison to alternative methods. Nevertheless, the accuracy of the results relies on the realism of the structural model and on the appropriate choice of the ground motions set.
4. **Hybrid Method:** The hybrid method enhances the accuracy of the analysis by employing both empirical and analytical approaches. However, it is the most complex method as it integrates experimental testing with computational analysis.

In the current thesis, the analytical methodology will be implemented.

Three analytical approaches, namely cloud analysis (Cornell et al. 2002), incremental dynamic analysis (IDA) (Vamvatsikos and Cornell 2002) and multiple strip analysis (MSA) (Singhal and Kiremidjian 1996), have been widely used for the development of probabilistic demand models (i.e., relationships between seismic demands and IMs) towards the derivation of fragility curves.

IDA and MSA are practically similar with a noted difference on scale-factors used for selecting ground motions. IDA uses one set of ground motion records scaled to different IM levels that are considered. By contrast, MSA adopts multiple sets of ground motion records for individual IM levels.

Our approach was a mixed one, because it started with the development of IDA curve to evaluate the record-to-record variability and then, for the evaluation of the probability, we preferred to use a visualization of the results similar to the one proposed in the case of the multi stripe analysis.

In the following paragraphs, both IDA and MSA will be introduced.

4.2 Incremental Dynamic Analysis

Incremental Dynamic Analysis was first developed in 1977 by Bertero; in the following years, many researchers, such as Luco and Cornell, contributed to further developing the concepts behind this method of analysis; recently, it has been adopted by the U.S. Federal Emergency Management Agency (FEMA) and established as the state-of-the-art approach to determine global collapse capacity.

In this paragraph, the IDA method will be explained according to the work done by Dimitrios Vamvatsikos and C. Allin Cornell in the paper: “Incremental Dynamic Analysis” [17].

The final aim of the IDA method, intended as a parametric method to estimate the performances of a structure with respect to one or more seismic actions, is to obtain a curve of response parametrized versus intensity level; in order to do that the ground motion record is scaled by a factor, applied to the structure and then the structural response is recorded.

The method is based on the following steps:

1. Consider a single acceleration time history, selected from a ground motion database (see the next paragraph for the criteria used in the selection of the ground motion data), which is called “unscaled accelerogram” a_1 ;

2. To account for more severe or milder ground motions, the amplitudes of the unscaled accelerogram are uniformly scaled up or down by a scalar $\lambda \in [0 + \infty)$ called scale factor (SF) or Intensity Measure (IM):

$$a_\lambda = \lambda \cdot a_1$$

The set of Intensity Measures should be chosen in such a way that the IMs can cover the whole range of behaviour of the structure (starting from the elastic one, going through the non-linear field up to the collapse of the structure).

3. Selection of a Damage Measure (DM) that is an observable quantity that is part of, or can be deduced from, the output of the corresponding nonlinear dynamic analysis.
4. The dynamic nonlinear analysis can be performed to obtain a record of the DMs of the structural model at each level IM of the scaled ground motion.
5. The values so obtained are then plotted versus the intensity level as continuous curves (that are the result of a process of interpolation).

4.2.1 General properties of IDA curves

The IDA curve is a non-monotonic function of the IM and it is peculiar to a very specific accelerogram and structural model, because when subjected to different ground motions a model will often produce quite dissimilar responses that are difficult to predict a priori; nevertheless it is possible to identify some general properties that are in common between IDA curves that belong to different studies, in particular we can find some common pattern such as:

- Elastic linear region at the beginning.
- Nonlinear region that follows the elastic branch.
- Flattening of the curve in a plateau in the correspondence of the maximum IM value where the DM tends to “infinity”.

Between the nonlinear region and the plateau we can have 2 different situations:

1. Softening case: the curve sharply “softens” after the initial buckling and accelerates towards large drifts and eventual collapse (Figure 31a).
2. Hardening case: as it can be seen in Figure 31, the curves (c) and (d) follow a twisting pattern made of consecutive segments of “softening” and “hardening, this means that sometimes the structure experiences acceleration of the rate of DM accumulation while other times a deceleration occurs that can be powerful enough to momentarily stop the DM accumulation or even reverse it.

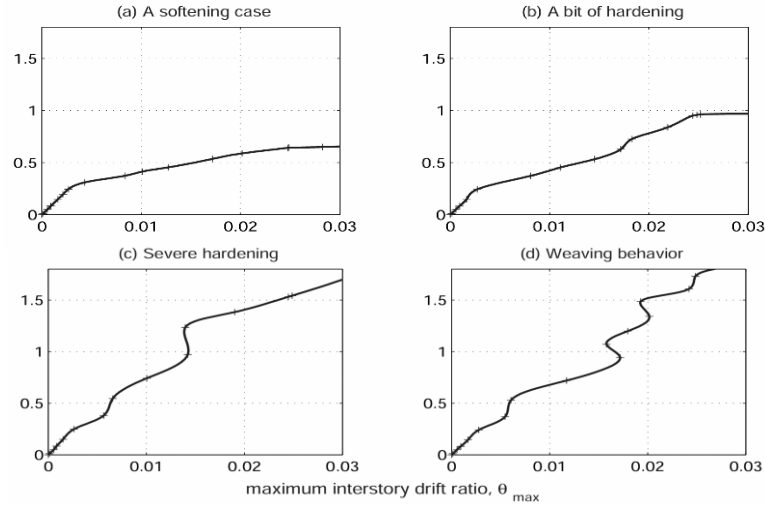


Figure 31: IDA curves of a $T_1 = 18$ sec, 5-storey steel braced frame subjected to 4 different records. [17]

Cornell also observed the phenomenon of the “structural resurrection” (Figure 32) which is an extreme case of hardening that occurs when a system is pushed all the way to global collapse at some IM (i.e., the analysis code cannot converge, producing “numerically infinite” DMs), only to reappear as non-collapsing at a higher intensity level, displaying high response but still standing.

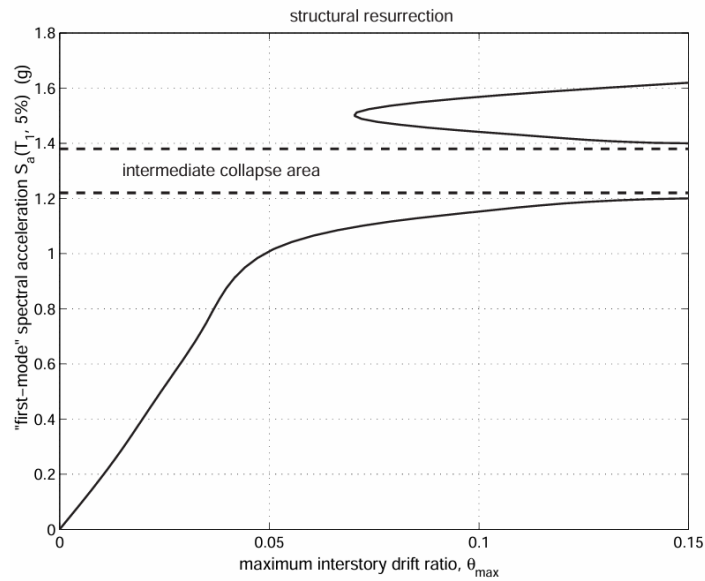


Figure 32: Structural resurrection on the IDA curve of a $T_1 = 13$ sec, 3-storey steel moment-resisting frame with fracturing connections [17]

4.2.2 Multi-record IDAs

A single-record IDA study cannot fully capture the behaviour a building may display in a future event. The IDA can be highly dependent on the record chosen, so a sufficient number of data set are required to cover the full range of responses. In this way it is possible to perform some statistical analysis of the results so obtained from the analyses and to extend the previous

findings, which can thus characterise the structure in a more general way. The approach used is the same as that described in a “single record IDA study” paragraph.

4.2.3 Spline interpolation of IDA curves: Centripetal method

Once we have obtained a set of discrete points from the analysis, the key thing now is to choose the most suitable technique to interpolate the given points to get a “smooth” curve.

According to what Cornell proposes in his paper “Applied Incremental Dynamic Analysis”, the best choice is to use the centripetal method, first introduced by E.T.Y. Lee in his paper “Choosing nodes in parametric curve interpolation” (computer-aided design).

To briefly explain Lee work, the basic concept behind the centripetal model is to find a spline that can go through all the elements of a given a random set of points and that is able to create a “fair shape”; in order to explain the idea behind this method he uses a parallelism between what the algorithm does and what happens in the real word when an object follows a path.

“Imagine someone driving on a curved highway. It becomes quite obvious that the driver does not try to maintain an approximately uniform speed. Anticipating a sharp turn in the road, the driver would significantly slow down, because the centripetal force necessary to keep the driver in a natural posture or to keep the car from skidding becomes too great if the speed is not reduced, ... In a way, 'fair' or 'pleasing' is identified with the comfort of the driver during the travel.”

Thus, let the curve be $P(t)$, the interpolating conditions are:

$$P(t) = P_i, 0 \leq i \leq n$$

where $t_0 < t_1 < \dots < t_n$ are certain chosen parameter values called the interpolating nodes and the parametric interval shall be normalized so that $t_0 = 0$, $t_n = 1$.

There can be different kinds of parametrization such as the uniform parametrization or the cumulative chord length parametrization, but the centripetal model is one of the most used because it is quite “stable”. In mathematical terms what the algorithm does is to compute the square root of the Euclidean distance of two consecutive points in the curve $|P_i - P_{i-1}|^{\frac{1}{2}}$ and this distance is then normalized with respect to the cumulative sum:

$$t_i - t_{i-1} = \frac{|P_i - P_{i-1}|^{\frac{1}{2}}}{\sum_{j=1}^n |P_j - P_{j-1}|^{\frac{1}{2}}} \quad \text{for } 1 \leq i \leq n$$

It should be mentioned that when the data points are unevenly spaced, the centripetal method gives much better results than the uniform parametrization and the chord length method, because the final curve is smooth, and it is quite similar to the curve that a person would draw if he was asked to join “naturally” all the points.

In Figure 33, is shown the interpolation of the points which belong to a “raw” IDA curve (black line) using the centripetal method (red line)

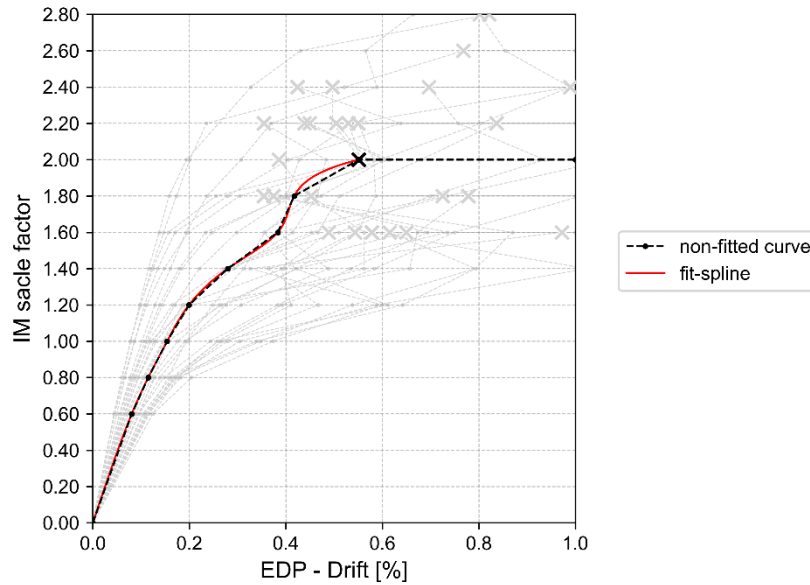


Figure 33: Non-fitted IDA curve vs fitted IDA curve using the centripetal model

4.3 Multi-stripe analysis

Multi stripe analysis was first introduced by Ajay Singhal and Anne S. Kiremidjian in their paper “*Method for probabilistic evaluation of seismic structural damage*” (1996), in which they have developed a systematic approach for estimating fragility curves and damage probability matrices for different structural systems, based on nonlinear dynamic analysis of the structure rather than on heuristics or on empirical data [18].

The results of MSA approach are quite similar to IDA ones, however, there is a slight difference in the methodology used: with IDAs, the workflow is to select one set of ground motions and scale them for different IMs; conversely, the approach adopted with MSA is diametrically opposed, a set of IMs is chosen and different sets of ground motions are scaled for each IM. As a consequence, the points in the IDA analyses can be interpolated to create a curve (Figure 34.a), while, the visual representation of MSA analyses is much clearer due to the distinct division between the n-points that are collapsing and the N-points that are in the “safe zone” (Figure 34.b).

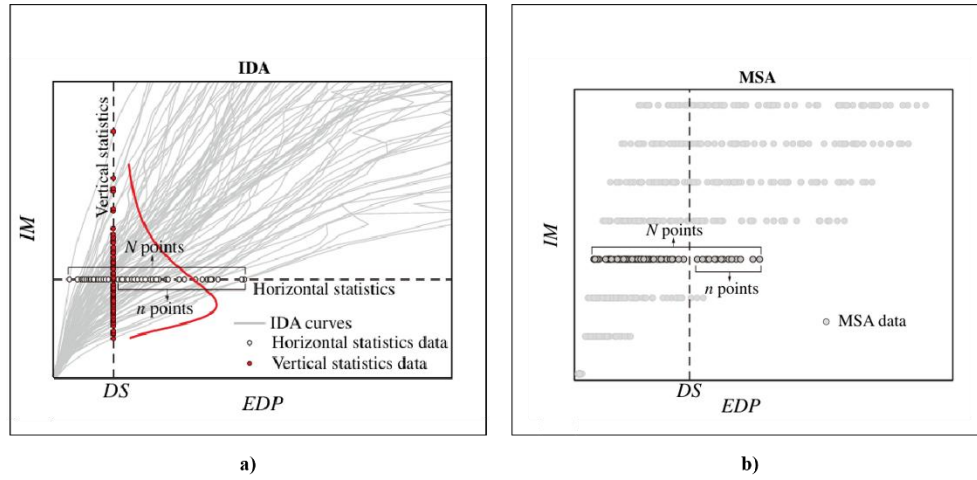


Figure 34: Example of IDA curves and MSA data [15]

4.4 Performance-based earthquake engineering assessment framework

In the past, in order to state whether a structure was safe or not, it was preferable to use sets of prescriptive provisions that were a direct consequence of the most commonly used performance indicators in structural engineering (such as drifts, accelerations, and strains). Today, as a direct consequence of the needs of stakeholders and policy makers, this approach has evolved to take into consideration parameters that can be easily understood by everyone, such as downtime or repair costs.

The approach herein presented, considers the seismic hazard, structural response, damage, and repair costs associated with restoring the building to its original condition using a fully consistent probabilistic analysis [19].

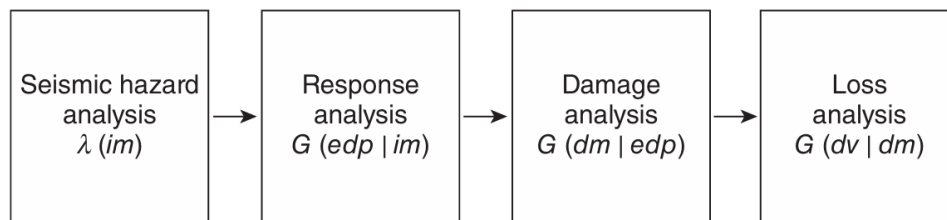


Figure 35: Performance-based earthquake engineering framework (Yang et al. 2009) [19]

The PBEE framework proposed by the Pacific Earthquake Engineering Research (PEER) Center (Moehle and Deierlein 2004, Goulet et al. 2007, Solberg et al. 2008, Yang et al. 2009, ATC-58 2010, Bradley and Lee 2010) can be explained by the following equation:

$$\lambda(DV > dv) = \int_{im} \int_{dm} \int_{edp} G(dv|dm) dG(dm|edp) dG(edp|im) d\lambda(im)$$

Where:

$G(dv|dm)$, $G(dm|edp)$, $G(edp|im)$ are the conditional probabilities of the performance measures DV, DM, and EDP given an intensity measure $IM = im$

As it is shown in Figure 35, in the framework proposed by PEER, the performance assessment is divided into four analysis steps:

- a) **Seismic hazard analysis:** The output of this first term is a seismic hazard curve, $\lambda(IM)$, which quantifies the annual rate at which a given value of the seismic intensity measure (IM) will be exceeded.
- b) **Response analysis:** $P(EDP > edp)$ The output of response analysis are statistical functions that relate engineering demand parameters (the response of structural and non-structural components, such as drifts or stresses) to the hazard experienced by the structure. Precisely the aim is to use conditional probability functions $G(edp|im)$ to represent the statistical relationship between EDP and IM.
- c) **Damage analysis:** $P(DM > dm)$ The damage states that structural and non-structural components experience after an earthquake can be characterized in terms of fragility curves; this phase aims to obtain a quantitative description of the damage state (DM) when the EDP has reached a certain threshold value by the means of the function $G(dm|edp)$.
- d) **Loss analysis:** $P(DV > dv)$ this final step translates the results of the damage analysis (DM) to decision variables (DV) that can be used by stakeholders to make risk management decisions; this is made explicit in the term $G(dv|dm)$.

Lastly, performance levels or limit-states are important ingredients of Performance Based Earthquake Engineering (PBEE), and the IDA curve contains the necessary information to assess them. However, some remarks related to this formulation of PBEE should be addressed:

- We need to identify a “rule” that when it is reached it can detect the presence of a limit state that has been exceeded. For monotonic IMs, such a rule is generated by a statement of the form: “If $IM > C_{IM}$ then the limit-state is exceeded” [17]. In the present thesis, to solve this issue, we have assumed that after the first collapse the limit state is always reached, neglecting the phenomenon of structural resurrection.

- The conditional probability is assumed to be the same for successive earthquake events. This implies the structure is non-deteriorating or is restored to its original condition immediately after any structural damage due to an earthquake [19].

It's important to clarify that the aim of this thesis is not to implement the whole PBEE framework, since the work that follows does not comprehend the hazard and the loss analyses.

4.4.1 Engineering characterization of ground motions: Arias intensity, energetic criteria for ground motion truncation

In general, ground-motion severity can be considered as a function of amplitude, frequency content, and duration [20]. All these three aspects are chosen because they can be intuitively associated to their direct effects on the structure itself. Concerning the amplitude, the larger is the amplitude, the higher are the damages that the ground motion will cause to the structure; conversely, the frequency content is also important, because it is referred to the resonance phenomenon and, finally, the duration is relevant in dynamic non-linear analyses, because it is related to damage accumulation.

However, given a complete record of an accelerogram, the definition of its significant part is not a straightforward process, many duration measures can be treated, but for the purposes of this thesis, the Arias Intensity will be discussed as a mean to reduce also the computational time needed to perform the analyses.

To better define what Arias Intensity (I_A) is, it is a cumulative ground-motion intensity measure (IM) that simultaneously captures multiple characteristics of a ground motion record such as amplitude, frequency content, and duration. It is a useful indicator of damage potential for a range of civil engineering structures. [21]

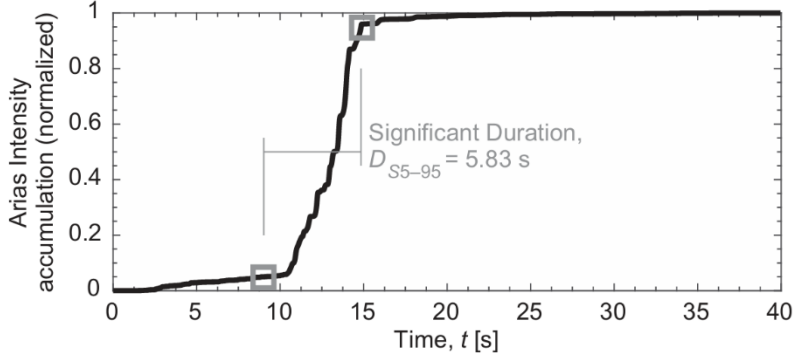


Figure 36: Illustration of significant duration for the Treasure Island ground motion during the 1989, based on 5% and 95% thresholds [20]

Mathematically, it is computed evaluating the time integral of the squared acceleration, as given by Eq:

$$AI = \frac{\pi}{2g} \int_0^{t_{max}} [a(t)]^2 dt$$

Using the Arias intensity, it is possible to provide an alternative definition of duration by considering the time in which a given percentage of the total energy imparted by the ground motion time series occurs. It can be demonstrated that the energy contained in the ground-motion time series is proportional to the cumulative squared acceleration, and we can consider a time t_X at which X% of the total squared acceleration has accumulated:

$$\frac{\int_0^{t_X} [a(t)]^2 dt}{\int_0^{\infty} [a(t)]^2 dt} = \frac{X}{100}$$

Hence, the significant duration (DS) can be defined as:

$$D_{SX-Y} = t_Y - t_X$$

That is the time difference between the accumulation of two different percentages of the cumulative squared acceleration, X% and Y% (where $Y > X$)

The values of X and Y are empirical, but there is a physical basis about their choice that is related to the arrival time of P and S-waves. It is almost universally considered to be 5%, and the two most common values of Y are 75% and 95%. These two metrics are subsequently referred to as the 5–75% significant duration, DS5–75, and the 5–95% significant duration, DS5–95, respectively [20].

4.4.2 Selection of the DM and post-processing of the results

In this paragraph, two important concerns should be correctly pointed out: the selection of a suitable Damage Measure and the postprocess of the results.

Equally important to the analysis is the postprocessing of the resulting data and perhaps the most important issue is selecting a suitable IM and DM [17]. About the selection of a suitable damage measure, there are many parameters that can be monitored during the analysis (peak floor accelerations, velocities, out of plane drifts, in plane drifts, ...) but, according to what Vamvatsikos and Cornell proposed in their paper “Applied Incremental Dynamic Analysis”, our choice was to monitor the in-plane drift ratio θ_{max} (the maximum over time and over all stories of the interstory drift ratios recorded during the time history analysis [17]) because it can be related to several limit states and to global dynamic instability.

The second key aspect that must be addressed here is related to the necessity of an appropriate post-processing phase of the results of the analyses. After the completion of the simulations of all the increments and all the models, the software collects a large amount of “raw” data that should be carefully analysed and postprocessed. Our workflow is designed to terminate when the model encounters its first non-convergence, however, in such cases, there can be significant numerical errors. This phenomenon becomes evident by plotting the capacity curves related to the IMs that are not converging, Figure 37: Specifically the reaction force-displacement curve (Figure b) initially exhibit a smooth trend then, further advancing in the analysis, clear discontinuities and quick changes in its slope start to appear; the algorithm employed for this thesis is simple and it is based on monitoring three points of the curve each time, providing limitations for the slope variations and for the differences in terms of reaction force between two consecutive steps; additionally, a final check is used to neglect the cases in which the curve is relatively smooth, but one of its point is excessively distant with respect to the origin.

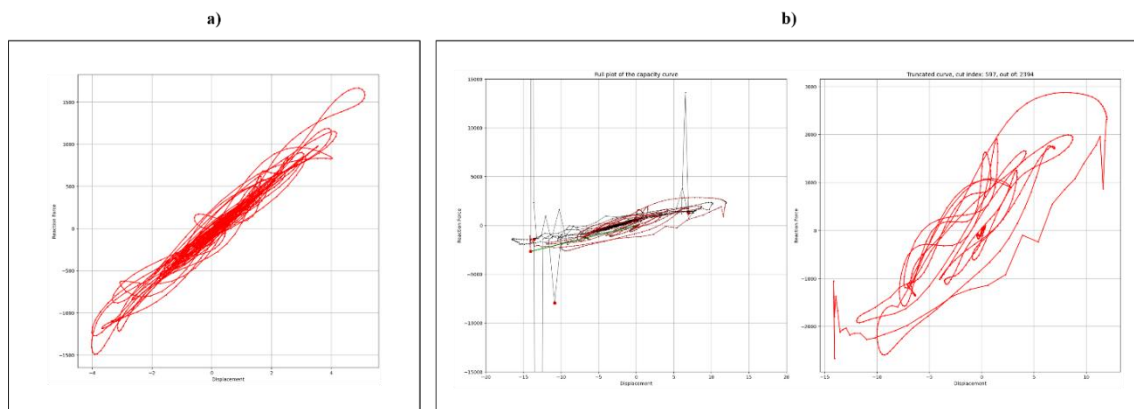


Figure 37: Capacity curves of the same accelerogram scaled for different factors: Figure a) smooth capacity curve, Figure b) discontinuities given by the non-convergence of the analysis.

4.5 Probability

The workflow, established using STKO and Python, is designed in such a way that each ground motion is scaled using scale factor and then the model is solved using OpenSees; this process terminates when the first non-convergence is reached. Consequently, two main typologies of analyses can be defined:

- Numerically convergent analyses.
- Numerically non-convergent analyses.

It is important to note that, since we are considering the Collapse Limit State, a key assumption that lies behind these analyses is to designate the analysis as “collapsed” both in instances where the inter-story drift threshold is exceeded (for numerically convergent analyses) and in the cases in which the convergence is not achieved.

4.5.1 Conditional probability

The conditional probability stands for the probability that an event E_1 has occur given the fact that an event E_2 has already occurred:

$$P(E_1|E_2) = \frac{P(E_1 \cap E_2)}{P(E_2)}$$

With: $P(E_1 \cap E_2)$ The probability that both the events occur simultaneously

$P(E_2)$ is the probability of occurrence of the event E_2 (since the event E_2 has occurred, $P(E_2)$ should be positive).

So this expression could be rewritten:

$$P(E_1 \cap E_2) = P(E_1|E_2) \cdot P(E_2)$$

According to the standard definition of conditional probability, the usual formulation, namely the Bayes formula, can also be recalled:

$$P(E_1|E_2) = \frac{P(E_2|E_1) \cdot P(E_1)}{P(E_2)}$$

4.5.2 Definition of the fragility function

As said before, the analyses can be classified in two categories:

1. Analyses that have reached convergence
2. Analyses that have not reached convergence

In both cases we want to assess the probability that for a given IM (Intensity Measure), the EDP (Engineering Demand Parameter) chosen is greater than a limit value EDP_{lim} (that can be obtained from the literature, in the regulations or on the basis of empirical observations). For this particular study, the limits established by the CNR[] are used as the criteria to determine the exceedance of the Collapse Limit State.

$$P[EDP > EDP_{lim}]$$

The two typologies of event are mutually exclusive since the analysis is either collapsing numerically or reaching the converge, hence:

$$P(E_1 \cup E_2) = P(E_1) + P(E_2)$$

It follows that the formula should be decomposed into two terms (one for each category of analysis – convergent or non-convergent):

$$P[EDP > EDP_{lim}] = P[(EDP > EDP_{lim}) \cap P(conv)] + P[(EDP > EDP_{lim}) \cap P(non_conv)]$$

Hence, imposing that if the analysis is non convergent, it also implies that it has reached the Collapse Limit State:

$$P[EDP > EDP_{lim}] = P[EDP > EDP_{lim}|conv] \cdot P[NC] + P[EDP > EDP_{lim}|non_conv] \cdot P[C]$$

Where:

- $P[C]$ is the probability of collapse
- $P[NC]$ is the probability of non-collapse

The assertion that “*the non-convergence of the event can be interpreted as a collapse*” is expressed in mathematical terms as follows:

$$P[EDP > EDP_{lim}|non_conv] = 1$$

It is also possible to write:

$$P[NC] = 1 - P[C]$$

This implies:

$$P[EDP > EDP_{lim}] = P[EDP > EDP_{lim}|conv] \cdot (1 - P[C]) + 1 \cdot P[C]$$

Hence, extending this approach to all the intensity measures:

$$P[EDP > EDP_{lim}, IM = x] = P[EDP > EDP_{lim}|conv, IM = x] \cdot (1 - P[C], IM = x) + 1 \cdot P[C, IM = x]$$

That is: “*The probability that, for a given intensity measure, the EDP is higher than the EDP_{lim} is the result of the sum of two terms: the conditional probability that the $EDP > EDP_{lim}$ for*

convergent events, multiplied by the probability that the analysis is convergent, plus the conditional probability that $EDP > EDP_{lim}$ for non-convergent analyses (that is equal to one), multiplied by the probability that the analysis has collapsed”.

It is to be noted that this is the probabilistic formulation of the fragility curve that will be adopted in the analyses of the following chapters.

Now the meaning of each term is going to be explained:

1. First term

The first term of the fragility equation is:

$$P[EDP > EDP_{lim} | conv, IM = x]$$

That means, for a given intensity measure, this is the probability that an event is converging and exceeding the EDP limit at the same time. It is then multiplied by the probability of non-collapse of the event.

So, all the analyses that didn't reach the collapse condition will be taken into consideration.

The MSA approach is used to plot the results of the analyses, for each IM of each event that has reached the convergence, the maximum inter-story drift is reported. To distinguish between collapse and non-collapse, it is necessary to set a limit for the EDP (in our analyses, as reported in the paragraph 2.1.3, from the CNR the inter-story drift limit is considered at 0.5% of the inter-story height). In this way, the total number of converging events that have collapsed is obtained for each IM (marked using red dots in Figure 38).

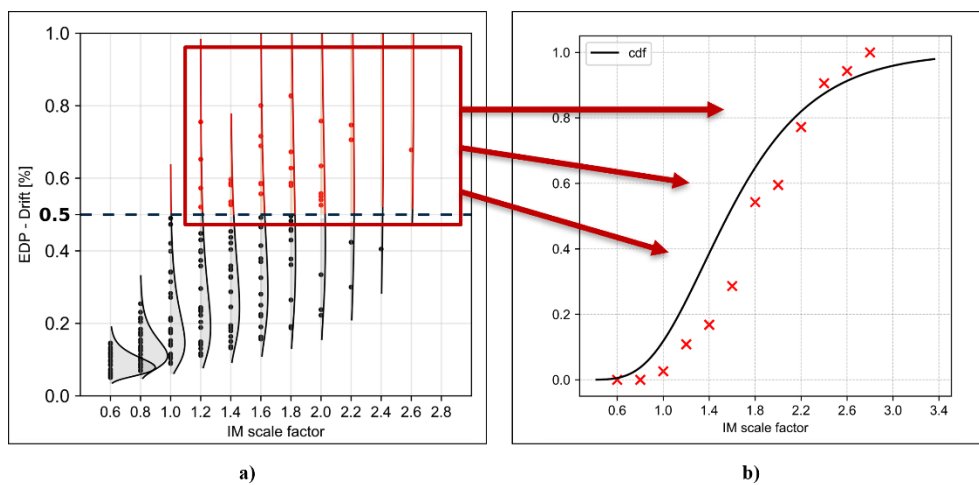


Figure 38: Cumulative density functions for different IMs and the related probability of exceedance of the imposed threshold.

Finally, to evaluate the probability of exceedance of the EDP_{lim} , for each IM, the CDF of the event is computed as it is displayed in Figure 38.

2. Second term

The second term of the equation is:

$$1 \cdot P[C, IM = x]$$

That means, for a given intensity measure, this is the probability that an event is non-converging, assuming that all non-convergent analysis exceed the value established as EDP limit.

Hence, the probability $P[C, IM = x]$ is obtained exclusively considering the analyses that are not reaching numerical convergence, for each Intensity Measure. This is achieved by first computing their Probability Density Function (Figure 39.a) and then computing the CDF (Figure 39.b).

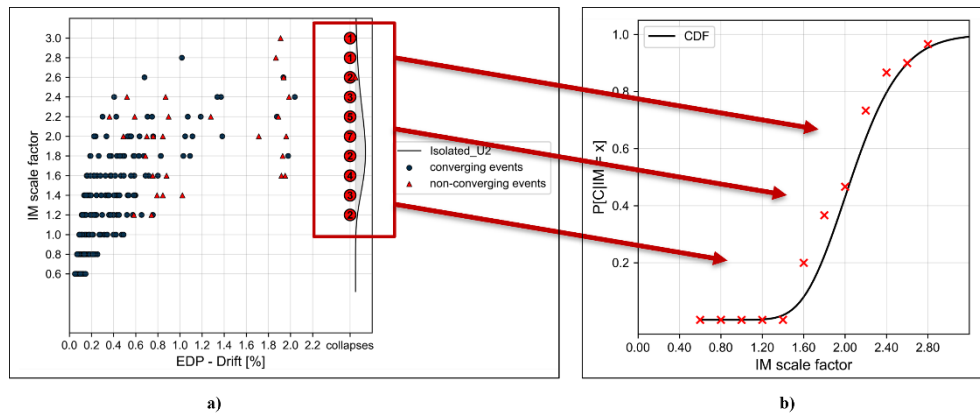


Figure 39: Probability Density Function for the collapsing events and the relative Cumulative Density Function.

Ultimately, the fragility function is obtained as the sum of the two terms:

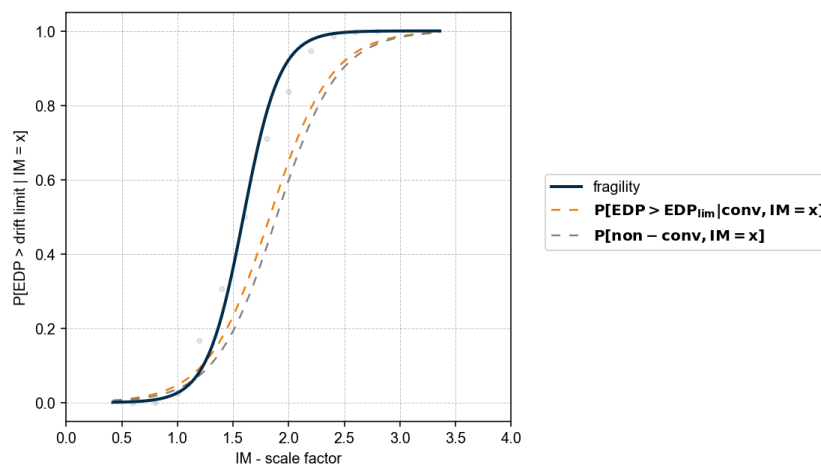


Figure 40: Fragility curve as the sum of the 2 terms.

5. Description of the elementary aggregate case study

The numerical model of this elementary case study has been developed and fully investigated in two previous theses; only slight changes have been introduced for the current study, but the overall geometry was kept the same in order to exploit the deep knowledge that resulted from the previous investigations. In this chapter, the geometry and the results of the analyses will be enucleated. The URM aggregate is composed of 3 units that are almost symmetrical from the geometrical point of view, this choice was made to avoid that differences in the material and in the geometry could interfere with the global structural response; four cases will be analysed: fully connected, semi-connected with mortar m1, semi-connected with mortar m3 and completely isolated. The semi-connected case was reproduced using an interface layer of 3 cm between the longitudinal walls of adjacent units and assigning a mortar material to this layer.

The aim of this thesis is to implement a workflow which integrates the STKO model and Python scripts to perform a fragility analysis of an aggregate building; in particular, the analysis has been conducted several times, each time introducing a change in the degree of connection between the units.

5.1 Numerical modelling

5.1.1 Geometry

The structure of the elementary aggregate is composed of 3 units, each one with 3 storeys. The in-plan configuration is almost identical for every unit, each one having a dimension of 8 m x 12.6 m x 11.2 m in respectively longitudinal, transverse, and vertical directions. The geometry of the front and back wall is reported in Figure 41.

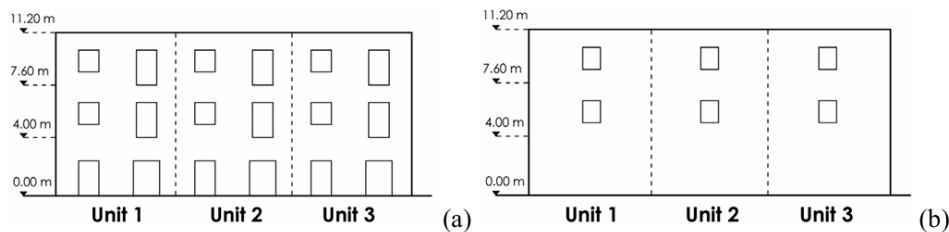


Figure 41: Reference aggregate's geometry: (a) Front wall; (b) Back wall [24]

The aggregate model has an elongated dimension along the longitudinal direction (x axis) and perpendicularly one shorter side along the transversal direction (y axis)

From left to right in the x axis the units illustrated in Figure 42 are: “Unit 1, Unit 2 and Unit 3”.

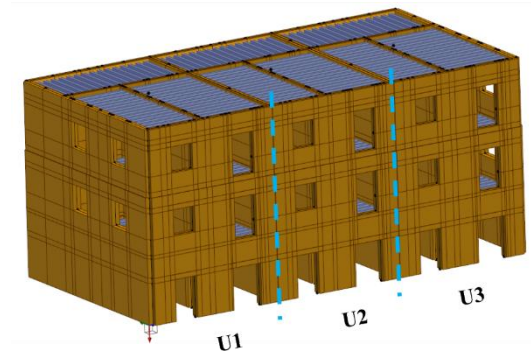


Figure 42: STKO 3D model of the aggregate building

In the longitudinal direction, the aggregate has 3 walls which have been called "front wall", "central wall" and "back wall".



Figure 43: Front wall, mid wall and back wall

As illustrated in Figure 44, the external walls of the aggregate and the internal wall of each unit have few openings, while for the partition wall between the different units, it was decided to avoid the placement of any opening.



Figure 44: From left to right: example of external wall, internal wall and partitioning wall between the units

The floor beams were arranged in accordance with the orientation of the floor slab and were assumed to be embedded into each wall.

The thickness of the external walls is 50 cm for the first two floors and 40 cm for the upper level; the thickness of the other walls is 35 cm and 30 cm for the last floor (additional details can be found in the appendix).

5.1.2 Material properties

The model was constructed using two types of materials: masonry and wood.

Average values were used for wood properties for beam sections (400x200 mm):

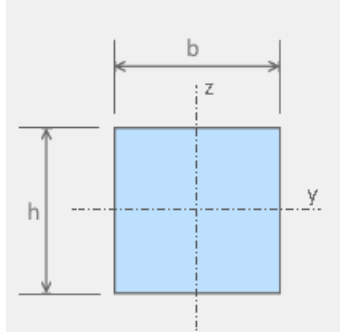


Table 4: Wood physical properties and embedded settings

Penalty factor	5e+07
Constrain rotations	yes
E [MPa]	10000
G [MPa]	300

The masonry material properties used for the model were derived from the calibration performed in the study "Seismic response of different masonry building aggregate configurations by a refined FE Model" [22]. The study was about exploring the potential beneficial impact of the aggregate effect in URM units. The model was created using the homogenized masonry technique in STKO to replicate experimental tests performed on an existing masonry building analysed at the University of Pavia [23].

The parameters obtained from the calibration of the masonry are reported in Table 5 and are the results of characterization tests that have been carried out on samples.

To provide a more detailed description, terracotta bricks with an average compressive strength of 16 MPa on cubic samples were chosen, along with a mortar composed of hydrated lime and sand in a volume ratio of 1:3 and a compressive strength between 2 MPa and 3 MPa. The elastic modulus was determined to be 1490 MPa while the tensile strength was reduced to 0.15 MPa to better match the experimental results.

Table 5: Masonry physical properties calibration from study

f_t	f_{cp}	G_t	G_c	E_m	ν
[MPa]	[MPa]	[N/mm]	[N/mm]	[MPa]	[—]
0.15	6.2	0.07	14	1490	0.2

The assumed material properties of the masonry can be associated with the classes of "Squared block masonry" outlined in Table C8.5.1 of the circular of the NTC.

Table 6: Tab C8.5.1, NTC2018 - Masonry categories

Tipologia di muratura	f (N/mm ²)	τ_0 (N/mm ²)	f_{v0} (N/mm ²)	E (N/mm ²)	G (N/mm ²)	w (kN/m ³)
	min-max	min-max		min-max	min-max	
Muratura in pietrame disordinata (ciottoli, pietre erratiche e irregolari)	1,0-2,0	0,018-0,032	- -	690-1050	230-350	19
Muratura a conci sbozzati, con paramenti di spessore disomogeneo (*)	2,0	0,035-0,051	- -	1020-1440	340-480	20
Muratura in pietre a spacco con buona tessitura	2,6-3,8	0,056-0,074	- -	1500-1980	500-660	21
Muratura irregolare di pietra tenera (tufo, calcarenite, ecc.,)	1,4-2,2	0,028-0,042	- -	900-1260	300-420	13 ÷ 16(**)
Muratura a conci regolari di pietra tenera (tufo, calcarenite, ecc.,) (**)	2,0-3,2	0,04-0,08	0,10-0,19	1200-1620	400-500	
Muratura a blocchi lapidei squadrati	5,8-8,2	0,09-0,12	0,18-0,28	2400-3300	800-1100	22
Muratura in mattoni pieni e malta di calce (***)	2,6-4,3	0,05-0,13	0,13-0,27	1200-1800	400-600	18
Muratura in mattoni semipieni con malta cementizia (es.: doppio UNI foratura ≤40%)	5,0-8,0	0,08-0,17	0,20-0,36	3500-5600	875-1400	15

As said before, two different typologies of interface material for the units were considered (material m_3 emulates the behaviour of a stiffer connection, while material m_1 is associated with a lower degree of interconnection between units). The two have been modelled with *DamageTC3D* and a summary of the material properties is displayed in Table 7.

Table 7: Properties used in the model for the different typologies of mortar considered

	F_{cp}	f_{c0}	f_{cr}	E_m	E_{ms}	ε_b	f_{tm}	G_t	G_c	ν
	[MPa]	[MPa]	[MPa]	[MPa]	[MPa]	[-]	[MPa]	$\frac{[N]}{[mm]}$	[N/mm]	[-]
m_1	1.0	0.7	0.1	100	50	0.02	0.04	0.05	18.25	0.15
m_3	3.06	2.14	0.31	306	153	0.02	0.11	0.09	22.32	0.15

Lintel material properties were chosen assuming a unique solid brick. Material properties are reported in Table 8.

Table 8: Lintel physical properties

f_t	f_{cp}	G_t	G_c	E_m	ν
[MPa]	[MPa]	[N/mm]	[N/mm]	[MPa]	[-]
1.6	16	0.12	30	9600	0.2

In the study, the mortar surrounding lintels was defined differently from the mortar used as an interface between units. Specifically, the mortar around the lintel needed to behave purely elastically under compression and have no strength under tension to capture the sliding of the lintel. To achieve this specific behaviour, a customized constitutive model was introduced using the user-defined settings available for the *ASDConcrete3D* model, described in Table 9.

Table 9: User-defined mortar parameters

Elasticity	E [MPa]	1490
	ν [–]	0.2
Tension	T_e	[0; $6.71141 \cdot 10^{-7}$; 1]
	T_s	[0; 0,001; 0,001]
	T_d	[1; 1; 1]
Compression	C_e	[0; 1]
	C_s	[0; 1490]
	C_d	[1; 1]

5.1.3 Loads, masses and conditions

Two types of loads were considered

- Beams' distributed load equal to 2.5 kN/m, applied to the element as *EdgeForce*;
- Masonry self-weight, equal to the product between the specific weight of the masonry ($\gamma_m = 17 \text{ kN/m}^3$) and the thickness of the shell, applied to the shell as *FaceForce*.
- Stairs load equal to 4 kN/m^2 to take into account for the presence of these elements (even if they were not explicitly modelled) and applied as *EdgeForces* at the edges of transversal walls, both at the beginning and end of the staircase

Since STKO distinguishes between loads and masses, all the loads mentioned were converted to masses and applied as *FaceMass* for the walls and *EdgeMass* for the edges; this operation is necessary for the modal and non-linear dynamic analysis.

A fixed boundary condition was applied at the base of the structure to avoid displacements and rotations along all axes.

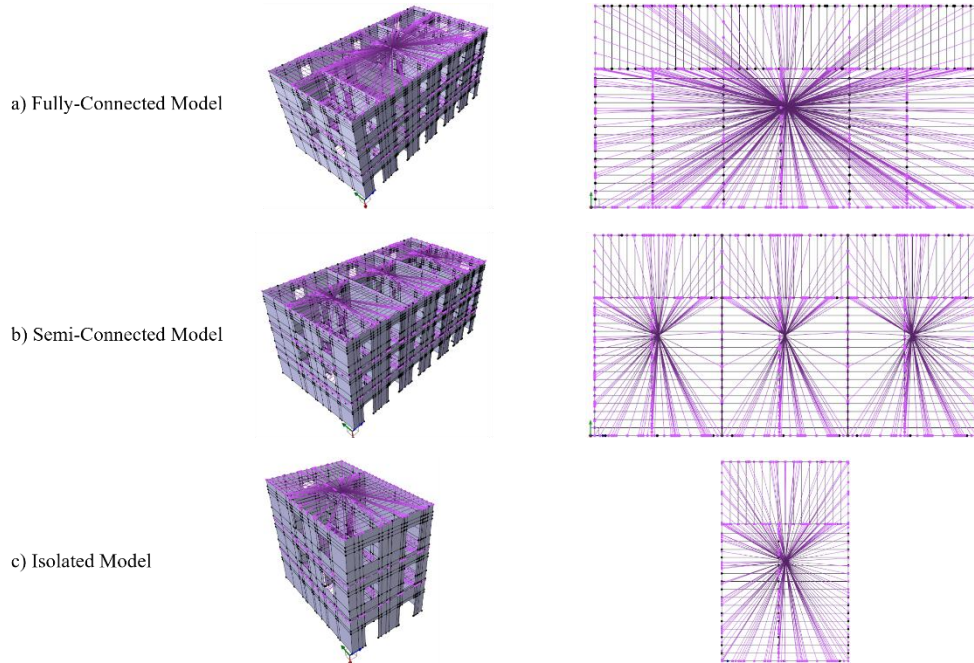


Figure 45: Model geometry for the three cases considered, emphasizing the rigid diaphragm.

5.1.4 Mesh architecture

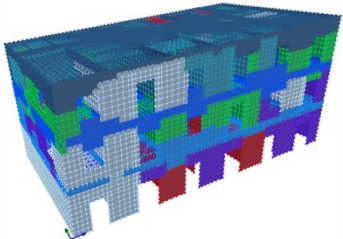
To run the analyses, it is necessary to assign a mesh to the model itself; to foster a balance between the accuracy of the results and the computational time needed for the analysis, a global mesh size of 350 mm has been chosen (such a coarse mesh was acceptable thanks to the use of *ASDConcrete3D*, which is insensitive to mesh size variations), and a finer mesh of 15 mm was chosen for interface material layers (to ensure a square aspect ratio of the mesh).

The mesh was refined to 300 mm in the case of Semi-Connected models.

STKO allow the user to choose to partition the model, enabling parallel computing using different processors and, consequently, decreasing the time needed to complete the analysis; The criteria used for the partition are to subdivide the model in such a way that each processor handles around 4000-5000 elements. As it is shown in Figure 46, 8 processors were utilized for the Fully-Connected model, 10 for the Semi-Connected models and 4 for the Isolated Units models.

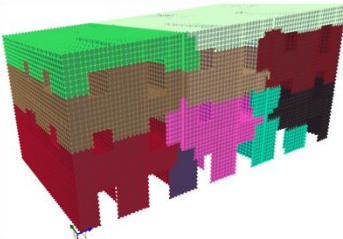
Fully-Connected Model

Color	ID	Nodes	Elements
	0	2318	4135
	1	2519	3385
	2	2227	3620
	3	2474	3741
	4	2556	3964
	5	2477	3868
	6	2260	3663
	7	2511	3630



Semi-Connected Model

Color	ID	Nodes	Elements
	0	4164	7177
	1	4381	7277
	2	4472	7590
	3	4575	7524
	4	4502	7434
	5	4576	7421
	6	3985	6864
	7	4627	7433
	8	4473	7305
	9	3889	7003



Isolated Model

Color	ID	Nodes	Elements
	0	2411	3886
	1	2601	3510
	2	2411	3928
	3	2449	4068

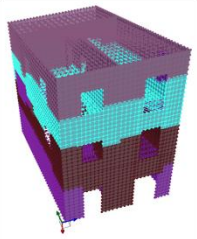


Figure 46: Visual representation of the model partition

5.2 Dynamic properties of the elementary aggregate

This section explains the analyses performed. Three types of analyses were conducted: vertical analysis, modal analysis, and non-linear dynamic analysis. Each was performed separately, following the initial vertical analysis.

5.2.1 Vertical analysis

In the vertical analysis, both vertical and self-weight loads are applied linearly at each step.

The vertical analysis was performed in all simulations as the first analysis; particular care was put in the choice of the right algorithm for the operations of numbering the degrees of freedom (*DOF_Numberer*): *Reverse Cuthill-McKee* was used for single processor analyses and *parallel reverse Cuthill-McKee* algorithm for parallel computing.

The same approach should be applied in the case of the choice of the system solver, necessary for solving the differential equations: *UmfPack* was used for uniprocessor analysis, while *Mumps* is employed for parallel processors. Given the complexity of the problem and the need to handle nonlinear equation systems, the Krylov-Newton method was used.

To ensure result reliability, a convergence test was performed using the norm displacement increment test with a tolerance of 0.0001. A Load Control integrator with a time series definition was used to manage load increments over time. In the vertical analysis, a linear time series definition was applied to linearly increment the load factor at each time step.

After the first vertical analysis, a *wipeAnalysis* deletes all analysis settings imposed in previous analyses.

5.2.2 Modal analysis

In the modal analysis, the first 10 vibration modes were considered for each model, assessing their periods, the vibration frequencies and the participation mass factors. Parallel computing cannot be employed for the modal analysis in STKO, therefore, one single partition needs to be used and the model should be processed by one single processor. The *genBandArpack* solver employed for eigen analysis doesn't offer any customization for the constraint and numbering options and the default options must be adopted. This limitation can have an impact on the model validity, this is also reflected in the necessity to carefully evaluate the analysis's results and check for computational issues.

5.2.3 Non-linear dynamic analysis

Dynamic analysis is the most reliable technique for assessing the behaviour of a structure during an earthquake, since it evaluates the actual inertial forces induced by a real seismic event, solving the equations of motion. Since STKO distinguishes between masses and loads, it is necessary to apply the masses to the model components.

The acceleration data were retrieved from a set of 30 ground motions, which was used to ensure a statistical distribution of the ground motion data (for further details about the ground motion selection see Table 15 and the paragraph 5.4.1).

The damping was introduced using Rayleigh method, considering a damping ratio of 0.03 and a range of frequencies between the first and fifth mode.

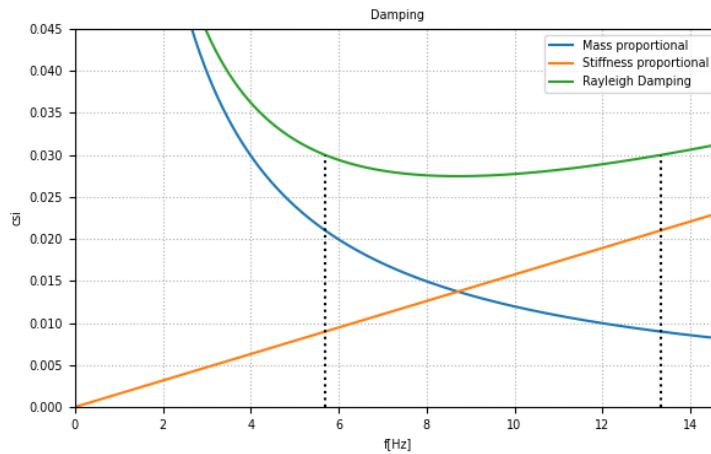


Figure 47: Example of Rayleigh damping introduced for the Semi-connected model

For solving the differential equations, the TRBDF2 (Trapezoidal Rule-Backward Differentiation Formula 2) method was employed; it is a numerical integration method that is widely used in dynamic and transient analyses and that combines two different methods (the Trapezoidal Rule and the Backward Differentiation Formula 2), ensuring the accuracy and the stability of the results.

The analyses were conducted using an adaptive time step, considering each time a number of steps equal to the number of increments of the ground motion recording and a total duration consistent with the one of the ground motion considered, ensuring a step duration of 0.005 s (coinciding with the sampling rate of the signal).

5.3 Dynamic characteristics of the models

The dynamic properties of the models were retrieved from the modal analysis. The period and the modal participation ratios in the x and y directions for the first five vibration modes are reported for the fully-connected case, the semi-connected model (Table 10) and the isolated ones (Table 11).

Table 10: Eigenvalues analysis results for the fully-connected and the semi-connected cases.

	Fully-connected			Semi-connected					
				m1			m3		
	T	Mx	My	T	Mx	My	T	Mx	My
Mode	[s]	[%]	[%]	[s]	[%]	[%]	[s]	[%]	[%]
1	0.164	66.34	0.53	0.176	67.22	1.68	0.172	69.27	0.12
2	0.152	0.64	72.24	0.14	2.93	67.96	0.139	0.24	71
3	0.119	9.33	0.05	0.121	5.82	1.53	0.121	6.57	0.18
4	0.075	0.001	0.06	0.0755	0.02	0.08	0.0755	0.001	0.032
5	0.074	0.003	0.006	0.0751	0.25	0.28	0.0751	0.008	0.007

Table 11: Eigenvalues analysis results for the isolated model

	Isolated units								
	Unit 1			Unit 2			Unit 3		
	T	Mx	My	T	Mx	My	T	Mx	My
Mode	[s]	[%]	[%]	[s]	[%]	[%]	[s]	[%]	[%]
1	0.196	70.69	0.002	0.199	71.27	0	0.195	70.77	0.03
2	0.141	0	70.76	0.138	0.01	72.57	0.142	0.14	70.01
3	0.109	1.31	0.2	0.109	1.16	0.06	0.109	1.31	1.03
4	0.073	13.76	0.24	0.074	15.54	0.07	0.074	4.37	1.61
5	0.072	0.04	0.003	0.068	0.01	0.01	0.074	0.53	0

In all cases, the fundamental mode is along the longitudinal direction (x-axis), the second mode is along the transversal direction (y-axis), and the third mode is around the z-axis. The following tables display the first three modal shapes of the models.

Table 12: First 3 modal shapes of the Fully-Connected aggregate [24]

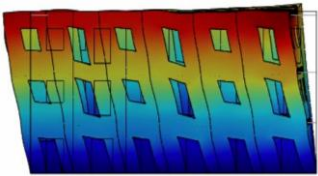
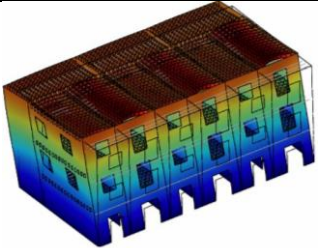
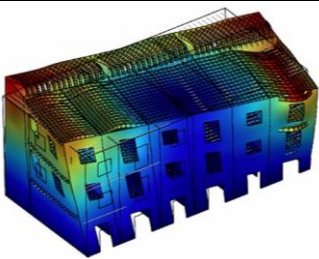
	1 ST mode	2 ND mode	3 RD mode
Fully Connected			

Table 13: First 3 modal shapes of the isolated units [24].

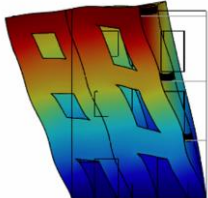
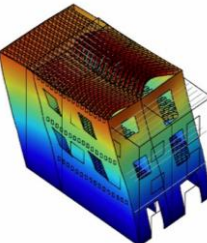
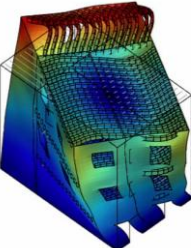
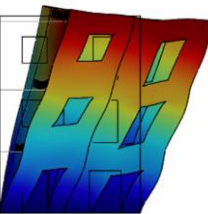
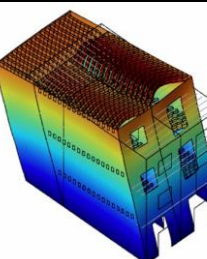
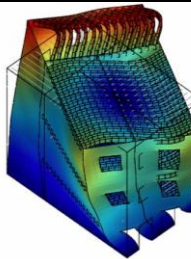
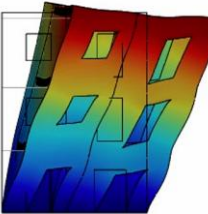
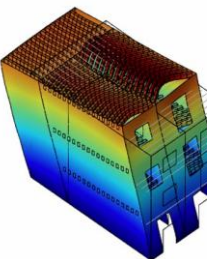
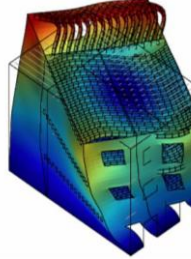
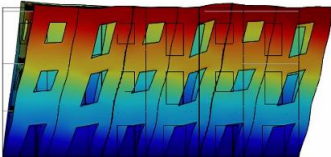
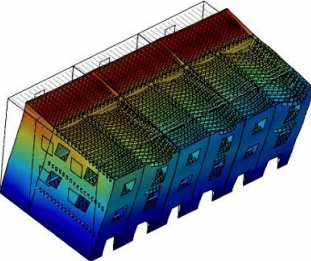
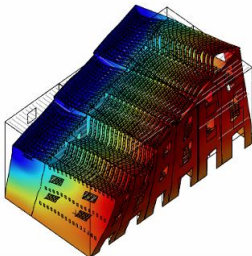
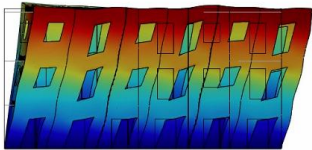
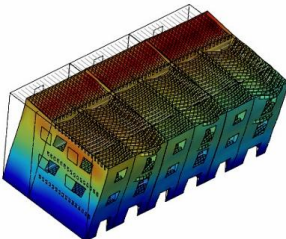
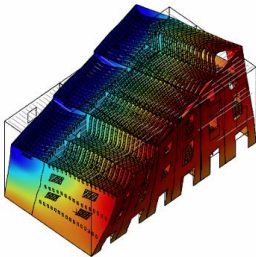
	1 ST mode	2 ND mode	3 RD mode
Isolated unit (U1)			
Isolated unit (U2)			
Isolated unit (U3)			

Table 14: First 3 modal shapes of the Semi-Connected aggregate [24].

	1 ST mode	2 ND mode	3 RD mode
Semi Connected (m1)			
Semi Connected (m3)			

5.4 Non-linear dynamic analysis results – derivation of fragility curves

5.4.1 Ground motion selection

Ground-motion selection provides the link between seismic hazard and response analyses. It is therefore critical that selected ground-motion ensembles are consistent with hazard analysis results [20].

In this thesis, we used a set of 30 ground motion records, retrieved from the Archive of Italian Department of Civil Protection, HEAD (Unified Hellenic Accelerogram Database), FDSN Web Service databases. The ground motions are mainly obtained by the Italian accelerometric network (Rete Accelerometrica Nazionale, RAN), HL (National Observatory of Athens Seismic Network) and SM (Icelandic Strong Motion Network).

The selected ground motions take into account a wide range of PGA and are recorded in different Italian regions, in Greece and Iceland. These ground motions are within a specified range: magnitude M_w between 5.0 and 6.6 and EC8 soil classification from A to D.

The main features of the set of 30 accelerograms are summarized in Table 15. The ground motions were applied only in the longitudinal direction of the aggregate to study in depth the effect of the presence of adjacent units under different degrees of unit-interconnection.

5.4.2 Intensity measure

As many authors have highlighted, the choice of the right set of IMs is crucial, they serve as a connection between probabilistic seismic hazard analysis and probabilistic structural response analysis [25]. This is explained by the fact that, often, the hazard is provided in the form of ground-motion IMs. It is therefore necessary to select ground-motion ensembles that are consistent with the IMs from PSHA to achieve hazard consistency [20].

The spectral acceleration at the fundamental period of the structure ($S_a(T_1)$) was taken as the Intensity Measure for the following analyses.

5.4.3 Engineering demand parameter (EDP)

In this thesis, the collapse limit state is considered, and the inter-story drift is assumed as the EDP. The limit state is reached when the 0.5% threshold is exceeded, as it is indicated by the regulations.

During the analyses, several monitors were placed along the structure (either in the front, back and middle walls), tracking the displacements of the selected node along the x axis.

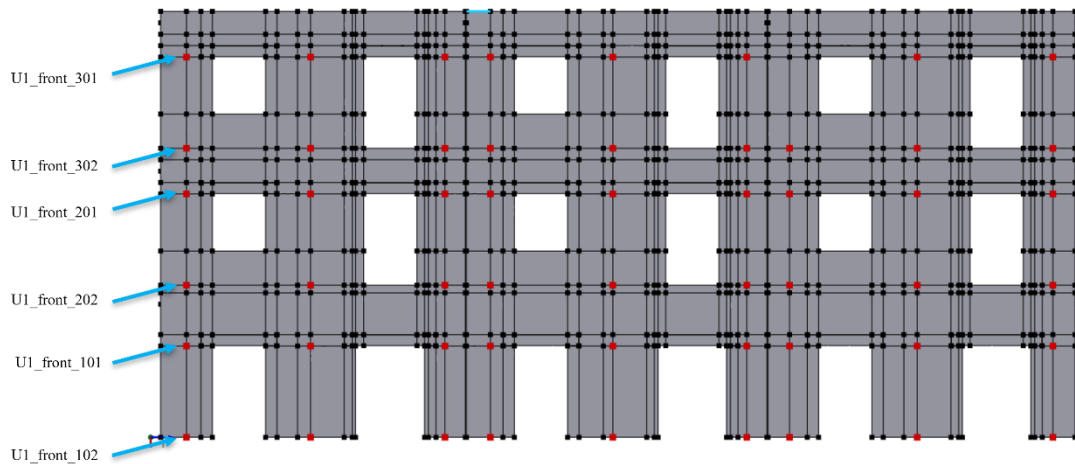


Figure 48: Example of monitor placement and naming for the front wall of the semi-connected model

This analysis, the EDP choice and the monitor location have taken advantage of the results of previous thesis ([26] and [24]) which have investigated the structure mainly using a non-linear dynamic approach and also conducting one non-linear dynamic analysis using the ground motion recording of the event: “*L’Aquila – v Aterno – Colle Grilli*”, in the North-South direction.

Both the studies have highlighted the central role of the front wall in affecting the behaviour of the whole ensemble: the front wall has the highest number of openings, consequently, it shows the lowest resistance, being the first to experience damage. When this happens, the rigid diaphragm redistributes the forces among the other walls, which increases their damage and crack openings.

The increased flexibility of the front wall, due to the presence of various openings, is also reflected in its highest longitudinal displacement demand among all longitudinal walls; conversely, in the dynamic analysis, the back wall configuration remains almost unchanged.

For all these reasons and given the results of some preliminary non-linear dynamic analyses executed on the model at the beginning of this study, our choice was to process and analyse only the front wall monitors (even if the monitors were placed in every longitudinal wall), retrieving the in-plan inter-story drift for each floor.

Table 15: Ground motion selection

Year	Event_ID	Station name and site classific. (EC8)	Magnitude [M _w]	Epicentral distance [Km]	PGA [g]	Duration [s]	Sampling interval [s]
2016	EMSC- 20161030_0000029	Pasciano cimitero INGV (B)	6.6	22.9	0.36	50.76	0.005
2016	EMSC- 20161030_0000029	Pasciano cimitero INGV (B)	6.6	22.9	0.40	50.76	0.005
2016	EMSC- 20161030_0000029	San Lorenzo a Pinaco INGV (B)	6.6	28.8	0.21	148.84	0.005
2016	EMSC- 20161030_0000029	Pozzo Varoni IMAA CNR (B)	6.6	27.8	0.20	99.42	0.005
2016	EMSC- 20161030_0000029	Collecetra IDPA CNR IMAA CNR (B)	6.6	28.3	0.38	75.29	0.005
1986	GR-1986-0006	KALAMATA (C)	5.9	4.6	0.22	35.88	0.005
1986	GR-1986-0006	KALAMATA (C)	5.9	4.6	0.30	35.88	0.005
1981	GR-1981-0001	KORINTHOS (B)	6.6	30.2	0.24	50.70	0.005
1981	GR-1981-0001	KORINTHOS (B)	6.6	30.2	0.30	50.70	0.005
1981	GR-1981-0001	XYLOKASTRO (B)	6.6	35.9	0.29	41.92	0.005
2016	EMSC- 20160824_0000006	AMATRICE (B)	6	8.5	0.38	27.90	0.005
2009	IT-2009-0009	L AQUILA V. ATERNO COLLE GRILLI (B)	6.1	5	0.45	100.00	0.005
2009	IT-2009-0009	L AQUILA V. ATERNO AQUIL PARK ING. (B)	6.1	1.8	0.35	100.00	0.005
1997	IT-1997-0004	COLFIORITO (D)	5.7	2.8	0.26	44.45	0.005
2016	EMSC- 20161026_0000095	Castelsantangelo sul Nera (C)	5.9	2	0.38	30.00	0.005
2016	EMSC- 20161030_0000029	Castelsantangelo sul Nera (C)	6.6	6.7	0.29	100.00	0.005
2012	IT-2012-0011	MOGLIA (C)	6	15.8	0.17	115.00	0.005
2012	IT-2012-0008	Mirandola (C)	6.1	16.1	0.26	130.15	0.005
2012	IT-2012-0011	SAN FELICE SUL PANARO (C)	6	6.1	0.22	170.01	0.005
2018	EMSC- 20181226_0000014	Santa Venerina (A)	5	5.3	0.30	57.91	0.005
2012	IT-2012-0011	Loc. Cortile Carpi MO (C)	6	9.3	0.44	100.01	0.005
2012	IT-2012-0010	Novi di Modena MO (C)	5.5	6.8	0.26	60.01	0.005
2016	EMSC- 20161030_0000029	Domo RI (B)	6.6	22.6	0.35	60.48	0.005
2016	EMSC- 20161030_0000029	Spelonga (B)	6.6	16.9	0.29	54.97	0.005
2016	EMSC- 20161030_0000029	Spelonga (B)	6.6	16.9	0.19	54.97	0.005
2009	IT-2009-0009	L Aquila Italy (B)	6.1	2.5	0.26	90.0	0.005
2000	IS-2000-0053	Solheimar (B)	6.5	17.8	0.43	55.0	0.005
2008	IS-2008-0054	Selfoss-City Hall (A)	6.3	4.3	0.33	72.0	0.005
2012	IT-2012-0011	MIRANDOLA MRN (C)	6	5.1	0.22	63.0	0.005
2012	IT-2012-0011	GAVELLO (C)	6	13	0.31	150.0	0.005

5.4.4 IDA curves

This section presents IDA curves resulting from the 6 models analysed. Each point of the curve is defined by a specific IM-EDP combination and then the curve is constructed simply by joining together the points.

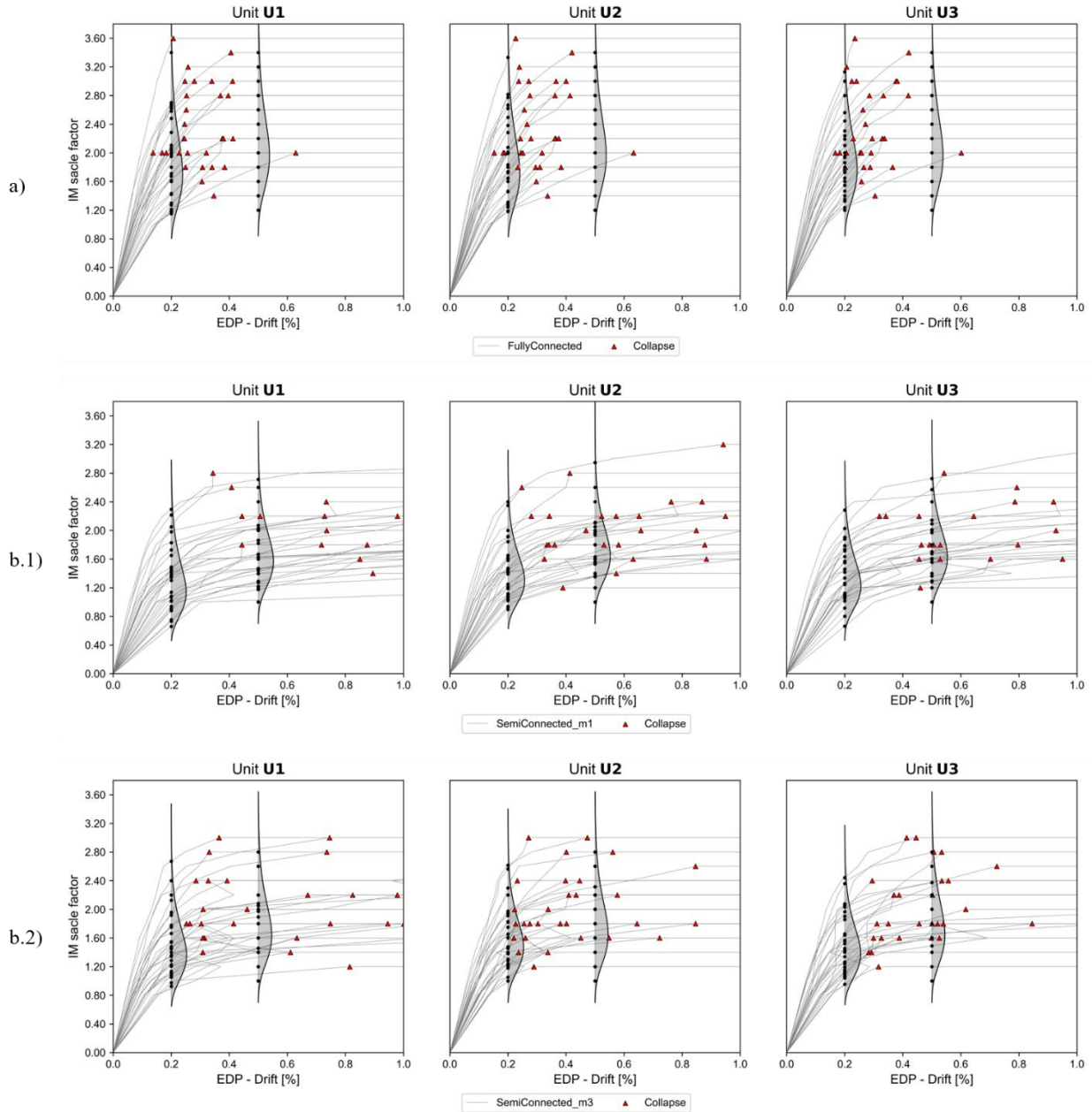


Figure 49: IDA curves obtained for a set of 30 ground motions. a) Fully-connected case, b.1) Semi-connected case, m1 b.2) semi-connected case, m3

It is important to highlight that, due to the complexity of the model herein considered, the models will produce IDA curves with a markedly irregular trend. It was also assumed that after the first nonconvergence successive IM will cause collapse of the structure. For this reason, after the collapse point, IDA curves are kept constant.

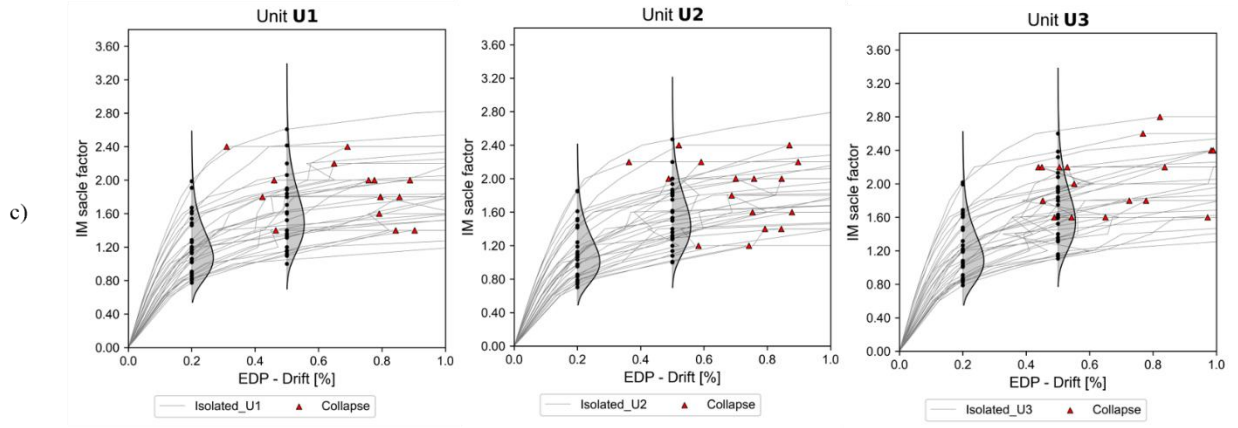


Figure 50: IDA curves obtained for a set of 30 ground motions. c) Isolated cases

Additionally, as D. Vamvatsikos and C.A. Cornell suggested in their paper [17], once the Damage Measure and the Intensity Measures are extracted from the analyses, the set of discrete points can be interpolated using different typologies of functions, without performing additional analyses. In the next figure, the IDA curves interpolated using spline functions are reported.

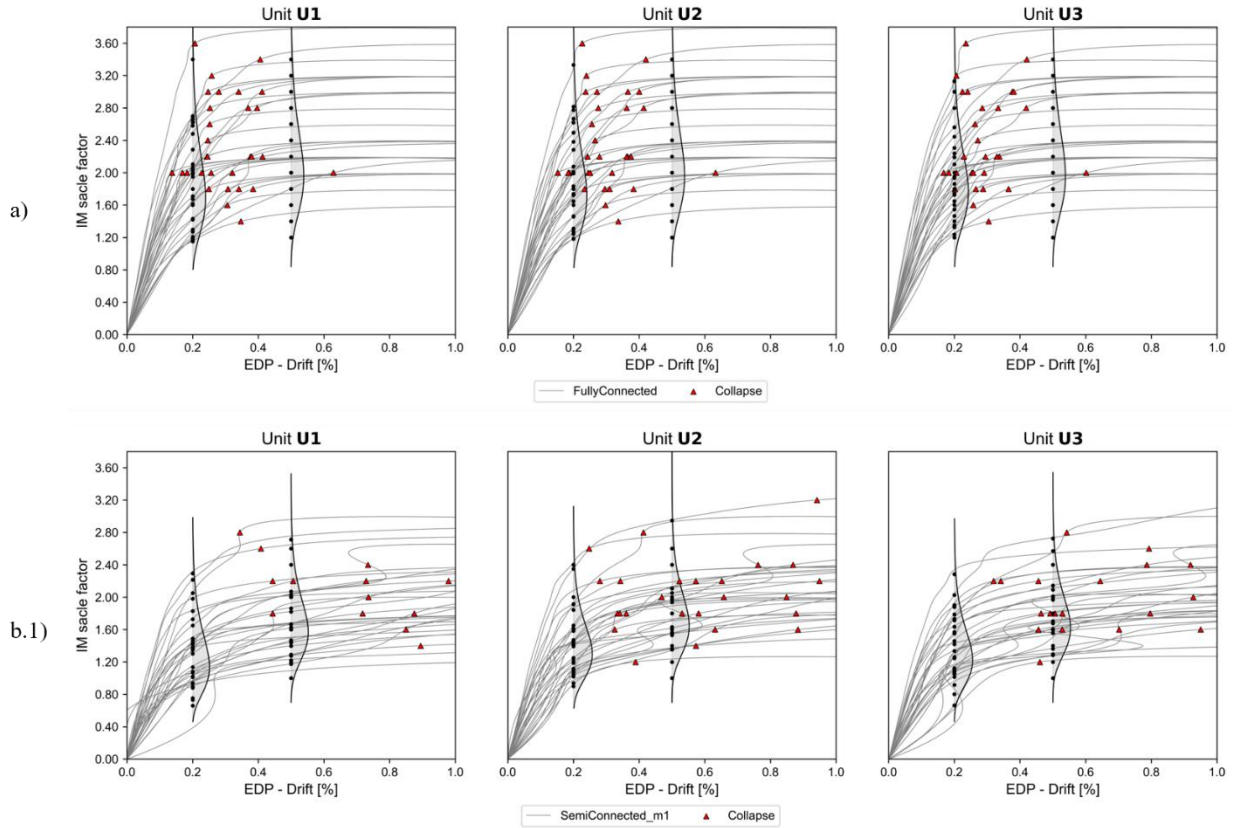


Figure 51: Interpolated IDA curves obtained for a set of 30 ground motions. a) Fully-connected case, b.1) Semi-connected case, m1

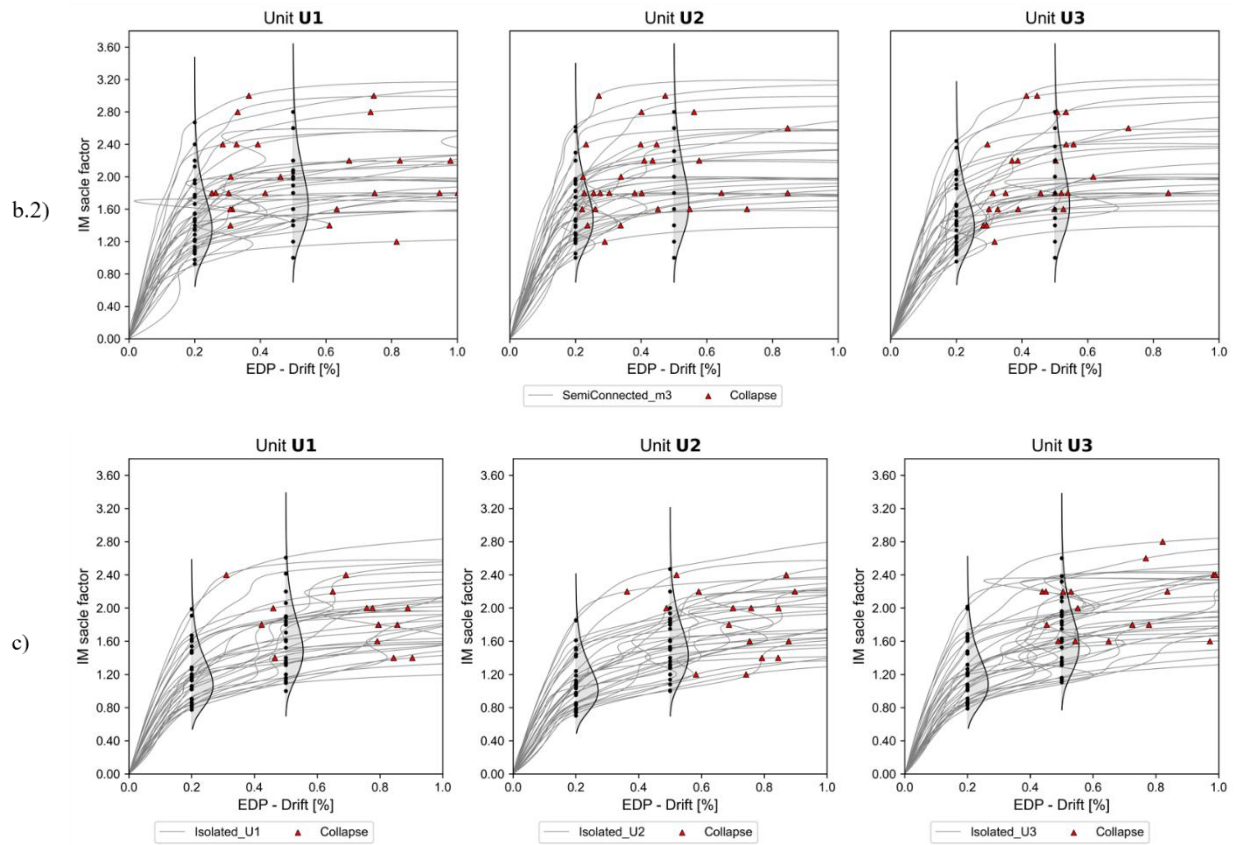


Figure 52: Interpolated IDA curves obtained for a set of 30 ground motions. b.2) semi-connected case, m3 c) Isolated cases

At the beginning, almost all the curves exhibit a distinct linear trend which terminates between EDP comprises in the interval 0.2% - 0.4%. This first segment is followed by the characteristic “twisting” pattern that can commonly be found in IDA curves, and it is generated by consecutive hardening and softening regions; finally, the curve flattens out in a plateau in the correspondence of the maximum IM value, where the DM tend to go towards “infinity”.

Figure 51.a (fully-connected case) shows that the model tends to collapse at low drift, even at higher levels of the Intensity Measure. However, this trend does not hold for the semi-connected model (Figure 51.b.1 and b.2), particularly in the case with material m1, or for the isolated models (Figure 51.c). These models can reach high levels of inter-story drift without collapsing. Nonetheless, it is important to note that, overall, the isolated models tend to collapse at lower IM levels.

The results of the Fully-Connected model indicate that it suffers limited damage, consequently it can be deduced that its response to seismic inputs was predominantly elastic; this result is consistent with the ones obtained in [24].

As expected, isolated units behaved similarly, which was used as a base to emphasize the effect of the different degrees of connection in their behaviour. Fully-connected models, although presented identical drift measures and shape of the hysteretic curves, exhibited considerable differences in terms of reaction at base. Exploring lower degrees of interconnection, in the semi-connected model (especially with weaker interface materials, like m_1 case) we start to see the first differences in the units' behaviour: in particular it is possible to see in Figure 51.b.1 that the middle unit (unit U2) displays a higher number of collapses for lower levels of EDP. This evidence can be interpreted by the fact that the external units are free to oscillate, while the central one is constrained by U1 and U3; this configuration limits the displacements and stresses of the middle unit, which are redistributed from the unit 2 towards the external ones.

This fact can also be seen plotting the capacity curves of the three units (Figure 53). These curves are obtained considering the reaction force at the base of each unit and the displacements of a control node located in the barycentre of the unit.

The central unit presents a symmetrical curve, conversely, the unit U1 shows a larger reaction force in the correspondence of the negative direction and the unit U3 shows a greater reaction force for the positive direction. This is clear evidence of the redistribution of stresses from the central unit to the external ones, Figure 53.

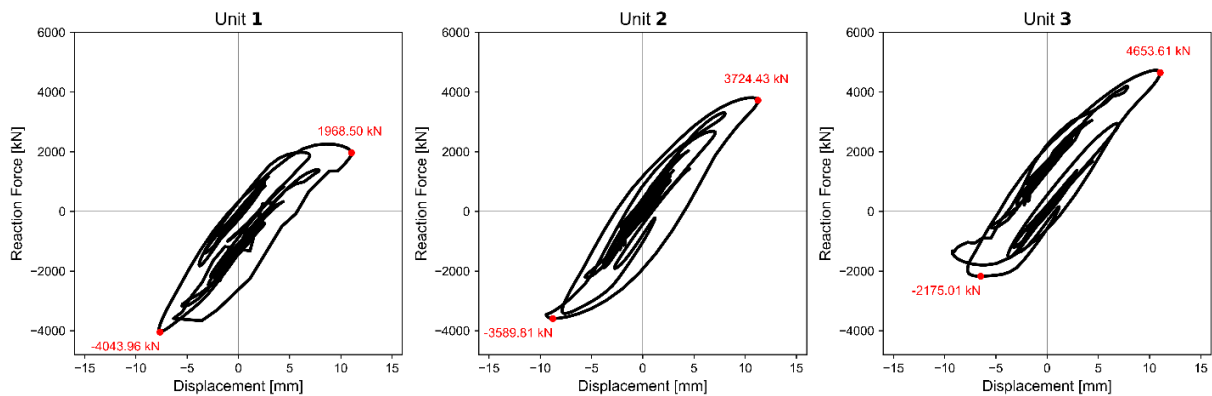


Figure 53: Capacity curves for the fully-connected model.

The analysis of the capacity curves of the semi-connected model, particularly considering the maximum displacements reached by each unit, sheds light on the distinctions in the asymmetrical behaviour of the first unit (that is the most severely affected by the seismic event) and the other two units, which, on the contrary, demonstrate a nearly symmetrical response (Figure 54).

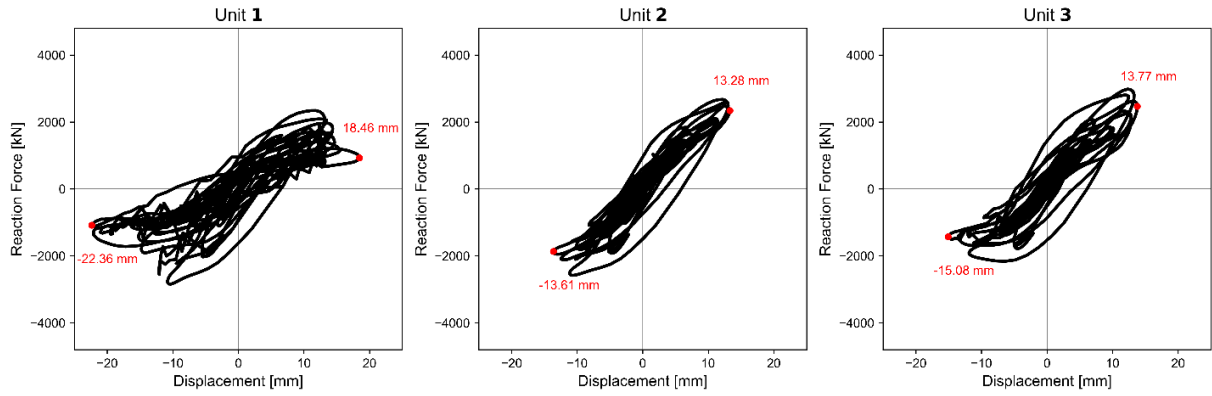


Figure 54: Capacity curves for the semi-connected model

In all the plots, the IDA curves are overlapped with two probability density functions in the correspondence of two values of inter-story drift equal to 0.2% and 0.5 %. The Fully Connected model has the greatest record to record variability, showing collapses in a great range of IMs, while the other cases tend to exhibit a more uniform behaviour.

It is important to highlight that although IDA curves in general exhibited similar behaviour among units, capacity curves exhibited considerable differences and showcase the limitations of choosing a single parameter such as the in-plane drift to evaluate the response of such complex buildings. This is further emphasized considering that these models are regular buildings with rigid diaphragms, which do not represent the actual structural configurations found in the historical centres of mediterranean regions. For this reason, the study is further extended by analysing a real case study aiming to determine other possible measurable variables that better capture the “aggregate effect”.

5.4.5 Multi Stripe Analysis (MSA)

The MS Analyses relate in a single graph the results in terms of IMs and EDP. The approach is the opposite with respect to the one used for implementing IDA curves: for a fixed IM multiple ground motions are considered. Consequently, even with this method, it is necessary to process the model several times, exploring a vast range of IMs. In the following figure, the results for all the four models considered are reported.

In Figure 55 and Figure 56, the results of both converging and non-converging analyses are plotted using blue dots and red markers respectively.

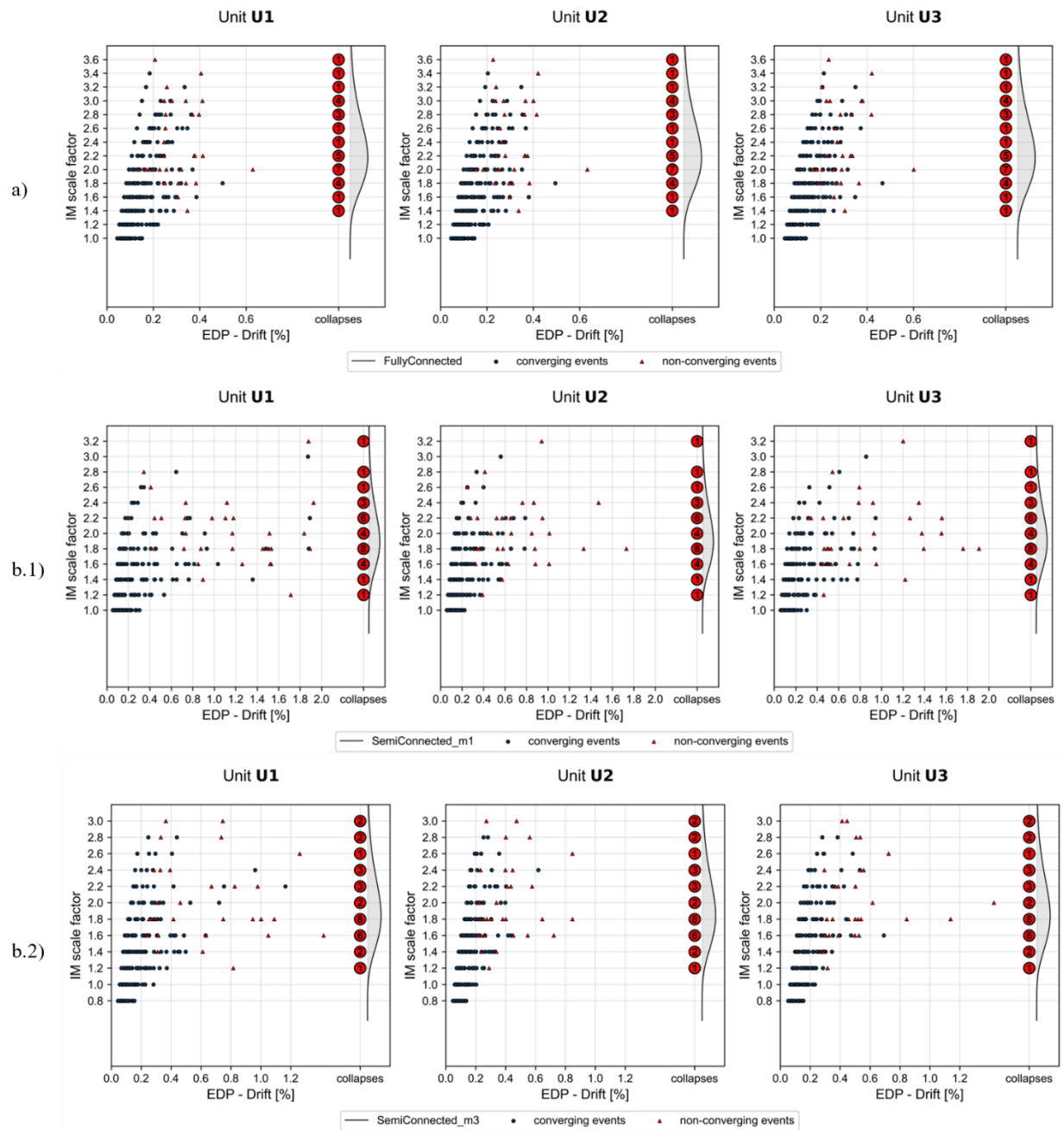


Figure 55: MSA analysis for the Fully Connected case (a) and Semi Connected case (b)

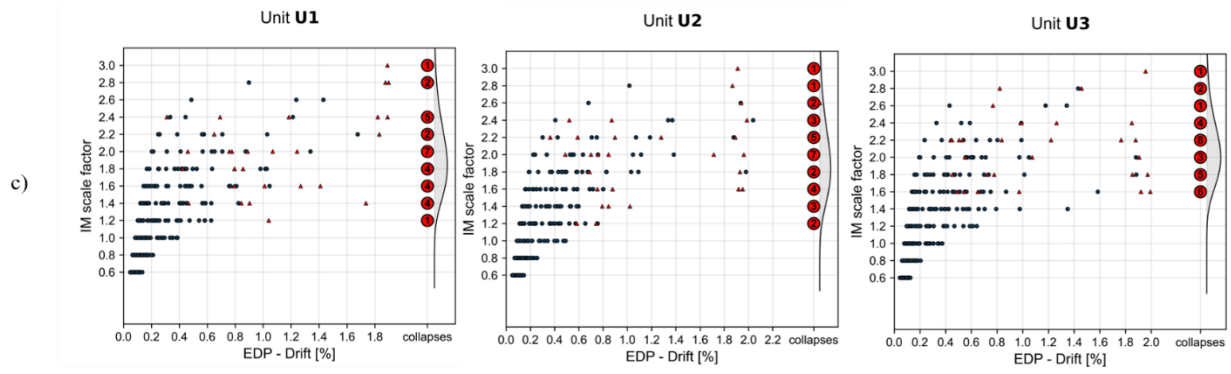
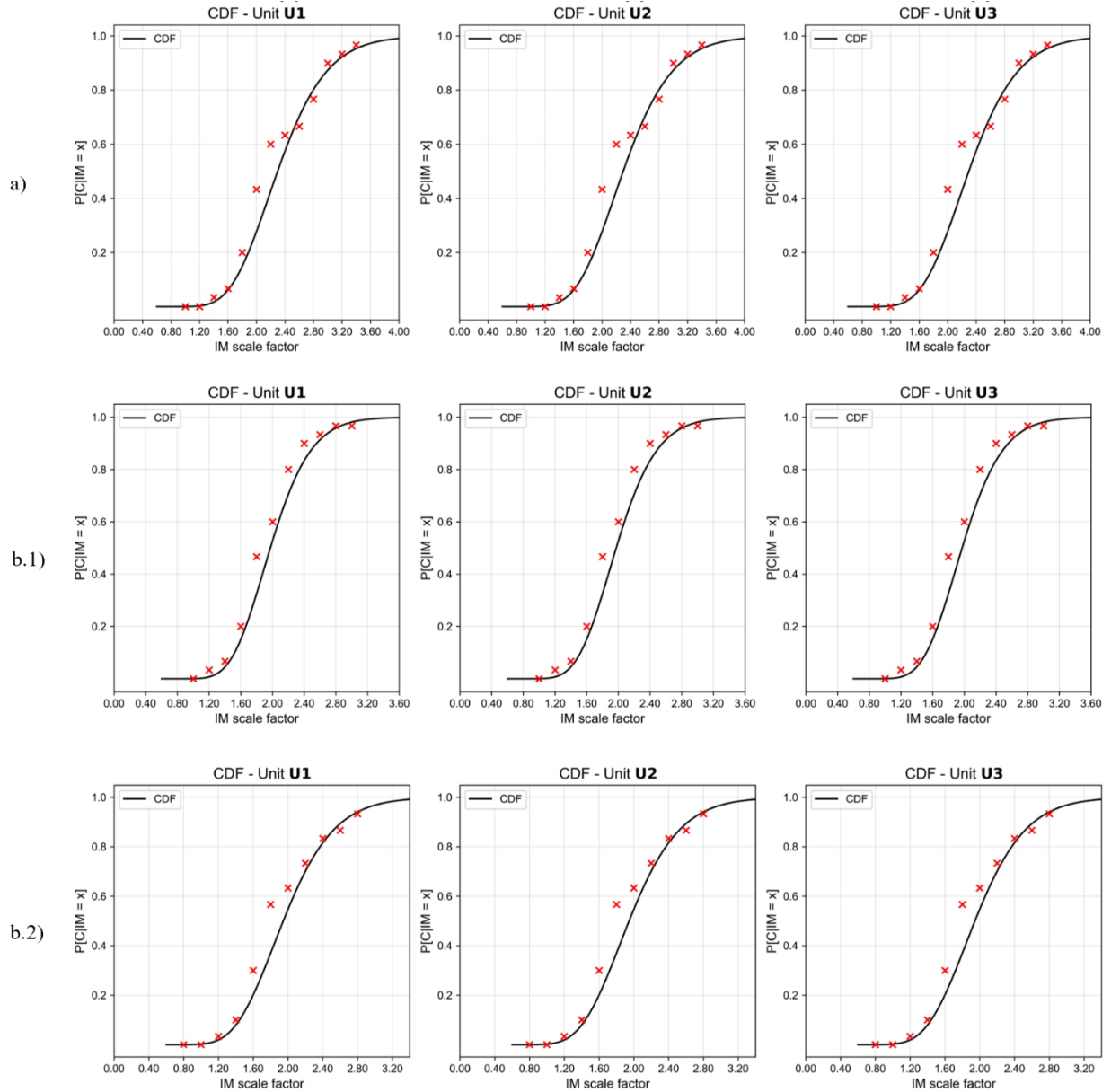


Figure 56: Figure 50: MSA analysis for the isolated cases (c)

Then, as it was reported in chapter 4.5, it is necessary to distinguish between converging and non-converging analyses. So, considering only the non-converging events, the cumulative probability of collapse for non-converging analyses is computed.



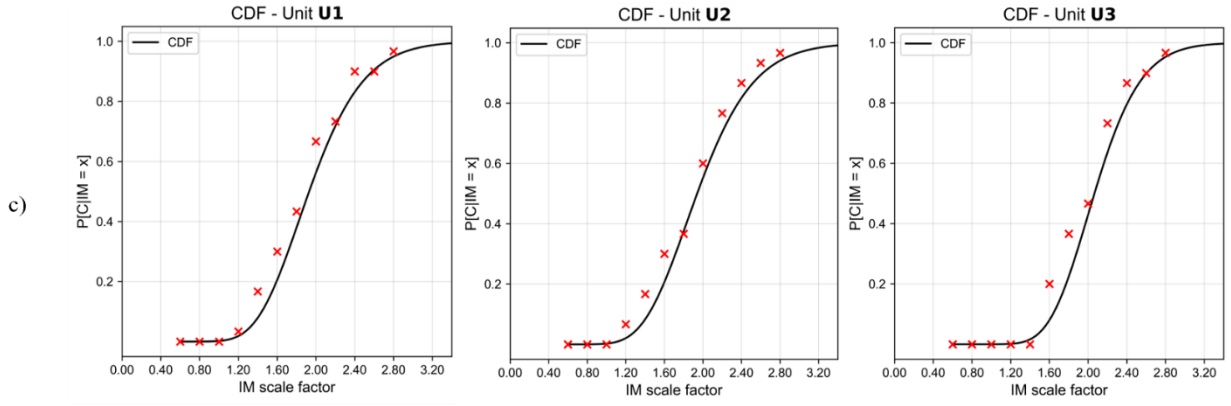


Figure 57: Cumulative Density Function for the a) fully-connected case b) semi-connected case c) isolated models.

In order to compute the probability of collapse of converging analyses, it is necessary to define a threshold (EDP_{lim}) which if exceeded, marks the event as “collapsed”. For the present thesis, the limit considered is in terms of inter-story drift and it is set at $EDP_{lim} = 0.5\%$.

The following plots show the Multi-Stripe Analysis of the several models, colouring the drift values that exceed the limit value of 0.5%. For each IM, the Probability Density Function of the inter-story drifts is computed, Figure 58.

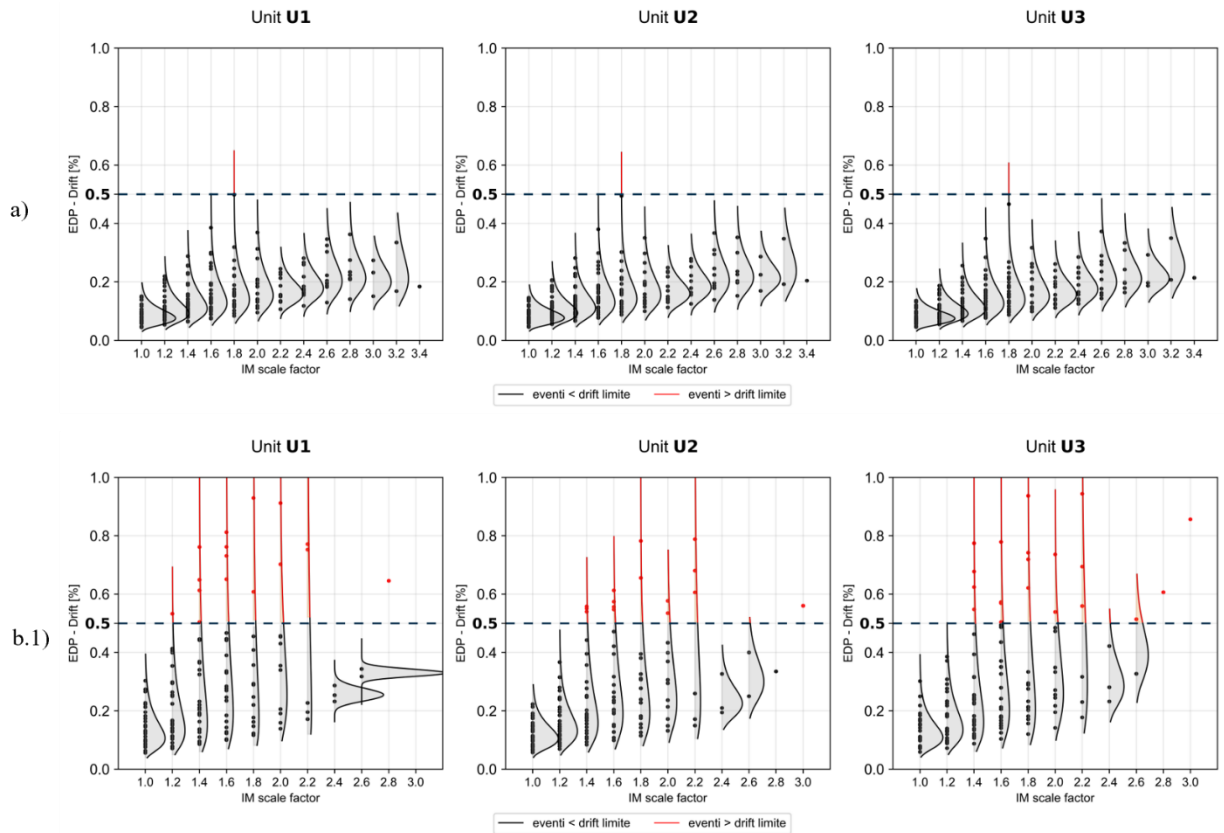


Figure 58: MSA for converging analyses and PDF of the intensity measures obtained for the fully-connected and semi-connected cases

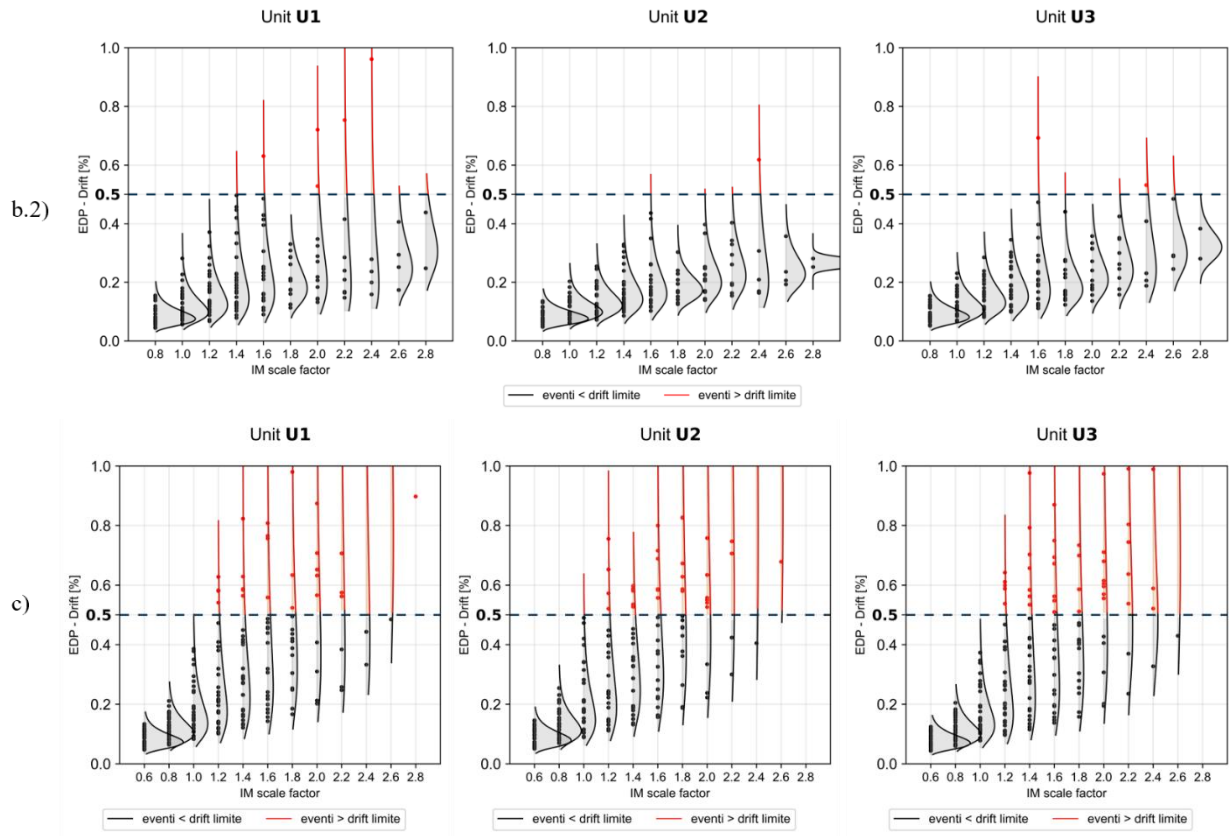


Figure 59: MSA for converging analyses and PDF of the intensity measures obtained for the semi-connected and isolated cases.

As it is displayed in Figure 58, for each intensity measure the Probability Density Function of the inter story drift values is computed. For the semi-connected case with material m_1 and in the case of the isolated units (Figure 58.b.1 and Figure 58.c respectively) the trend that the probability distributions follow is what we expected: increasing the IM there's an increase in the number of events which are over the threshold. This condition is not true in the case of the fully-connected model and the semi-connected case with material m_3 , but their behaviour confirms the trend that was previously manifest in IDA curves and that now is evident: increasing the stiffness of the interconnection between the units leads the aggregate model to collapse at lower levels of inter story drift, conversely the IM range is more extended. Aiming to better understand this phenomenon, a damage analysis was performed selecting two ground motions.

5.4.6 Damage Analysis

To further investigate the damage mechanisms that cause the premature collapse that is manifest in Figure 60.a, a damage analysis has been carried out on a set of two ground motions (accelerogram 9 and 15) which have showed a premature collapse, both in terms of intensity measure and in terms of maximum EDP reached (Figure 60).

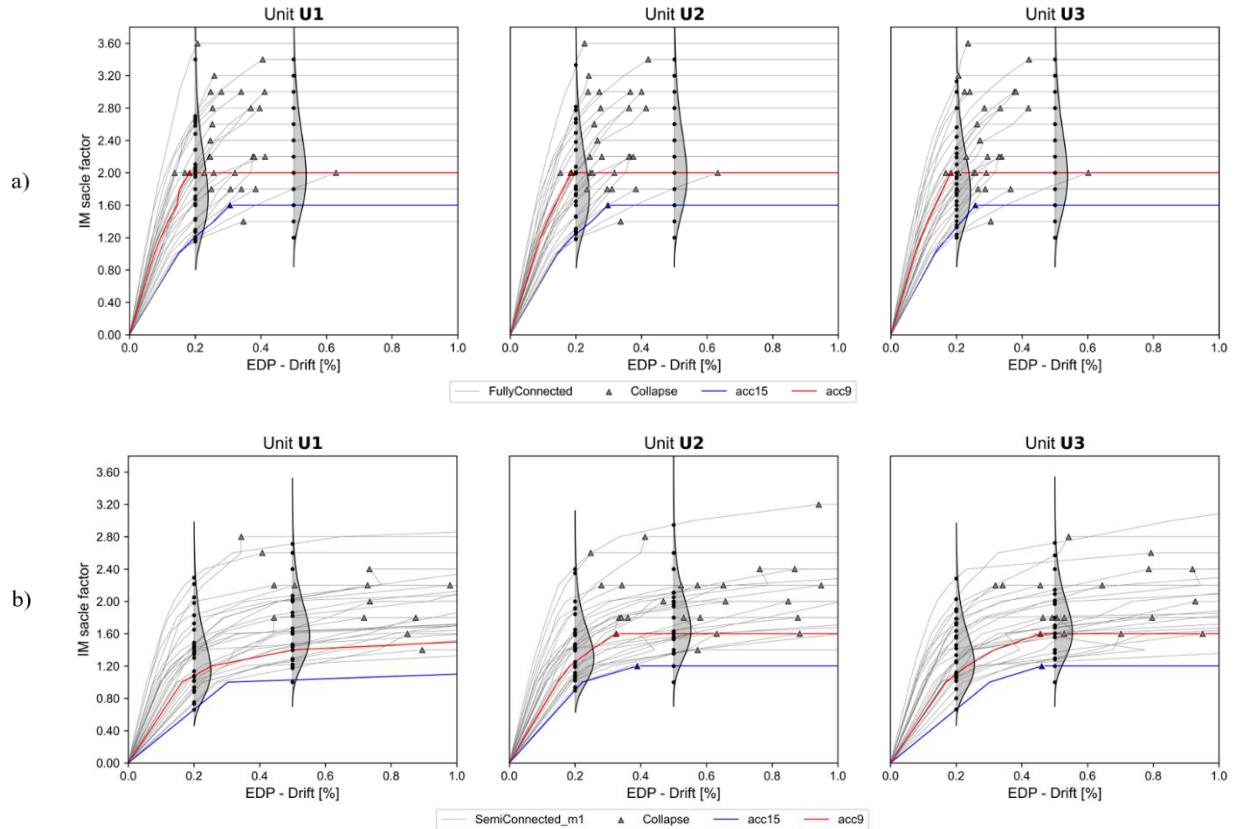
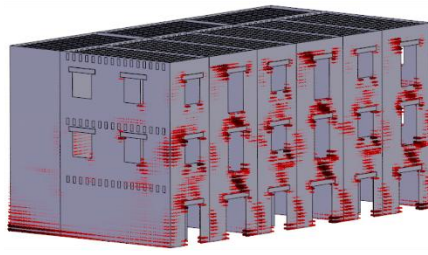


Figure 60: IDA curves for the fully connected and semi connected m1 cases (accelerograms 9 and 15 are highlighted in red and in blue respectively).

As expected, the first wall to be damaged by the ground motion is the front wall, due to its greater flexibility, induced by the higher number of openings. Initially, shear cracks start to form in the spandrels between the openings; this process is particularly pronounced in the thinner elements, but later it will spread also to the other spandrels.

Due to the presence of rigid diaphragms at each floor, when the longitudinal front wall is damaged, the forces are redistributed to the other walls, including both longitudinal and transversal masonry panels.

acc9



Fully-Connected Model



Semi-Connected Model

Figure 61: Initial damage for the fully-connected and the semi-connected model.

The presence of the rigid diaphragm, joined with the presence of the transversal walls, has the beneficial effects of reducing the displacements of the central units, but on the other hand, this also influences the redistribution of the stresses among the units, with the external ones that result to be more compressed. This condition is pictured in Figure 62 when, after the initial damage experienced by the front wall, it is evident the crushing of the back wall in the correspondence of the two external units (that is also the cause of the non-convergence of the analysis).

When the analyses are completed, the final damage plot shows significant damage in the semi-connected model, while the fully connected case exhibits a limited degradation, implying that the more rigid is the connection, the better is the collaboration between units. Additionally, this also confirms the initial hypothesis that the aggregate response was mainly elastic; this is consistent with the IDA curves results that have shown collapses with low inter-story drift values. The greater damage reported by the semi-connected model, especially for the first unit, can be justified by recalling the pounding effect. This phenomenon is specific to adjacent buildings that vibrate and collide repeatedly during an earthquake, causing severe damage.

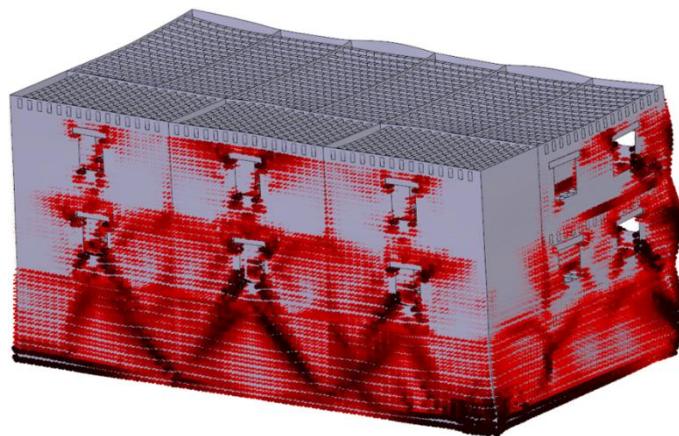


Figure 62: Crushing of the back wall of the external units for the fully-connected case.

In this case study, the collisions are possible if the interface material of the connections between the units is damaged enough to allow each unit to move independently.

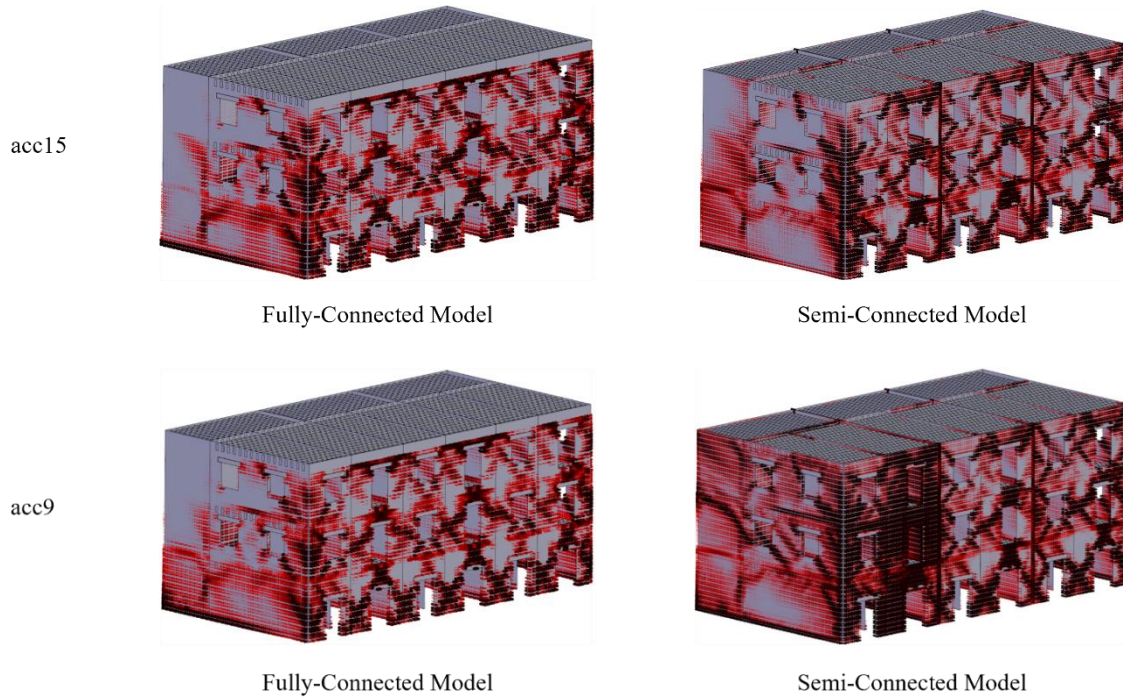


Figure 63: Final damage for the fully-connected and the semi-connected model, for the accelerogram 9 and 15.

5.4.7 Proposed fragility curves

The fragility curves for the different models were created by varying the degree of interconnection between the units, ranging from the fully connected model to the one which considers each unit separately. Each fragility curve was obtained by carrying out 30 nonlinear dynamic analyses for a range of different levels of intensity measure for a total of 1361 analyses. The data obtained were extrapolated using STKO monitors; due to the large amount of data (about 40 GB), Python was used to elaborate them and extrapolate the fragility curves.

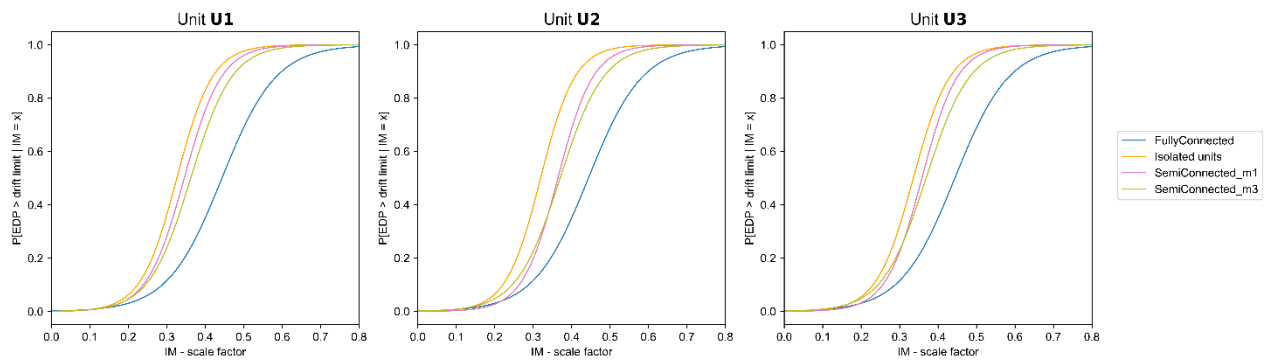


Figure 64: Comparison of the fragility curves for different degrees of interconnection between units.

As it is pictured in Figure 64, the fragility curves obtained confirm the initial hypothesis, which wanted to demonstrate the existence of a beneficial effect that a building ensemble can retrieve from the aggregate configuration (the so called “aggregate effect”). By superimposing the fragility curves related to different model cases, it becomes clear that the curves associated with the fully-connected model and with the isolated ones provide the upper and the lower boundary for the fragility curves, respectively. The semi-connected models represent an intermediate category.

Comparing the different units, the trend exhibited by the curves associated with the fully-connected case and the isolated models, remains almost identical in each unit. On the contrary, it is possible to observe a slight change in the curves related to the semi-connected models. In the external units, the two curves show a progression that is similar to the one of the isolated models, while, in the case of the unit U2, the semi-connected curves are shifted to the right, resulting in a moderate decrease in its probability of collapse. This evidences the beneficial impact that central units experience as a product of the constraining action provided by the adjacent units and the stress redistribution to the external units as a consequence of the improved connection.

These findings are consistent with the pieces of evidence obtained from the damage plot and they also confirm the role that a more rigid interconnection between the units has in enhancing the performance of the building ensemble to the seismic event.

6. Description of a real example of aggregate:

Palazzo Ducale in Popoli, Abruzzo

The ducal palace of Popoli was built at the end of the 15th century by order of Giovanni Cantelmo to make it the new house of the lords of the Popoli fiefdom to better participate in the economic activities and markets of the village that, since the enemy invasions had chased, have moved from the castle to the place that even today is the actual centre of the town.



Figure 65: The case study aggregate in the historical centre of Popoli (Italy). The façades facing the square, reported with the ten units (from U1 to U10 from left to right)

The palace is a great example of aggregate building because it is the result of an “assembly” of different residential cells that were given the form of a palace only in the 15th-16th centuries, features some typical elements of 15th-century noble palaces, including the entrance hall to the courtyard with a trapezoidal plan and a three-arched loggia and a series of windows, representing important examples of Abruzzi Renaissance architecture.

The courtyard is the best-preserved portion of the structure and forms the architectural backdrop to Piazza Duchi Cantelmo. It also preserves a fine façade built in 1824. [27]

6.1 Evolution of the aggregate

The primitive settlement in Popoli developed in the Middle Ages between the street parallel to the main road axis of the town and the connection to the market square. The first dwellings were developed in terraces that were adapted to the contours of the land.

An important aspect is that the houses were structured to have the workshop on the ground floor and on, the first floor, a couple of rooms for the owners' accommodation.

Towards the end of the 15th century, the ducal palace was built as the result of the fusion of the existing residential units in the area; the palace had the typical elements of the noble palaces of this period: an entrance hall gives access to the courtyard loggia from which all the rooms of the palace can be reached. While the upper floor kept its residential use, the shops were centralised in the square so in the ground floor there was only a large room with small openings that was used as a warehouse.

In 1834, the facade of the Ducal Palace was restored by the Muzj family, the new owners of the palace, who further developed the building in height by adding a storey; internally, vaults were added, probably as false ceilings of the overlying 16th-century wooden floors. [27]

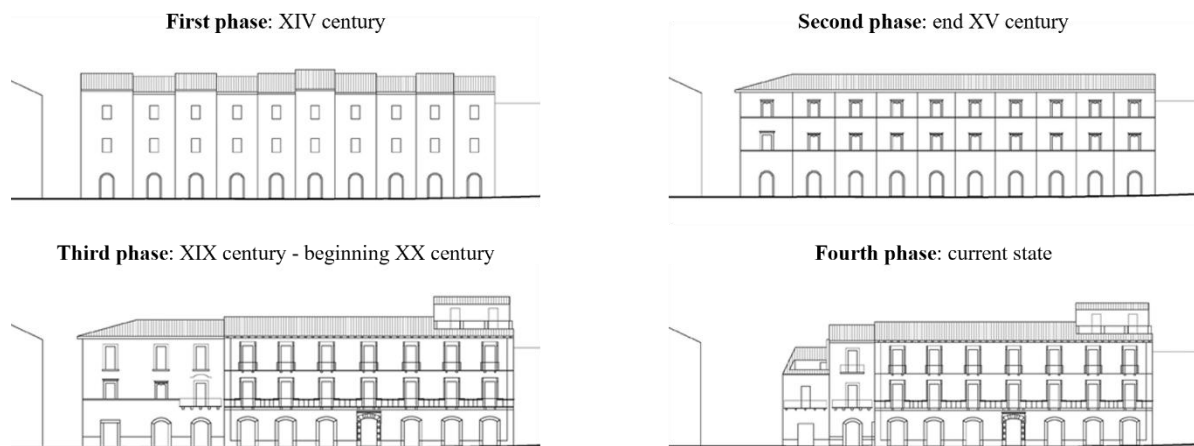


Figure 66: Hypothesis about the evolution of the aggregate over time

Towards the end of the 19th century, as a consequence of the progressive decline of the place, the building was split into smaller units using partition walls made of brick or (more recently) of hollow bricks; these changes were also reflected externally with the opening of new windows without following a particular criterion.

The ducal palace underwent a further evolution both due to the disruption of the first unit of the aggregate, destroyed in a bombing of World War II, and to the combination of interventions that now make it difficult to understand the building as a whole.

6.2 Numerical modelling

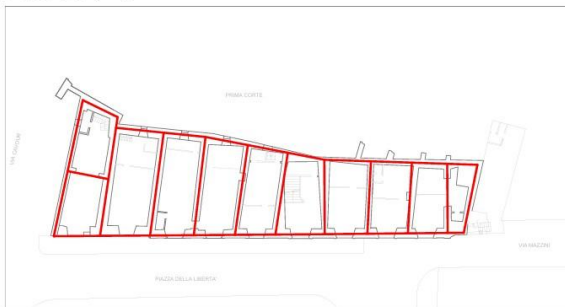
6.2.1 Geometry and simplification hypothesis

The aggregate considered is a part of a more complex building.

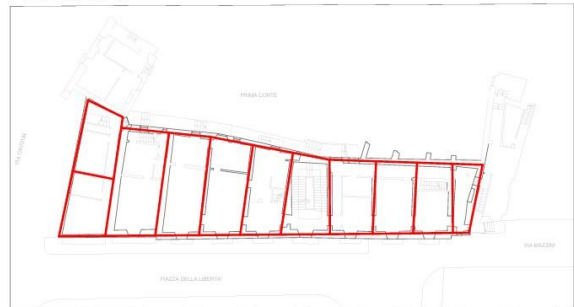
Since the original geometry of the building described so far is very complex, it has been schematised and simplified overlaying all four levels, considering as a reference line for the structural layout of the building the one that almost has an equal distance from the 2 sides of the wall and avoiding considering walls that have a thickness smaller than 20 cm.

The same approach was used for the walls, 20 different typologies of panels were identified measuring the average thickness of each panel and gathering different categories together rounding and averaging the thickness measured to reduce and simplify the model.

FLOOR -1



FLOOR 0



FLOOR +1



FLOOR +2



Figure 67: Proposed schematization and simplification of the structural layout for the four levels of the structure.

The aggregate is composed of 10 units and over three levels, except for unit 1 (which only has 2 floors) and units 9 and 10 (which exhibit four levels).

The total dimensions of the aggregates are 48.49 m along the longitudinal direction, on the transverse direction, the longer side measures 16.47 m while the shorter one is of 8.2 m; the total height of the building is 18.096 m.

For a better comprehension of the structural plan, see the figures in the appendix



Figure 68: Front and back wall (model from Revit)

In the longitudinal direction, only the external walls of the aggregate have been modelled and that will be denominated “Front Wall” and “Back Wall”. The Front wall has a regular disposition of the openings along the façade, while the Back wall’s disposition of the openings does not respect the actual division of the aggregate in subunits but is the consequence of the process of fusion and transformation of each single unit, resulting in a not regular distribution of the openings. The units have been identified from U1 to U10 from left to right.

The opening’s disposition for each wall can be observed in Figure 69.

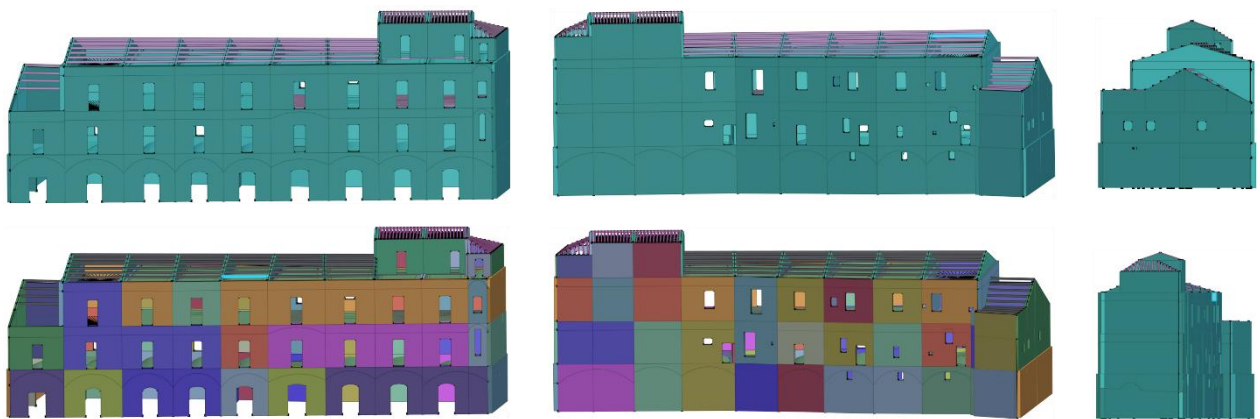


Figure 69: 3D STKO model for front, back and lateral walls.

The aggregate units’ floors were modelled using shell elements, except for level and 2 of unit 2 where the vaults have been replaced by a rigid diaphragm, because during the analysis, probably due to some errors in the geometry that exceeded the software tolerance, these elements kept having problems in the final results (Figure 71).

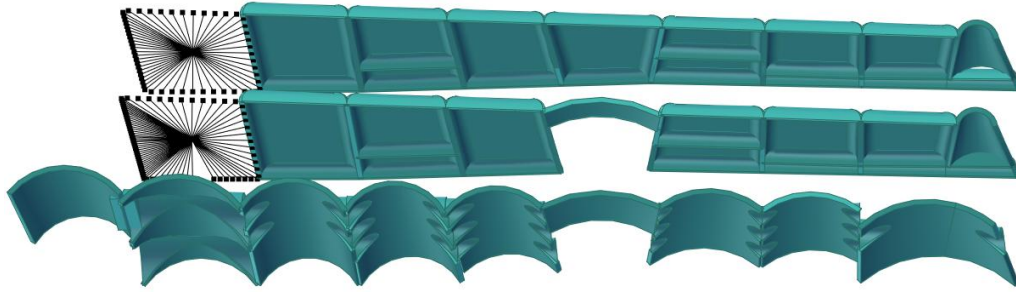


Figure 71: 3D STKO model, vaults and rigid diaphragms

Finally, it should be mentioned that, as mentioned in the introduction of this chapter, this case study is not isolated, instead it is a part of a larger, more complex building ensemble. However, the focus of the analysis is only on the aggregate and the other entities are considered only through their interactions with the case study. Analysing the in-plan configuration of the Palazzo Ducale, the aggregate interacts with the rest of the structure only in four contact points which can be modelled in STKO using a *fix* constraint, limiting the displacements in y-direction.

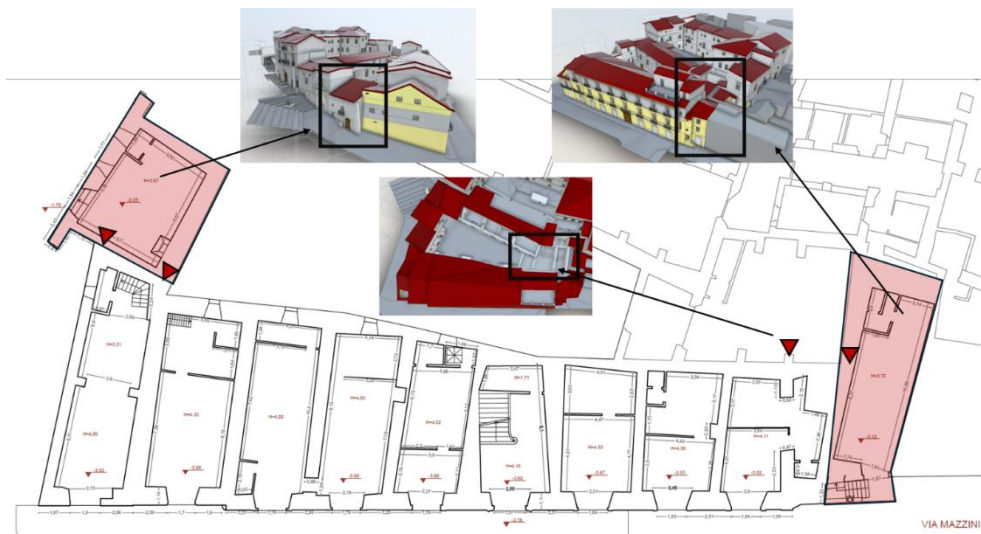


Figure 70: Modelling hypothesis regarding the placement and the typologies of constraint to simulate the interaction between the aggregate and the other buildings.

Consequently, two models have been developed:

- **Isolated model**, in which the aggregate is considered as it was not surrounded by other structures.
- **Constrained model**, in which the interaction between the case study and the other structures is emulated by the insertion of a Fix condition in the lines that stand for the contact point between the structure and the aggregate in STKO limiting the displacements in the y direction (the red lines in Figure 72).

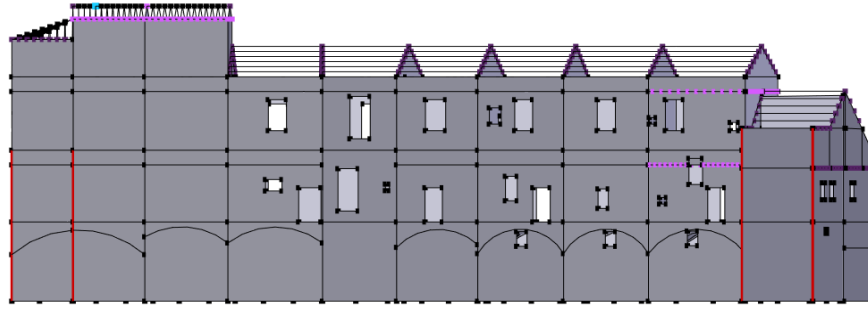


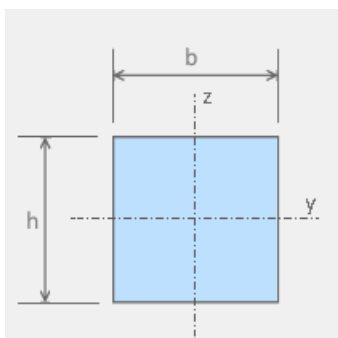
Figure 72: Fix condition to emulate the interaction between the aggregate and the rest of the structure

Three types of analyses have been conducted on the models. The first one was a static vertical analysis; the second one was a modal analysis, which helped us to identify the fundamental mode of the structure and then we have also used some of the outputs (such as the eigenvectors and frequencies) as input for the dynamic analyses (for instance to model the damping of the structure on the basis of Rayleigh damping). Lastly, the third typology of analysis was a dynamic analysis of the structure applying a set of selected ground motions.

6.2.2 Material properties

Two typologies of materials were used for the model of the aggregate: wood and masonry.

The following tables contain the dimensions of the sections used and the physical properties of the material (standard values for a wood section according to NTC18).



	z [mm]	y [mm]
Floor's beams	200	100
Roof's beams	200	100
Roof's beams (small)	140	100
<hr/>		
E [MPa]	11500	
G [MPa]	300	

All materials that compose the masonry walls are modelled using the ASDConcrete3D constitutive model explained in the chapter. Masonry material parameters used were taken from table C8.5II from NTC18 (here reported as Table 2) and in particular since there was no detailed

characterization of the masonry, during the modelling it was made the assumption that all the masonry belonged to the category “Muratura a conci sbozzati con paramenti di spessore disomogeneo”.

Table 16: Masonry physical properties

	f_t	f_{cp}	G_t	G_c	E	ν	w
	[Mpa]	[Mpa]	[N/mm]	[N/mm]	[Mpa]	[-]	[N/mm ³]
Walls	0.07	2	0.083	20.68	1230	0.2	0.00002
Vaults	0.1505	4.3	0.095	23.73	1200	0.2	0.000018

6.2.3 Loads, masses and conditions

The self-weight of the wood beams was obtained from the specific weight of wood (5.5 [kN/m³]) and then applied as *EdgeForce* to the beams.

To obtain the loads and the masses of the elements, the specific weight of the elements (Table 16) was multiplied by their thickness (Figure 73) and is applied as *FaceForce* distributed on the shells.

An additional load was applied to the vaults to emulate the presence of 5 cm of screed having a specific weight of 0.000018 [N/mm³].

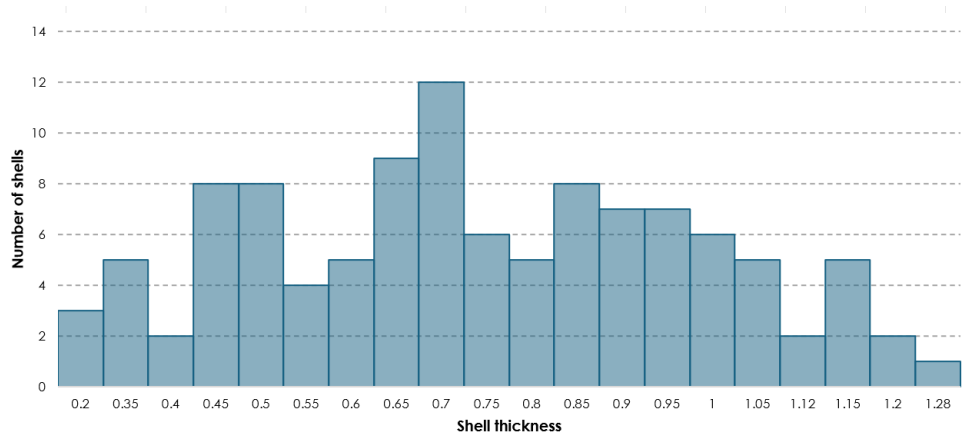


Figure 73: Shell thicknesses and the related number of elements

Since Opensees does not automatically convert the load into masses, it is necessary to compute the masses separately and to apply them to the elements for the dynamic analyses.

6.2.4 Mesh architecture

For the mesh, the choice was to use a global mesh size of 400 mm for all the shells and the beams, while for the eigenvalue analysis it was decided to use a mesh of only one element for the beams in order to neglect their local mode in the analysis. The global mesh size was chosen

because in this way it is possible to discretize the model achieving a balance between result accuracy and computational resources. This coarse mesh was acceptable, thanks to the use of ASDConcrete3D, which is insensitive to mesh size variations.

For the analyses, a total of 9 processors have been used, each handling approximately 7000 partition elements (Figure 74).

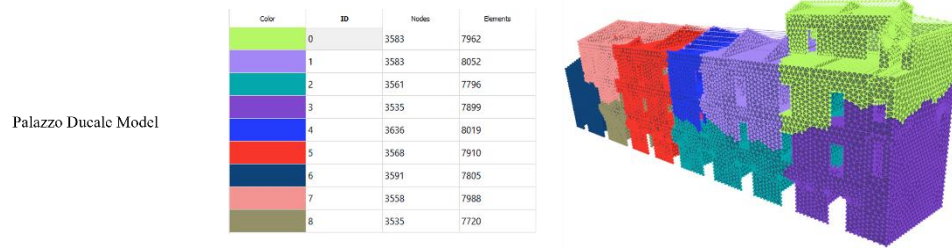


Figure 74: Partitioning of the Palazzo Ducale model

6.3 Dynamic properties of Palazzo Ducale

Modal analysis was conducted to study the models, extracting their dynamic properties including vibration modes, frequencies, and modal participation factors. Table 17 shows the periods and modal participation ratios in the x and y directions for the first 5 vibration modes of the aggregate; two cases have been considered: Constrained case and isolated case.

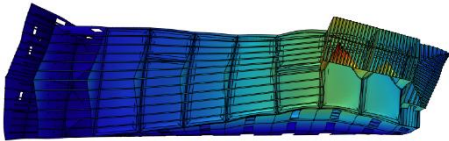
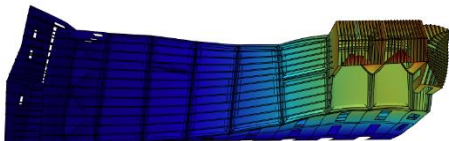
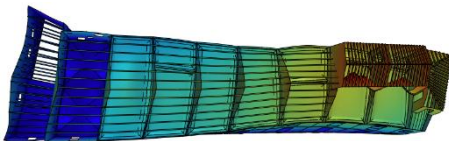
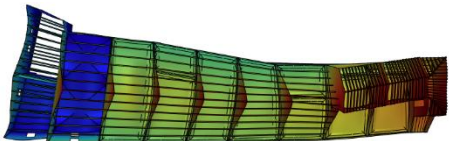
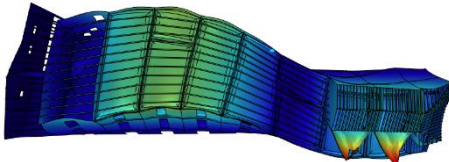
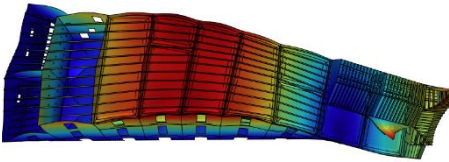
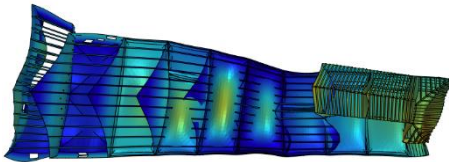
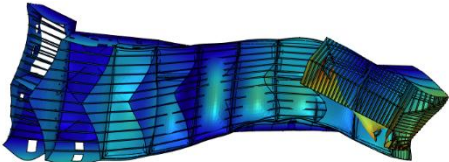
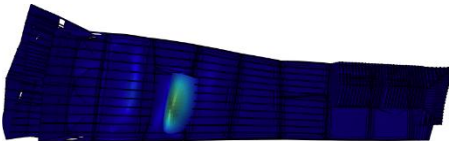
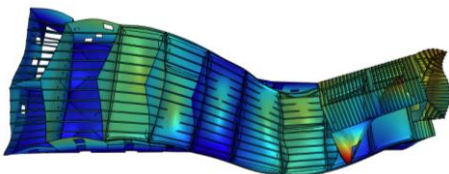
Table 17: Eigenvalues analysis results for the constrained and the isolated model

	Constrained model			Isolated model		
	T	Mx	My	T	Mx	My
Mode	[s]	[%]	[%]	[s]	[%]	[%]
1	0.221261	16.0927	28.7012	0.256818	0.002217	32.2978
2	0.215581	50.9402	7.15913	0.218274	64.67	1.13736
3	0.174074	0.309011	10.5314	0.190593	2.66301	21.6321
4	0.16092	2.54332	0.002602	0.162758	1.44797	3.06367
5	0.149402	0.24184	0.001756	0.159989	1.00732	2.24724

In both the models considered in the analysis, the first mode predominantly is about the y-direction, while the second mode is in the x-direction. Table 18 displays the first five modal shapes of the two cases considered: Constrained model and isolated model.

As it can be seen from Table 17, the first three modes of vibration involves the majority of mass of the structure, while the last two modes are about local vibrations mode which only excite local masses, showing the aggregate's tendency to exhibit a local behaviour, due to the presence of the vault at each floor (this issue was partially solved introducing a rigid diaphragm instead of using shell elements for the vaults of the first and second floor of the second unit).

Table 18: Five modal shapes for the constrained and the isolated model

	Constrained model	Isolated model
1 ST mode		
2 ND mode		
3 RD mode		
4 TH mode		
5 TH mode		

6.4 Non-linear dynamic analysis results

The ground motion selected was obtained using REXELweb [28]. REXELweb is an online tool available on the ITACA3.2 and ESM websites (databases of Italian and European accelerometric recordings). It provides a guided and user-friendly web interface for searching recorded accelerograms that are, on average, compatible with a given target spectrum. The parameters used in the software are summarized in Table 19.

Table 19: Parameters for the ground motion selection.

Soil category	C
Topographic category	T1
Nominal life	50 years
Latitude	42,1709° N
Longitude	13,8317° E
Usage class	II
Limit state	SLC
$M_{w,min}$	5.5
$M_{w,max}$	6.5
R_{max}	50 km

The selected ground motion was IT.CLO.00.HGE.D.EMSC-20161030_0000029, recorded at the station of Castelluccio di Norcia, 30/10/2016.

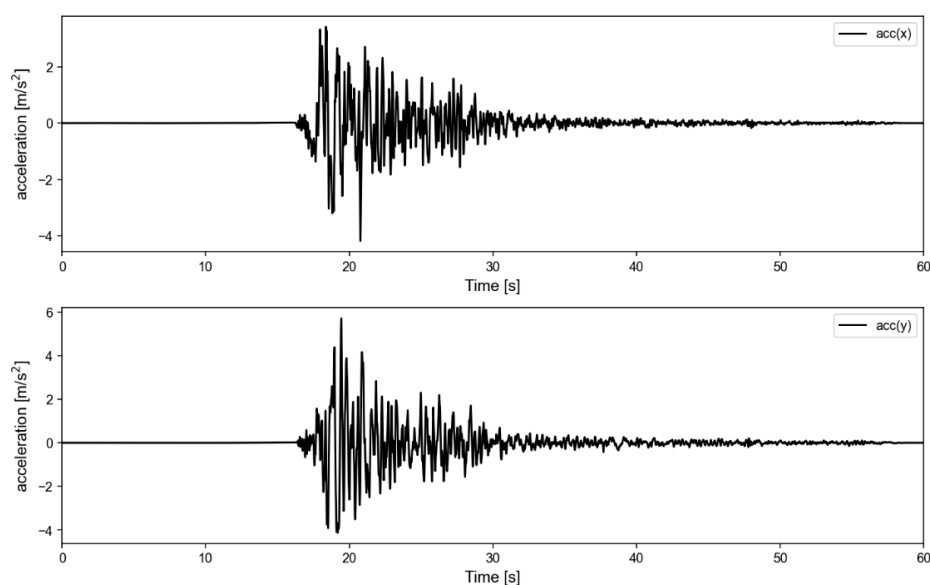


Figure 75: Acceleration time-history for the two components of the Norcia ground motion.

Figure 76 displays the evolution of the inter-story drift for two towering units (U8 and U9) on the fourth floor. The drift time history is compared with the accelerogram. Three points are highlighted: at the beginning, the amplitude of the acceleration is low and the structure exhibits almost no damage. The second point stands for the activation of some damage mechanism in particular in the towering units which result to be the most heavily affected by the seismic event and finally, the last point indicates the triggering an overturning mechanism of the façade. This condition terminates the analysis, since, even if the model continues to find a solution and the analysis is convergent, the results are not realistic.

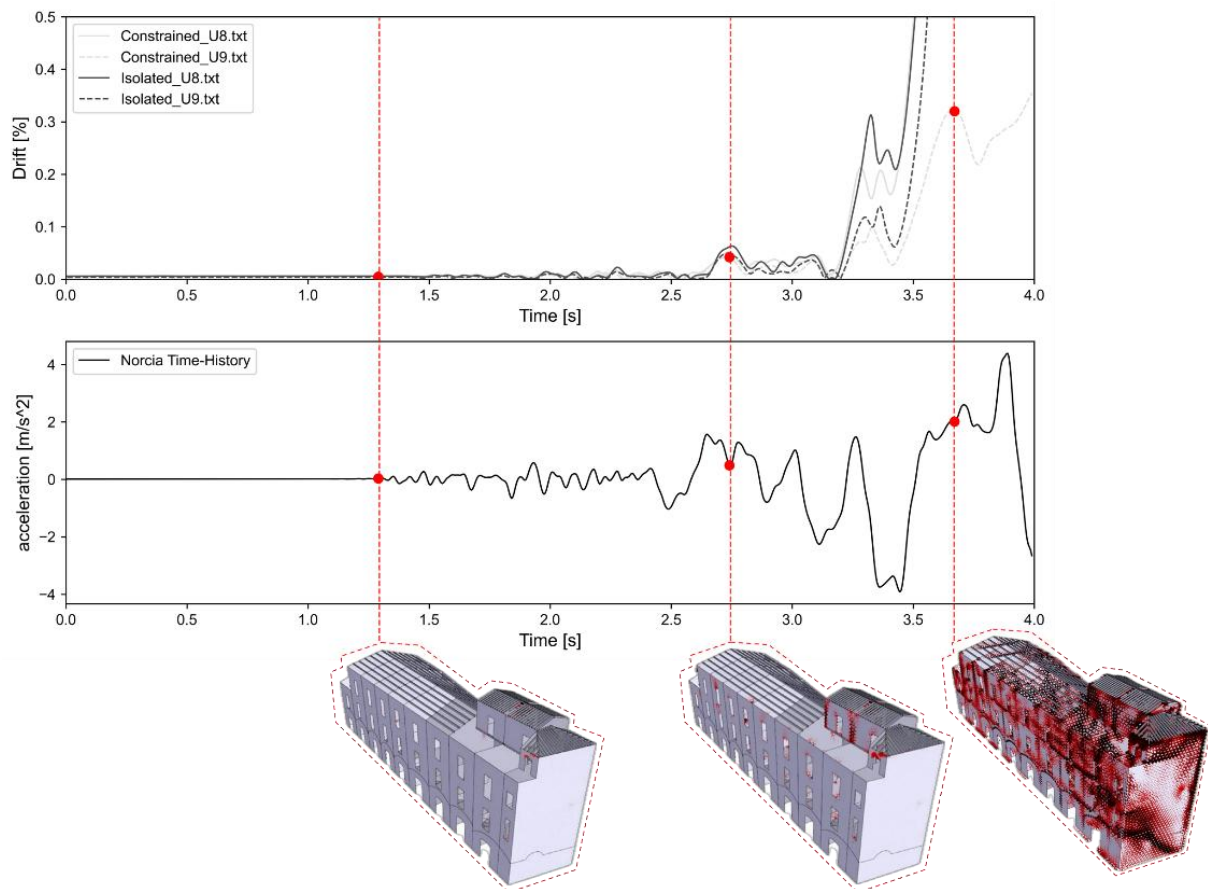


Figure 76: Comparison between the inter-story drift and the accelerations time-histories

6.4.1 Damage Analysis

The structure is almost regular in elevation for the first 7 units and, as anticipated by the modal analysis, the largest displacements occur on the transverse direction (y-axis). However, the presence of three towering units (on the right-hand side) has a great impact on the behaviour of the aggregate, since they result in being excited locally by the seismic event. This condition is portrayed performing a damage analysis of the building ensemble and, in Figure 77, it is

possible to observe the initial damage accumulation on the masonry panels of the structure. In particular, the panels located at the fourth floor of the building are primarily affected by the seismic event.

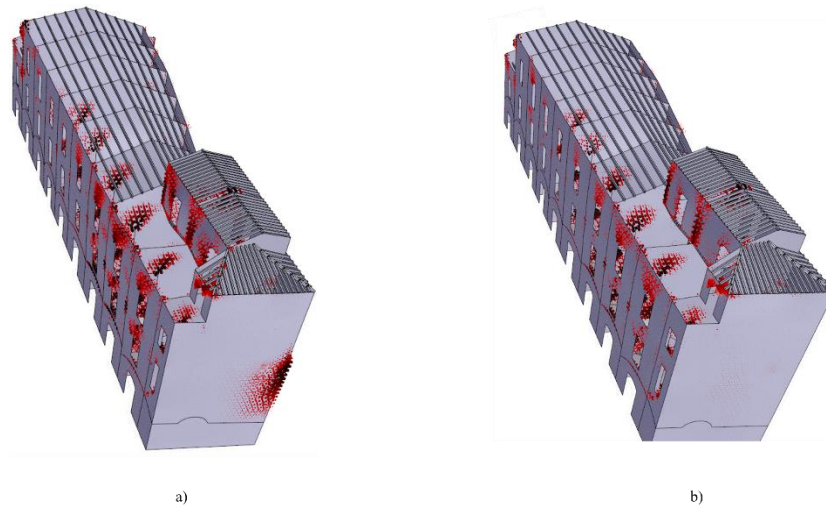


Figure 77: Initial damage for the two cases considered. a) constrained model, b) isolated model.

In Figure 77.a and b is pictured a comparison between the constrained model and the isolated models. It should be noted that, in the correspondence of the points at which the structure is constrained to the aggregate, the stress would concentrate and the phenomenon of damage accumulation starts to appear.

The continuation of the analysis reveals the existence of consistent damage on the back wall. Furthermore, this damage is observed to be present on the transverse walls, and subsequently on the front wall.

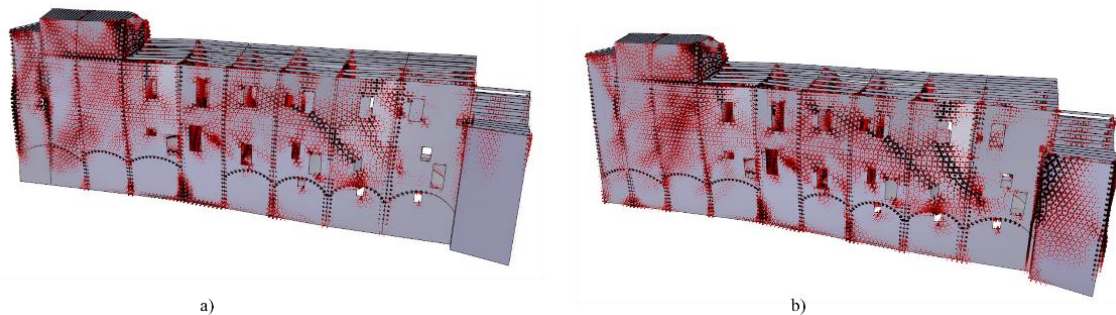


Figure 78: Damage for the back wall. a) constrained model, b) isolated model.

As previously explained, the damage accumulation can be seen in the correspondence of the points at which the structure is constrained, Figure 78.a.

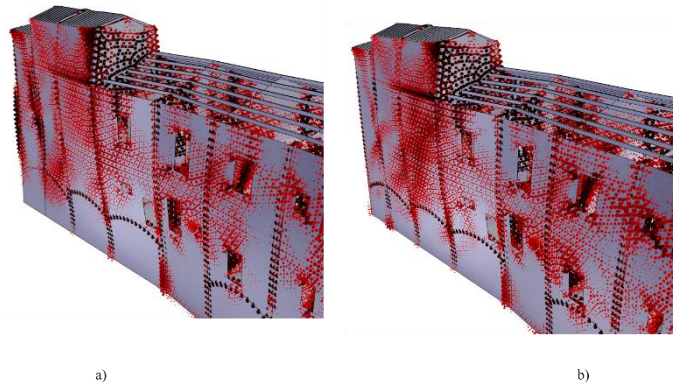


Figure 79: Damage for the back wall, detail of the large displacements attained for the towering units. a) constrained model, b) isolated model.

Shear cracks develop at discontinuities such as openings or where the thickness of the masonry panels changes. Additionally, the masonry at the base floor exhibits signs of crushing.

Finally, it should be noted that, as anticipated in Figure 76, the presence of constraints reduces the out-of-plane displacements of the structure,

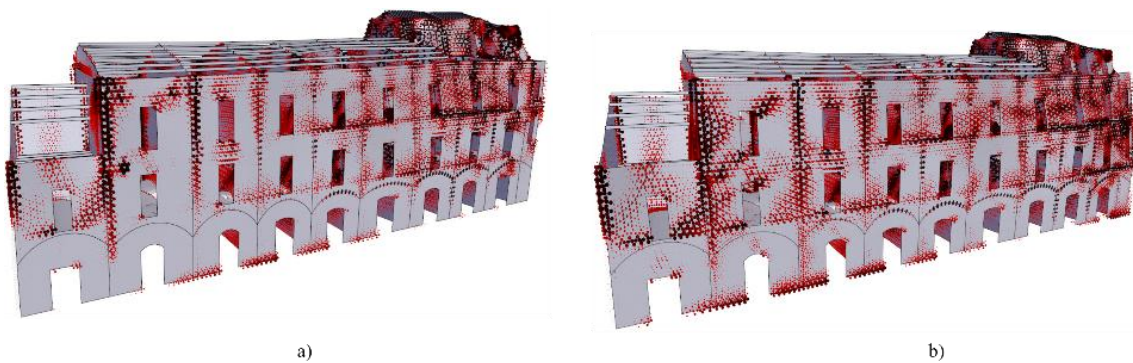


Figure 80: Damage of the aggregate front wall. a) constrained model, b) isolated model

As illustrated in Figure 80, the base floor results to be less affected by the seismic event, this can be mainly attributed to the significant difference in terms of thickness of the base walls compared to the panels of the other levels of the structure (which are substantially thinner) and to the effectiveness of the wall-to-vaults connection.

The issue of the effectiveness of the vault-to-wall connection has proven to be crucial for determining the final behaviour of the structure. Along the analysis, following the accumulation of damage on the structure, it is possible to observe a pronounced overturning of the walls, anticipated by a progressive reduction of the stiffness of the vaults.

In conclusion, this aggregate ensemble was such a complex model that necessitated a proper survey campaign and an adequate characterization of materials and connections between the different structural elements (such as vaults-walls connection or the wall-to-wall connection). Without these analyses, the uncertainties would lead to excessive model simplifications that would affect the final results.

This is manifest in the modelling of vaults of the upper levels, which were considered as structural components, but the uncertainty about their stiffness caused the triggering of kinematic mechanisms such as the out-of-plane overturning of the masonry panels. It is plausible to assume that, stiffening elements such as wooden beams, chains, etc, are located some under these vaults. Their presence would have been crucial in preventing or limiting the formation of these mechanisms.

Nevertheless, this study has demonstrated the limitations of a regular elementary case study, enhancing the necessity for further investigations concerning the influence of towering units in the final behaviour of the building and the impact that rigid diaphragms would have in the prevention of out-of-plane collapsing mechanisms.

7. Conclusions

Buildings in aggregate configurations are widespread throughout Europe and have been demonstrated to be extremely vulnerable to seismic events, nevertheless, the regulations do not address this issue in a comprehensive manner. This would often be reflected in the introduction of various simplifications in the model, neglecting the boundary conditions that adjacent units pose on the studied structure, namely the aggregate effect.

The present thesis is developed in this context, aiming to explore the potential beneficial effects that the structure could retrieve if considered in its aggregate configuration. Consequently, exploiting the results of previous studies based on an elementary aggregate purposely designed to isolate the effect of the different variables that affect this kind of structure's seismic behaviour, several non-linear dynamic analyses have been performed to assess the performance of the building ensemble and develop fragility curves.

The thesis considers two case studies: an elementary aggregate case study and a real aggregate that is the Palazzo Ducale of Popoli (PE). Both models were developed in 3D with STKO using similar modelling strategies. The masonry walls were modelled using 2D layered shell elements and a homogenized masonry approach using the ASDConcrete3D constitutive model available in STKO.

In the elementary aggregate model, various degrees of interconnection between the units were considered using three configurations: fully-connected model, semi-connected model and isolated units. In the Palazzo Ducale model, the interaction between the aggregate and the complex urban context surrounding the aggregate was considered, comparing the results obtained for the isolated and the constrained models.

The results proved that the individual unit has a beneficial effect if considered in its fully-connected configuration. The position of the unit in the context of the building ensemble also plays a crucial role in determining the final behaviour of the structures, resulting in the external ones being more affected by the seismic event, while the internal units can benefit from the confinement provided by the other structures.

In the current thesis for the elementary case study, IDA analyses are performed increasing the scale factor of 0.2 at each stage, until the model reaches the non-convergence. Consequently, the four models have been processed for a total of 1361 times and, since the average time

required to complete one analysis spans from two to four hours, it can be deduced that performing these types of analyses on a building is a time-consuming task, that, currently, has limited applications.

It should be noted that the average time required to perform one full analysis of the model depends primarily on several factors: the specific case under study (fully-connected, semi-connected, isolated or Palazzo Ducale), the duration of the ground motion and the point at which the model undergoes to non-convergence (as the solving algorithm, trying to solve the equations, reduces the time step and increases the increments). However, even if a high-performance workstation equipped with a 2022 processor (*AMD Ryzen Threadripper PRO 5965WX*) was used, solving complex models with a large number of degrees of freedom for a set of multiple accelerograms, remains a demanding task that requires weeks to be completed. That being said, since the analyses are performed with almost no human supervision, in future, using increasingly better processors will be reflected in an increase in the adoption of non-linear dynamic analyses and especially IDA analyses.

In conclusion, the present study implements a framework for the development of fragility analyses for selected case studies. The methodology developed is structured to integrate the modelling phase executed in STKO, the automatic scaling of the applied ground motion and the analysis of the model using OpenSees and Python.

The fragility curves, obtained applying the procedure described, confirm the presence of beneficial effects of in-aggregate configuration. However, despite the general consistency in IDA curve trends across units, a more detailed analysis of aggregate behaviour reveals significant differences in the capacity curves. These variations highlight the constraining action exerted by adjacent units on central ones, but they also expose the limitations of relying solely on in-plane drifts as a parameter to evaluate the behaviour of complex masonry aggregates.

This limitation is particularly relevant considering that the analysed models feature regular geometries and rigid diaphragms, which do not accurately reflect the structural configurations typically found in historical Mediterranean centres. To address these limitations, the study extends the analysis to a real case study. Furthermore, the findings highlight the need for further investigations into the influence of towering units on overall structural behaviour and the role of rigid diaphragms in mitigating out-of-plane collapse mechanisms.

7.1.1 Future developments

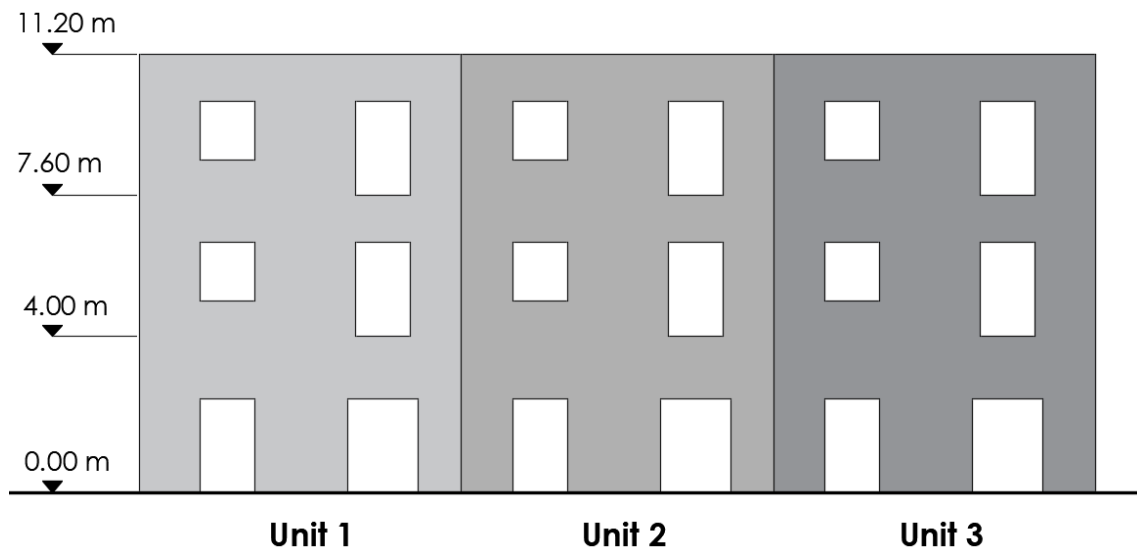
When the numerical non-convergence is reached, in some cases the drift level measured is not representative of the Collapse Limit State (in particular, this condition has been observed for the fully connected case and in the semi-connected case with stiffer connections among the units). It is likely to assume that this happens because the time step used in the analyses is not adequate. For future analyses, it should be recommended to reduce the time step, even doubling or tripling the number of increments, to obtain realistic values for the drifts.

In general, it should be pointed out that the chosen EDP may not be representative of the global behaviour of the structure, which collapse could be driven by other typologies of mechanisms, so it would be useful to evaluate other EDPs and to compare the fragility curves related to these cases.

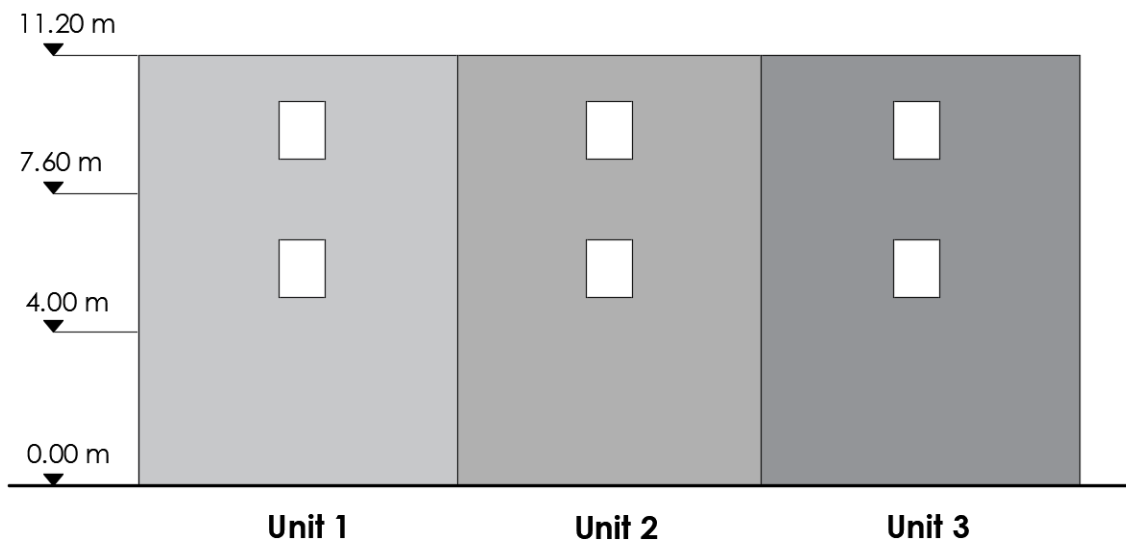
Lastly, in the Palazzo Ducale case study several issues have emerged, such as the importance of accounting for the presence of rigid diaphragms to distribute the forces among the masonry walls and to constrain the panels, avoiding the triggering of their out-of-plane overturning. For future analyses, it would be interesting to observe the differences between fragility curves representing different model choices and simplifications.

8. Appendix

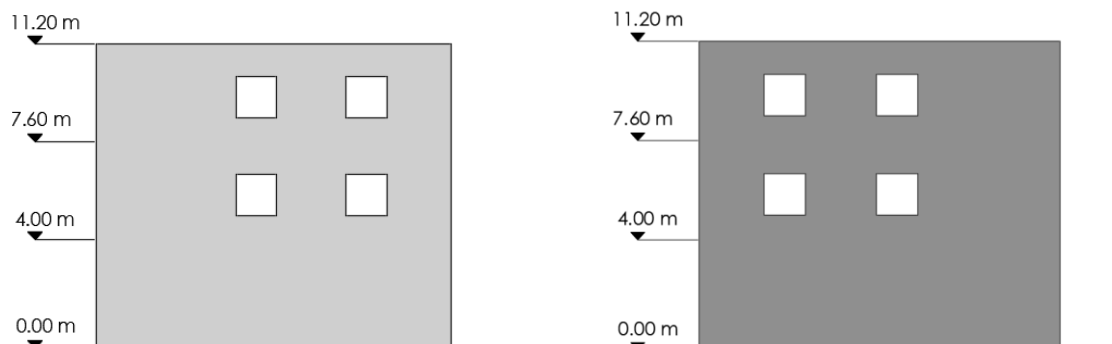
Front Wall



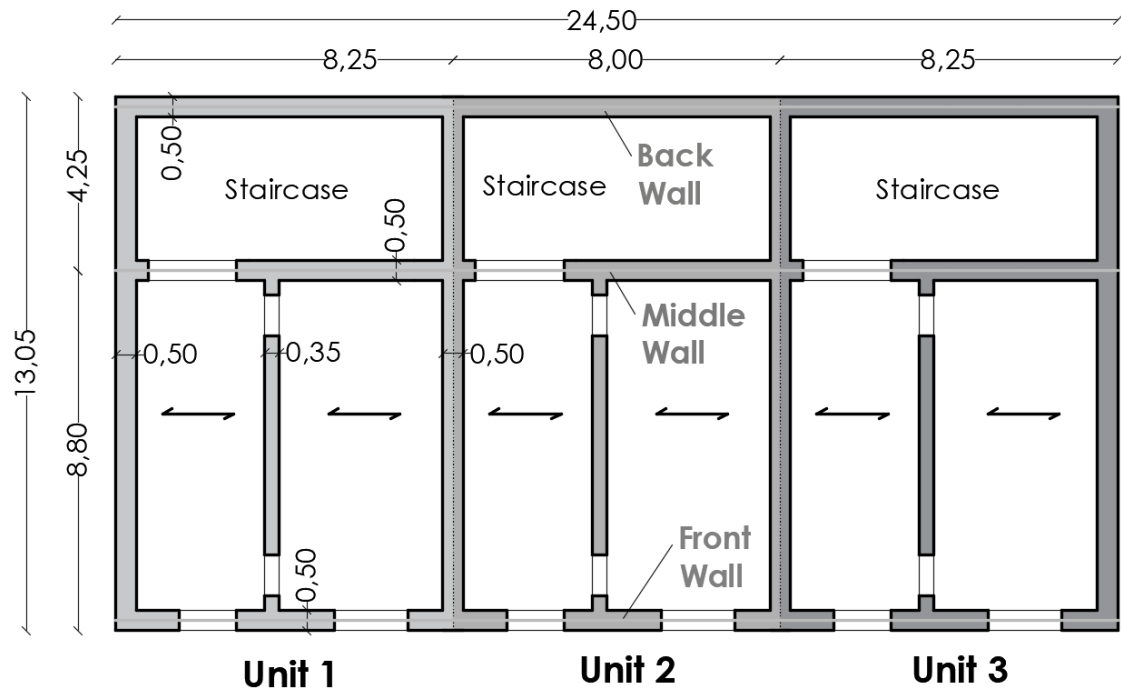
Back Wall



Transverse Walls



First Floor



9. References

- [1] S. C. F. d. P. G. M. A. P. Luigi Sorrentino, “Seismic behaviour of ordinary masonry buildings,” *Springer Nature*, 2018.
- [2] A. B. S. C. Michele Angiolilli, “Fragility curves of masonry buildings in aggregate,” *Springer Nature*, 2023.
- [3] C. N. D. RICERCHE, CNR-DT 212/2013, Roma, 2014.
- [4] S. L. S. C. Silvia Pinasco, “Unreinforced masonry buildings in aggregate of urban settlements: Current approaches and critical issues for the seismic vulnerability assessment,” *Elsevier*, 2025.
- [5] M. G. G. E. F. Valente M, “A. Historical masonry building aggregates: advanced numerical insight for an effective seismic assessment on two row housing compound,” *Eng Struct*, 2019.
- [6] K. B. Igor Tomić, “Shake-table test on a historical masonry aggregate: prediction and postdiction using an equivalent-frame model,” *Bulletin of Earthquake Engineering*, 2023.
- [7] S. M. F. S. M. H. & F. G. Mazzoni, “OpenSees Command Language Manual,” 2006.
- [8] F. S. M. H. & F. G. L. McKenna, “Nonlinear Finite-Element Analysis Software Architecture Using Object Composition,” *Journal of Computing in Civil Engineering*, 2010.
- [9] F. McKenna, “Object-oriented finite element programming: Frameworks for analysis, algorithms and parallel computing,” *University of California*, 1997.
- [10] M. Petracca, “OpenSeesDocumentation,” 2022. [Online]. Available: <https://opensees.github.io/OpenSeesDocumentation/index.html>.

- [11] L. P. R. R. S. Z. G. C. E. S. Massimo Petracca, "Micro-scale continuous and discrete numerical models for nonlinear analysis of masonry shear walls," *Construction and Building Materials*, vol. 149, pp. 296-314, 2017.
- [12] A. H. J. C. J. Oliver, "An implicit/explicit integration scheme to increase computability of non-linear material and contact/friction problems," *Computer Methods in Applied Mechanics and Engineering*, 2007.
- [13] J. W. & Son, "Model Code for concrete structures," 2010.
- [14] e. a. Water, "Guidelines for Nonlinear Finite Element Analysis of Concrete Structures," 2020.
- [15] X. W. A. Yutao Pang, "Cloud-IDA-MSA Conversion of Fragility Curves for Efficient and High-Fidelity Resilience Assessment," *Journal of Structural Engi*, 2021.
- [16] X. L. L. J. M. Y. A. K. Xinyong Xu, "Dynamic Damage Mechanism and Seismic Fragility Analysis of an Aqueduct Structure," *Applied Sciences*, 2021.
- [17] C. C. Dimitrios Vamvatsikos, " Incremental Dynamic Analysis," *Earthquake Engng Struct. Dyn*, 2002.
- [18] A. S. K. Ajay Singhal, "Method for probabilistic evaluation of seismic structural damage," *J. Struct. Eng.*, pp. 1459-1467, 1996.
- [19] T. Yang, 12 - Assessing seismic risks for new and existing buildings using performance-based earthquake engineering (PBEE) methodology, vol. Handbook of Seismic Risk Analysis and Management of Civil Infrastructure Systems, K. G. S. Tesfamariam, Ed., Woodhead Publishing, 2013, pp. 307-333.
- [20] B. A. B. P. J. S. Jack W. Baker, Seismic Hazard and Risk Analysis, Cambridge: Cambridge University Press, 2021.
- [21] N. A. & J. B. J. Macedo, "Arias intensity models for subduction zone earthquakes," in *Earthquake Geotechnical Engineering for Protection and Development of Environment and Constructions*, Rome, 2019.
- [22] F. D. T. S. V. M. P. G. C. Marilisa Di Benedetto, "SEISMIC RESPONSE OF DIFFERENT MASONRY BUILDING AGGREGATE CONFIGURATIONS BY A REFINED FE

MODEL,” in *9th ECCOMAS Thematic Conference on Computational Methods in Structural Dynamics and Earthquake Engineering*, 2023.

- [23] K. a. C. Magenes, “Seismic Testing of a Full-Scale, Two-Story Masonry Building: Test Procedure and Measured Experimental Response,” 1995.
- [24] L. Medei, Modelling and analysis of masonry building aggregates subject to various degrees of interconnection (Master thesis), Torino, 2024.
- [25] F. M. A. C. A. T. Marco Nale, “Fragility functions for local failure mechanisms in unreinforced masonry buildings: a typological study in Ferrara, Italy,” *Bulletin of Earthquake Engineering*, 2021.
- [26] S. Villar, Refined modelling and analysis of masonry building aggregates (Master Thesis), Torino, 2023.
- [27] G. S. Silvio Cafarelli, *Il palazzo Ducale di Popoli, dalla conoscenza alla conservazione*, Casa Editrice Tinari, 2008.
- [28] S. F. C. R. E. D. M. L. G. P. F. L. L. B. R. B. G. I. I. Sgobba, “The online graphical user interface of REXELweb for the selection of accelerograms from the Engineering Strong Motion database (ESM).,” in *39° Convegno Nazionale Gruppo Nazionale Geofisica della Terra Solida (GNGTS)*, (online), 22 – 24 giugno 2021.
- [29] M. K. G. Muthukumar, “Influence of Openings on the Structural Response of Shear Wall,” *Springer, New Delhi.*, 2015.

